KYAMBOGO UNIVERSITY

FACULTY OF ENGINEERING

DEPARTMENT OF CIVIL AND ENVIRONMENTAL ENGINEERING

"A Comparative Analysis of the Concentrated Plasticity, the Yielded Block Spread Plasticity, and the Spread cracking and yielding block Pushover analysis models"

BY

KIMEZE HENRY
(MSc. Structural Engineering)

REG No: 17/U/14591/GMES/PE

A DISSERTATION/THESIS SUBMITTED TO KYAMBOGO UNIVERSITY

GRADUATE SCHOOL

IN PARTIAL FULFILMENT FOR THE

AWARD OF A MASTER IN STRUCTURAL ENGINEERING

AUGUST 2022

0

APPROVAL

The undersigned approve that they have read and hereby recommend for submission to the Graduate School of Kyambogo University, a final dissertation entitled: A Comparative Analysis of the Concentrated Plasticity, the Yielded Block Spread Plasticity and the Spread cracking and yielding block Pushover analysis models in fulfillment of the requirements for the award of Master of Science in Structural Engineering Degree of Kyambogo University.

Dr. MICHAEL KYAKULA ------------------------- (Supervisor)

Date: -----25ᵗʰ August, 2022-----

Dr. MUHWEZI LAWRENCE------------------------- (Supervisor)

Date: -----25ᵗʰ August, 2022-----

DECLARATION

I, Kimeze Henry hereby declare that this submission is my work and that, to the best of my knowledge and belief, it contains no material previously published or written by another person nor material which has been accepted for the award of any other degree of the university or other institute of higher learning, except where due acknowledgment has been made in the text and reference list.

ACKNOWLEDGEMENT

TABLE OF CONTENTS

LIST OF FIGURES

LIST OF TABLES

ACRONYMS

M_{cr} Cracking moment

M_y Yield moment

M_o Ultimate moment

EXECUTIVE SUMMARY

Pushover analysis is mainly carried out using the concentrated plasticity model where by when a point reaches yield, a hinge is placed at that point. The other is the yielded block spread plasticity model, whereby when a point reaches yield, an elastic sub-element of the beam is replaced by a yielded block sub-element having a reduced cross section and second moment of area. Both of these models ignore cracking. This research seeks to determine the effect of considering cracking during modelling on the accuracy of estimating deformations in RC structures during pushover analysis by proposing a spread cracking and yielding block model.

For the single storey frame, a comparison between the proposed model and the yielded block spread plasticity model indicates an improvement in accuracy of the joint rotational, displacement, moment and lateral load capacities of the frame by 27.81%, 13.46%, 2.035% and 6.26% respectively in favour of the proposed model. The proposed model in comparison to the concentrated plasticity model, leads to an improvement in accuracy of the joint rotational, displacement, moment and lateral load capacities of the frame by 58.01%, 56.59%, 53.69% and 55.56% respectively.

For the three storey frame, a comparative analysis of the deformations given by both the proposed model and the yielded block spread plasticity model indicates that there is an improvement in accuracy of the joint rotational and moment capacities of the frame by 66.67% and 37.2% respectively at some joints.

Comparing the proposed model with the concentrated plasticity model, indicates that there is an improvement in accuracy of the joint rotational and moment capacities of the frame by 150% and 102.98% respectively at some joints. The improvement in

accuracy of floor displacements and inter-storey drift ratios is negligible. The accuracy of the lateral load capacity of the frame improves by 33.9%.

CHAPTER ONE: INTRODUCTION

1.1 BACKGROUND

Concrete is a brittle material with low tensile strength therefore making it prone to cracking during loading. Despite the advent of high-performance concrete, being a more durable material, the predisposition to cracking remains, (Montaignac, et al., 2012). RC structures crack when, moment exceeds a certain value because concrete is weak in tension thus parts under tension crack.

Implications of various levels of structural damage are particularly important in considering the response of reinforced concrete structures subjected to earthquake motions. In some cases, reinforced concrete elements must remain elastic or nearly elastic to perform their allocated safety function. Tests results indicate that nonlinearity occurs at load levels lower than initial yield. This is enough to reduce considerably the required design values. Therefore, linear elastic analysis based on "un-cracked" properties is not realistic and may be unreasonably conservative particularly for lightly reinforced concrete members. (Aristizabal-Ochoa & Dario, 1983)

According to EN 1998 (2004), Clause 4.4.1(5) P, in reinforced concrete buildings the stiffness of the load bearing elements should, in general, be evaluated considering the effect of cracking.

EN 1998 (2004), Clause 4.4.1(6) further instructs that unless a more accurate analysis of the cracked elements is performed, the flexural and shear stiffness properties of concrete elements should not exceed one-half of the corresponding stiffness of the un-

cracked elements. This is further evidence that cracking accounts for a significant reduction of stiffness in reinforced concrete structural elements and therefore there is need to consider the effect of cracking during analysis.

The stiffness degradation upon cracking can be ably illustrated by the moment curvature relationship of a concrete section whose derivation is detailed by Kyakula (2010). A positive moment curvature diagram OABC, is shown in Figure 1-1. Before cracking, the stiffness of the section is given by the slope of the line OD while the slope of the line OB gives the stiffness K_y of the yielded section. The maximum moment is defined as M_o and the slope of the line OC gives the stiffness K_o of the section at which this moment occurs.

The existing plasticity models take the stiffness of both the un-cracked and cracked sections as equal. From Figure 1-1, AB represents a reduction in stiffness of the section as the section cracks which is evidently different from the stiffness of an un-cracked section equal to the slope of the line OD. This shows that the assumption that the stiffness of both the cracked and un-cracked sections are equal overestimates the stiffness of a section after cracking and this leads to inaccuracies during analysis.

Presently there are many seismic analysis methods for structures, and many are still being developed, these include: Time history analysis (Response history analysis (RHA) and the Direct Integration Method), Static lateral force method, Modal response spectral analysis (RSA), Substitute structure method, Pushover analysis and Displacement based design (DBD).
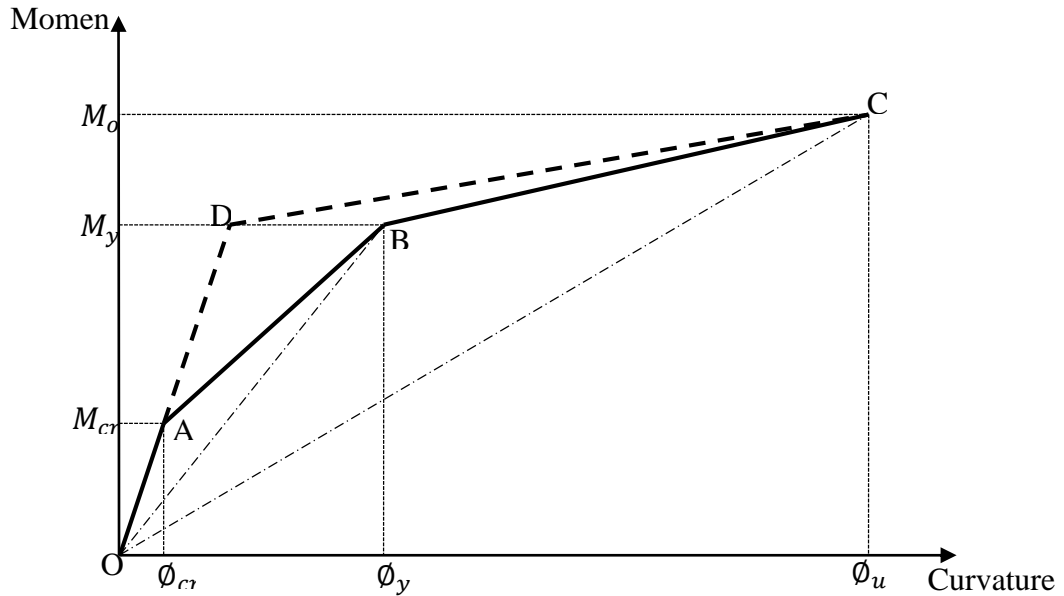
Figure 1-1: Moment Curvature relationship for a Typical RC section

(Kyakula, 2010)

Ideally, performance evaluation of structural systems subjected to earthquake loading should be based on nonlinear time history analysis. However, the intrinsic complexity and additional computational effort required does not justify its use in ordinary engineering applications. As a result of the above, nonlinear static, as opposed to dynamic, pushover analysis has been gaining significance over recent years as a tool of assessment and design verification. Despite its relative simplicity and ease of use, this numerical tool can provide information on many important response characteristics that cannot be obtained from an elastic static or dynamic analysis (Antoniou & Pinho, 2004).

The yield springs pushover analysis is based on the concentrated plasticity model, where it is assumed that the non-linear behaviour could be concentrated in springs at

the end of the beam. It has been reported that comparisons of the spread plasticity model and the concentrated plasticity model were carried out for cases of strain hardening ratios of 0.039, 0.03, and 0.016. (Filippou & Issa, 1988).

Strain hardening ratio, β = Post yield stiffness/Pre yield stiffness

And it was found that;

For β = 0.039, the concentrated plasticity model overestimated the maximum lateral displacement by 20% and the local girder rotation by 100% for the statically indeterminate structure sub assemblage.

For β = 0.03, the discrepancy in the maximum lateral displacement was about 50% and that in the girder rotation was 150%.

For β = 0.016, the discrepancy between the spread plasticity and the concentrated model was reportedly too large to be considered.

The purpose of pushover analysis is to evaluate the expected performance of a structural system by estimating its strength and deformation demands in design earthquakes by means of a static inelastic analysis, and comparing these demands to available capacities at the performance levels of interest (Krawinkler & Seneviratna, 1997).

In this research, the static pushover analysis was adopted as the preferred seismic performance evaluation tool. The expectation was that the pushover analysis would provide adequate information on seismic demands imposed by the design ground motion on the structural system and its components when cracking in beams is taken onto consideration.

1.2 PROBLEM STATEMENT

The inelastic behaviour of a beam/ structure has been modelled by hinges located at the yielded points. This has been found to be inaccurate because yielding (or Plasticity) spreads with loading and is not concentrated at a single point. This led to the spread plasticity model. In the spread plasticity model, it is assumed that the stiffness of the part of the beam that has not yielded is equal to the un-cracked stiffness of the beam which is not true because most of it has cracked, (Aktan & Nelson, 1989; Kyakula, 2010). However, when a beam cracks, its stiffness reduces. The existing models ignore the stiffness reduction due to cracking along the beam for parts of the beam that have not yielded. This does not accurately represent the behaviour of the structure. These models ignore the gradual spread of cracking in the member and therefore underestimate the flexibility of the beam and thus leading to errors in deflection, Joint rotation, and inter-storey drift ratios of structures. Accuracy could be improved further by adopting a spread cracking model to address the often neglected cracked but not yielded part of the beam.

1.3 OBJECTIVES

1.3.1 MAIN OBJECTIVE

To determine the effect of considering cracking during pushover analysis, on the accuracy of deflections, joint rotations, and inter storey drift ratios in reinforced concrete structures.

5

1.3.2 SPECIFIC OBJECTIVES

1. To determine the joint rotations, displacements and inter-storey drift from push over analysis of a structural frame using the concentrated plasticity model.

2. To determine the joint rotations, displacements and inter-storey drift from push over analysis of a structural frame using the yielded block spread plasticity model.

3. To determine the joint rotations, displacements and inter-storey drift from push over analysis of a structural frame using the spread cracking and yielding block spread plasticity model.

4. To compare the moment vs rotation curves, load vs displacement curves, and inter storey drift ratio curves obtained from the concentrated plasticity model, the yielded block spread plasticity model and the proposed spread cracking and yielding block model

1.4 RESEARCH QUESTIONS

a. What if the effect of considering cracking during pushover analysis on the Joint Rotations of a RC frame?

b. What is the effect of considering cracking during pushover analysis on the floor displacements of a RC frame?

c. What is the effect of considering cracking during pushover analysis on the inter-storey drift ratio of a RC frame?

d. What is the effect of considering cracking during pushover analysis on the moment capacity of a RC frame?

e. What is the effect of considering cracking during pushover analysis on the lateral load capacity of a RC frame?

1.5 SIGNIFICANCE

Cracking in beams leads to a reduction in stiffness and hence a reduction in strength of a beam, (Aktan & Nelson, 1989). Consider an un-cracked beam of any section, when a force/moment is exerted on the beam, the concrete in the entire section effectively contributes to the stiffness of the beam. When the load is increased to a critical level, cracks develop in the concrete at different locations (tensile region) along the beam. The concrete in the region that has cracked no longer contributes to the stiffness of the beam. Ignoring cracking during modelling therefore overestimates the stiffness and strength of a beam thus leading to inaccuracies in the determination of deflections, joint rotations and inter storey drift ratios in reinforced concrete structures. There is need to consider cracking during modelling of beams.

This research shall contribute to the body of knowledge and thus enable scholars to refer to it as they do further studies in a related field.

The results of this research shall provide insight into the effect of cracking on reinforced concrete beams and the entire structure thus enabling designers to make appropriate decisions.

1.6 JUSTIFICATION

Naturally, the reliability of analysis results would depend on uncertainties associated with the initial conditions and existing mechanical characteristics of the soil

foundation structure, the seismic effects, and the reliability associated with their perception and analytical modelling, (Aktan & Nelson, 1989)

Improving the accuracy and as such reducing uncertainties associated with cracking during the determination of beam deflections, joint rotations and inter storey drift ratios of reinforced concrete structures shall improve on the reliability of two-dimensional modelling and analysis of structures.

1.7 CONCEPTUAL FRAMEWORK

INDEPENDENT VARIABLE   **DEPENDENT VARIABLE**

MODELS

- Concentrated plasticity model
- Yielded block spread plasticity model
- Spread cracking and yielding block model

Push Over Analysis →

Comparison of:

- Load vs deflection curves
- Moment vs rotation curves
- Inter-storey drift ratios
- Moment capacities
- Lateral load capacities
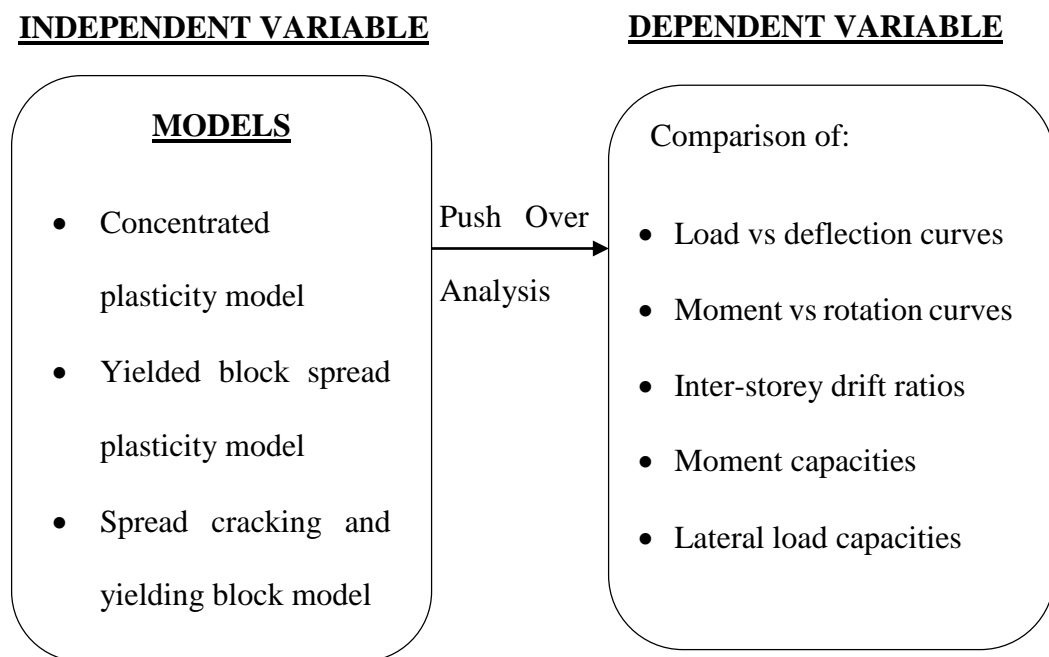
Figure 2: Conceptual Framework

1.8 CONTENT SCOPE

Regardless of whichever model was under investigation, analysis was terminated when the structural frame either formed a mechanism or on attainment of ultimate moment at any of the beam nodes whichever of the two came first. Both the existing and proposed models were subjected to push over analysis and the results of which were compared. Second order effects such as P-delta effect were not considered.

The work considered plane reinforced concrete framed structures without shear walls. It was assumed that only beams crack and/or yield, columns were assumed to remain elastic. One of the reasons for this was to enable the spread cracking and spread plasticity in the beam to be investigated without interference, because yielding of the column would change the properties of the structure. The other reason is the time frame for the research was not sufficient for the development of spread crack and plasticity models in the column.

Prokon structural analysis and design software was the preferred software package of use since it was locally available and relatively simple to use.

The work was limited to structures that are regular in plan. The aim was to avoid torsion effects, which tend to amplify structural displacements.

It was assumed that the masonry or any other in-fills and partitions were isolated from the structure such that their effect on the structural response was only in terms of increased mass and not stiffness of the structure.

This research was carried out on a computer in Kyambogo University, Kampala, Uganda for a period of one and a half years (1 ½ years).

CHAPTER TWO: LITERATURE REVIEW

Structural analysis refers to the determination of bending moment, shear force, axial forces, and Torsional moments. A more detailed analysis gives deformations such as, vertical deformations, horizontal deformations, joint rotations, and inters-storey drift ratio. In finite element modelling, stresses and strains are also determined.

Structures are usually in 3-dimension but can be analysed in 2-dimension and results aggregated to 3-dimension. When analysed in 2-dimension, they are referred to as plain structures.

2.1 THE STRUCTURAL MODEL

The model adopted is proposed by (Kyakula & Wilkinson, 2004). The model consists of column and beam elements.

Columns and beam-column joints are assumed adequately reinforced, confined and detailed so that they do not yield. The column element consists of axial force and elastic bending sub elements. The stiffness matrices of these sub elements are transformed to global co-ordinates then added to obtain the column stiffness matrix.

The beam element consists of the elastic bending, elastic axial, spread cracking and spread plasticity sub elements connected in series. The spread cracking sub element accounts for the gradual spread of cracking in the member, the shift of the point of contra-flexure, the variable location and actual length of the cracked zones. The beam element consists of inelastic regions of finite length where the plastic deformation takes place as well as cracked regions where cracking takes place. Infinitely rigid bars/

elastic sub elements and/or cracked sub elements connect the inelastic regions. The location and length of the inelastic regions, cracked regions and the rigid bars/ elastic sub elements varies depending on whether the combined moment due to gravity and lateral load has exceeded the cracking and or yield moment of the member.

When a member cracks, its stiffness reduces (its flexibility increases). The flexibility matrices of the elastic sub elements do not change, while those of the spread cracking and spread plasticity are zero before cracking and yielding respectively and increase as cracking and yielding increase. The flexibility of the beam shall be obtained by adding the flexibility matrices of elastic bending, spread cracking, and spread plasticity sub elements. Thus, the coefficients of the beam flexibility matrix increase (or coefficients of the beam stiffness matrix decreases) as cracking and yielding progress along the beam. The flexibility matrix of the beam is inverted, transformed into global coordinates, and then added to the global stiffness matrix of the axial sub element to obtain the global beam stiffness matrix.

The stiffness matrix K, of a free unsupported structure shall be obtained by assembling the column stiffness K_c, and beam elements stiffness K_b, matrices. Then the deformations, moments, shears and axial forces at joints found as in normal static analysis using uncondensed stiffness matrix adjusted for support conditions. Kyakula & Wilkinson (2004)

2.2 CONFINED CONCRETE

2.2.1 THE NOTION OF CONFINEMENT

According to Penelis & Kappos (1997), it has been recognised that strength, as well as deformability (ductility) of concrete, substantially increases whenever its state of stress is tri-axial compression. In practice a loading condition equivalent to hydrostatic compression results when transverse reinforcement in the form of closed ties (hoops) or spirals, prevent 'swelling' of an element when subjected to compression. The concrete which is affected by this favourable action of transverse reinforcement is called confined concrete.

Advantages of confinement

Confinement offers two main advantages regarding the seismic behaviour or concrete structural elements:

a) It increases strength of concrete, which compensates for possible losses caused by spalling, i.e. failure of the cover concrete in an element, which occurs whenever compressive strains in the cover exceed about0.4%

b) It reduces the slope of the descending branch of the stress-strain curve; therefore, it increases the maximum usable strain ε_{cu} to values much higher than 0.35% accepted by codes for flexure design.

2.2.2 PARAMETERS AFFECTING CONFINEMENT

According to Penelis & Kappos (1997), the main parameters involved in the problem of confinement are the following:

a) The ratio of transverse reinforcement. Typically, this is expressed as the volumetric ratio ρ_w, defined as the volume of hoops to the volume of the confined core of the member. The core is the part of the section enclosed by the centroidal axis of the hoop. Increasing ρ_w both the strength and the ductility of confined concrete increase.

The yield strength of the transverse reinforcement (f_{yw}). It is understood that the higher the strength of the stirrups, the higher the confining pressure they can exert.

b) The compressive force of concrete (f_c). Higher strength concrete is less ductile than lower strength concrete. Moreover, for the same amount of axial loading the lateral expansion (due to Poisson effect) of a concrete member is larger in the case of low strength, therefore it is anticipated that (passive) confinement will be more efficient in this case, since the hoops will be stressed more than in a high strength concrete member.

c) The spacing of hoops (s). For a given volumetric ratio of hoops (ρ_w), the efficiency of confinement increases as the spacing becomes closer, since the regions of the member which remain without confinement become smaller.

d) The hoop patterns. When multiple hoop patterns are used in a member, the regions of effectively unconfined concrete become smaller and strength and ductility increase.

e) The longitudinal reinforcement. Longitudinal bars also contribute, to a certain extent, in preventing the lateral expansion of the core, hence they increase confinement effects. The larger the diameter of the bars and the ratio ρ_w, the larger the contribution of confinement.

5

2.2.3 CONFINEMENT WITH HOOPS

Monotonic loading
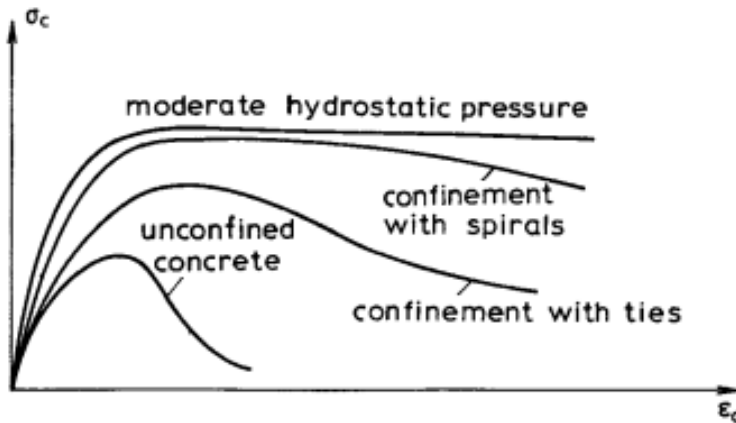
Figure 3: Stress-strain diagrams for concrete subjected to various types of confinement *(Penelis & Kappos, 1997)*

It should be noted that all curves for confined concrete are significantly different from the curve for unconfined concrete the latter corresponding to a specimen identical to the others but without reinforcement. The difference between confined and unconfined concrete is quite remarkable, as both strength and ductility are substantially larger in the case of confined specimens. The stress-strain curves are terminated at the point corresponding to the first hoop fracture detected. This point may be used for defining the limiting (or ultimate) strain of concrete (ε_{cu}), alternative definitions of (ε_{cu}) are based on specified drops in strength along the descending branch of the stress-strain curve and a buckling of longitudinal bars for columns. Recorded experimental values of (ε_{cu}) ranged from about 2.5 to 4.0%, which means that they are up to an order magnitude higher than the values 0.35 to 0.40% for unconfined concrete. This clearly shows the paramount importance of confinement regarding the earth-resistant properties of R/C members.

Experiments/ observations by Penelis & Kappos, (1997) have also shown that strength and ductility are affected by some basic parameters of confinement in R/C members such as:

a) Increase in the volumetric ratio (ρ_w) of hoops leads to an increase in strength and ductility.

b) Decrease of hoop spacing (s) results in an increment of strength and ductility

c) Changing the hoop patterns also affects the strength and ductility with the single hoop having an inferior performance to other multiple hoop patterns (Jack, et al., 1985).

d) Finally, regarding the influence of longitudinal bars on confinement, Sheikh & Uzumeri (1980) found that, at least in the case that adequate hoop reinforcement was present, the influence of these bars on the performance of the column was almost negligible.

Analytical Modelling

With regard to monotonic stress-strain relationships, it appears that the most commonly used models are those suggested by Park, Priestley and Gill (1982) and Sheikh and Uzumeri (1982), possibly because they were based on adequate in number, as well as reliable, experimental data Penelis & Kappos (1997). Both models use a parabolic form of ascending branch, the difference with unconfined concrete being that both the peak stress f_{cc} and the corresponding strain ε_{ccl} are increased by introducing the confinement index K. According to Park, Priestley and Gill (1982) the increased strength of confined concrete is

$f_{cc}=Kf_c$, where according to Kyakula (2010):

$$K=1+\partial \left(\rho_w \frac{f_{yw}}{f_c} \right)^b$$ (2.1)

∂ and b are empirical coefficients, that account for hoop patterns and spacing and are given by:

∂=0.55, b=0.75 for a single hoop pattern

∂=1.00, b=1.00 for double hoop pattern for example diamond shaped internal loop in an outer rectangular hoop or two orthognal cross ties acrosss an outer rectangular hoop

∂=1.00, b=1.00 for multiple hoop patterns

Regarding the strain (ε_{ccl}) corresponding to peak stress, Penelis & Kappos (1997) suggest a value $\varepsilon_{ccl} = K^2 \varepsilon_{cl}$, where $\varepsilon_{cl} = 0.2\%$ is the corresponding value for unconfined concrete.

According to Kyakula (2010),

$$\varepsilon_{cl} = \frac{2f_c}{E_{co}}$$

E_{co} is the slope of the tangent to the stress-strain curve at the origin and is given by:

$$E_{co} = 2.15x10^4 \left(\frac{f_c}{10} \right)^{\frac{1}{3}}$$
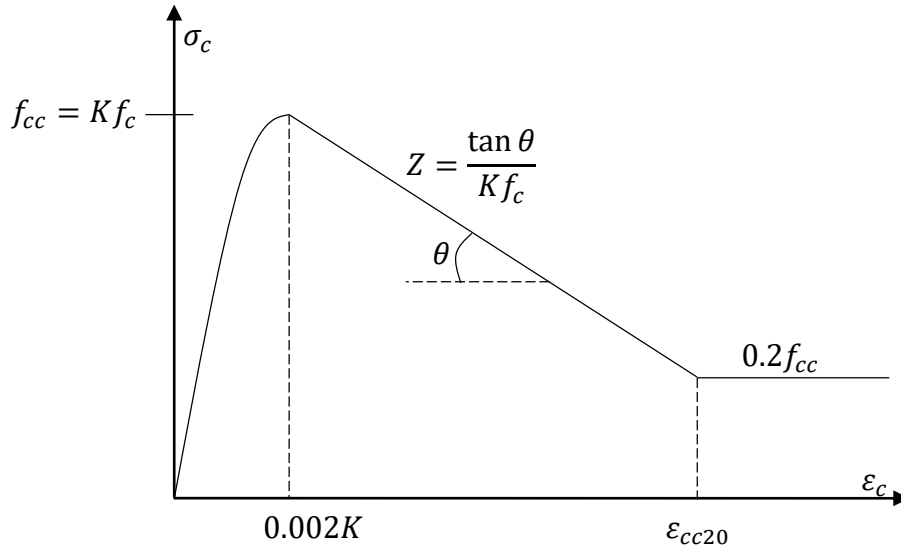
Figure 2-2: Stress-strain model for confined concrete subjected to uniaxial compression by Park, Priestley and Gill (1982)

Regarding the slope of the descending branch, Park, Priestley and Gill (1982) propose the following generalization of equations (2.2) and (2.4):

$$Z = \frac{0.5}{\varepsilon_{cc50} - \varepsilon_{ccl}} \qquad (2.2)$$

Where

$$\varepsilon_{cc50} = \frac{3 + 0.29 f_c}{145 f_c - 1000} + 0.75 \rho_w \left(\frac{b_c}{s}\right)^{1/2} \qquad (2.3)$$

For a rectangular section, the volumetric ratio ρ_w according to (Watson, et al., 1994), is given by

$$\rho_w = 0.5 (\rho_{sx} + \rho_{sy}) \qquad (2.4)$$

$$\rho_{sx} = \frac{5.41 A_b}{h_c s} \qquad (2.5)$$

9

$$\rho_{sy} = \frac{3.41A_b}{b_c S} \tag{2.6}$$

Cyclic loading

Cyclic tests on confined concrete specimens are less common than monotonic tests and possibly because of the limited data available it has been assumed that the hysteretic behaviour of confined concrete is the same as that of unconfined concrete. Tests by Mander, Priestley and Park (1988) with various amounts of transverse reinforcement, have shed some more light on the behaviour of confined concrete in cyclic compression. These tests confirmed that the monotonic curve is indeed the envelope of the cyclic loading curves and also that the shape of the unloading and reloading curves is similar to that observed for unconfined concrete (Penelis & Kappos, 1997).

Strength of concrete under the action of dynamic loading (Kyakula, 2010)

Concrete strength is higher in case of strain rates higher than the static ones.

The static strain rate $\bar{\varepsilon}_{cs}$ is given as CEB Code (1993)

$$\bar{\varepsilon}_{cs} = 3x10^{-5}S^{-1}$$

Typical strain rates $\bar{\varepsilon}_{cn}$, induced in structural members by earthquakes with normal frequency content range between $0.01 - 0.02s^{-1}$.

The maximum dynamic stress of confined concrete is given by:

$$f_{ccd} = f_{cc}\left(\frac{\bar{\varepsilon}_{cd}}{\bar{\varepsilon}_{cs}}\right)^{1.026a_s} \tag{2.7}$$

Where coefficient a_s is given by:

$$a_s = \left(\frac{1}{5 + 0.9f_{cc}} \right) \tag{2.8}$$

f_{cc} - the static strength of confined concrete

$\bar{\varepsilon}_{cd}$ - the dynamic strain rate

ε_{cld} - the dynamic strain corresponding to the maximum stress in the member. The dynamic strain is given by:

$$\varepsilon_{cld} = \varepsilon_{cl} \left(\frac{\bar{\varepsilon}_{cd}}{\bar{\varepsilon}_{cs}} \right)^{0.02} \tag{2.9}$$

2.2.4 OVERVIEW OF SEISMIC ANALYSIS METHODS

This section briefly discusses methods of seismic analysis that are currently in use for performance evaluation of structural systems subjected to earthquake loading.

(i)   Time History Analysis

In history analysis, the model of the structure is subjected to a base acceleration and the change in response of the model with time is determined. The total response is calculated at the end of a very small-time step. The analysis proceeds step by step, using the results of one step as the initial conditions of the next one. There are two basic methods of time history analysis, they are the response history analysis (RHA) and time history analysis by direct integration.

Response History Analysis

The response history analysis is carried out by superposition of normal modes. It is applicable to linear systems and uses the secant stiffness for each time step. Its major advantage is that it provides exact response of the idealised buildings because it avoids

11

the error in modal response spectral analysis which arise from combining modal maximum, without knowing the time variation of the modal responses. It also requires less computing time than time history analysis by direct integration because the determination of the normal modes and natural period is done only once. However, the response history analysis has limitations which include the requirement that at least three-earthquake ground motion records are considered. It also requires greater computational effort than modal response spectral analysis and is limited to linear systems. Only special structures are designed to remain elastic during the ultimate design earthquake. Structures of normal importance are designed to deform into the inelastic range without collapse (Kyakula, 2010).

Time history analysis by direct integration

Time history analysis by direct integration involves direct numerical integration of the equations of motion used in the analysis. Its major advantage is that its applicable to both linear and non-linear systems and gives accurate results compared to other methods. Its time step is considerably shorter than for response history analysis because it uses tangent stiffness. this method suffers from the limitation that it requires more time for computation and analysis of output data. Furthermore, there are uncertainties regarding the accuracy of the damping and stiffness matrices introduced into the model and their variation during loading.

Before the analysis, it is necessary to know, the geometry of the system (length of members, dimensions of cross sections, details of connections) and the strength of structural members (yield moments). The masses of the frame (assumed lamped at floor level or at joints), viscous damping ratio, and digitised ground accelerations at

the base of the structure are also required. Thus the structure is first analysed and designed by any simpler method of seismic design to determine the above parameters (Kyakula, 2010).

(ii)   Static lateral force method

The static lateral force method was developed to simplify both dynamic and inelastic considerations. The method relies on the fact that the maximum response of a dynamic system is dependent on the natural period, degree of damping utilisation of inelastic deformations to absorb large levels of energy leading to a reduction of design forces. After yielding, the member forces remain below the level they would have reached had the structure remained elastic. For structures with an initial period greater than or equal to the period for maximum spectral acceleration and also greater than the predominant period of the earthquake, lengthening of the structural period caused by yielding of the members helps to reduce the response. This method uses response modification factors to reduce the design forces such that during minor earthquakes, no damage is suffered, but during a major earthquake, structures may deform into the inelastic range without collapse. The static lateral force method computes the peak earthquake load as a function of; the geological location (zone factor), foundation soil (soil factor), intended use of the structure (importance factor), the weight of the structure, the fundamental period T_1 of the structure, the ductility expected (response modification factor) (Kyakula, 2010)

(iii)   Modal response spectral analysis

Modal response spectral analysis is also referred to as modal analysis. It is a dynamic analysis, where the peak values of the modal responses are determined from the

response spectrum and the pick response of the system is estimated by combining modal peaks by the complete quadratic combination (CQC) or the square root of sum of squares (SRSS) rule.

Since the mode shapes and periods of the structure are computed as part of the analysis, modal response spectral analysis gives a good understanding of the dynamic response of the structure. It also gives more accurate values than the static lateral load method and considerably reduces the computational time compared to the response history analysis, (RHA). Moreover, unlike the response history analysis, the response spectral analysis, uses a smoothed envelope spectrum, which makes the analysis independent of the characteristics of an earthquake.

The modal response spectral analysis has several draw backs as discussed below:

- The modal response spectral analysis (RSA) gives less accurate values when compared to the response history analysis, (RHA)

- The results of modal response spectral analysis, (RSA) are given in terms of peak responses only, and these do not occur as the same time.

- The response spectral analysis is linear and can only make approximations for non-linear behaviour.

Modal response spectral analysis is carried out by first determining the mass and stiffness matrix and estimating the modal damping ratios. The design spectrum is then constructed, and the natural frequencies and modes determined. For each mode, the effective modal masses and from these the maximum inertia forces for that mode are determined. Then applying the maximum inertia forces for each mode to the structure, the maximum values of the response parameters (moments, shears, displacements,

etc.) are determined through static analysis. For each response parameter, the response of the structure due to the effect of all the modes is determined by combining the responses by the square root of sum of squares, (SRSS) or complete quadratic combination, (CQC) rule for modal combination (Kyakula, 2010).

(iv) The substitute structure method

The substitute structure method is a spectral modal analysis procedure with the modification that the stiffness of members that are expected to crack or deform into the inelastic range is reduced. It is used to determine the design forces for reinforced concrete structures. To account for cracking, the actual structure is substituted for a structure, in which the stiffness of members expected to crack has been reduced. The reduction in the stiffness is related to the level of cracking expected. The damping ratio is also computed to fit in with the expected level of cracking.

The substitute-structure method is used to establish the minimum strength the components of the structure must have so that a tolerable response displacement is not exceeded, calculate the damping ratio for members that have yielded, and to check the displacements. It has the advantage of offering a simple method for calculating the damping ratio of structures deformed into the inelastic range. Also, the deformation limits (cracking level) expected is set for the different elements of the structure. The biggest drawback for the substitute structure method is that there is no basis for the level of stiffness reductions assigned to the structural members. (Kyakula, 2010)

(v) Pushover analysis

The pushover analysis is a method used to evaluate the expected performance of a structural system by estimating its strength and deformation demands in a design

15

earthquake. Gravity loads are applied to the structure followed by lateral loads in predetermined or adaptive patterns that approximately represent the relative inertia forces at floor levels. The structure is pushed under these load patterns to the largest displacements associated with the performance levels. The internal forces and deformations computed are used as estimates of strength and deformation demands, which need to be compared to available capacities.

It is used to derive base shear versus roof displacement relationship. Which relationship is used to calculate the ductility factor (R_u or μ), and over strength factor R_s which are part of the response modification factor R. It is also used to check the ductility demand.

The pushover analysis has the draw back that the present array of load patterns used in pushover analysis cannot capture the variant load demands expected in a design earthquake. In its present form it is only suitable for low-rise structures that vibrate primarily in the fundamental mode and in which higher mode effects are not very important. (Kyakula, 2010)

(vi)   Displacement based design (DBD)

It has been proposed that instead of starting by estimating the applied forces, then computing the internal forces and finally checking for the displacements, as is done in the static lateral force method, the analysis starts by estimating the target displacements (i.e. damage). Having obtained the target displacements, the forces that cause those displacements are determined. These forces are applied to the structure and internal forces calculated. Members are then detailed to be able to resist these

forces and to be ductile enough to achieve target rotations. Thus, the method uses displacements as the basis of design.

The advantage of displacement-based design is that one can consider explicitly the displacement demand (damage) in each member rather than assigning a single global response modification factor to the structure. The required force to be resisted becomes largely a function of damping, and thus it is directly related to the energy dissipation, hysteretic characteristics, and acceptable damage on local level.

However, the method suffers from the following limitations

- It has difficulty in handling structures with several prominent modes of response. This is because it assumes that the response of the multi degree of freedom structure can be related to the response of an equivalent single degree of freedom system by a shape function. This implies that a single displaced shape function controls the response of the structure and that this shape function remains constant throughout the time of response to the earthquake loading.

- Presently, the damping ratio used is computed by the substitute structure method, thus the limitations of the substitute structure method also affect the displacement-based method.

- Appropriate target displacement for a given structure are difficult to determine, yet the equivalent stiffness of a single degree of freedom system depends on the value of the target displacement chosen. (Kyakula, 2010)

CHAPTER THREE: METHODOLOGY

3.1 RESEARCH DESIGN

This research is computer based and is analytical in nature. It investigates the effect of introducing a model which considers cracking during pushover analysis of RC frames. The proposed model is compared to the two existing models of pushover analysis by assessing five parameters namely:

   a. Joint rotations

   b. Floor displacements

   c. Inter-storey drift ratios

   d. Moment capacities and,

   e. Lateral load capacities

To compare deformations obtained by the proposed model to those obtained by the existing models, two cases were considered. Case 1 involved the analysis of a single bay single storey frame while case 2 involved the analysis of a single bay three-storey frame. Both frames were fixed at the bottom and subjected to a gravity load made up of permanent and variable loads.

3.2 CASE 1: SINGLE STOREY – SINGLE BAY FRAME

3.2.1 INTRODUCTION

Case 1 aimed to use pushover analysis to investigate the performance and behaviour of reinforced concrete framed structures from the initiation of loading up to failure.

One of the limitations of pushover analysis is the determination of the best load pattern that can capture the variant loads due to earthquake at floor level. A single storey structural frame eliminates this problem. Three models were applied to the frame. These are:

- The proposed spread cracking and yielding block model (proposed model)

- The yielded block spread plasticity model (existing model)

- The concentrated plasticity model (existing model)

3.2.2 THE STRUCTURAL FRAME

The frame consists of 500mm square columns that are 3500mm high and fixed at the base. The beam has a depth of 500mm, a length of 7000mm, a web width of 300mm, an effective flange width and depth of 2480mm and 200mm, respectively. The joints were numbered as shown in Figure 3-1. It was assumed that the beam-column and the column-base joints were stiff. That is, they were sufficiently reinforced, tied, and detailed that they did not fail or deform locally.
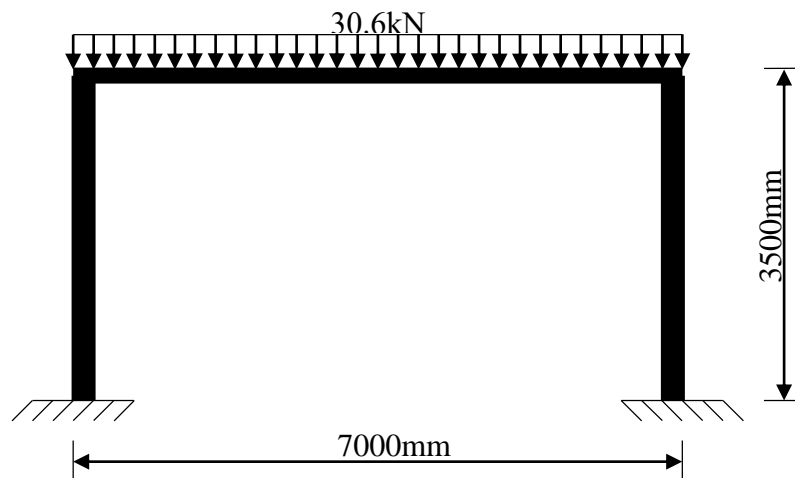
Figure 3-1 Sketch of the Proposed Single Bay Single Storey Frame

3.3 CASE 2: SINGLE BAY - THREE STOREY FRAME

3.3.1 INTRODUCTION

The frame in case 2 is a single bay-three storey structure. It was used to investigate the effect of considering the proposed model on the inter-storey drift ratios, joint rotations, and joint displacements in comparison with the existing models.

3.3.2 THE STRUCTURAL FRAME

The frame consists of 500mm square columns that are 3500mm high and fixed at the base. The beams has a depth of 500mm, a length of 7000mm, a web width of 300mm, an effective flange width and depth of 2480mm and 200mm, respectively. The joints were numbered as shown in Figure 3-2 below. It was assumed that the beam-column and the column-base joints were stiff. That is, they were sufficiently reinforced, tied, and detailed that they did not fail or deform locally.

Figure 3-2: Three Storey Single Bay frame sketch

3.4 PUSHOVER ANALYSIS

The analysis was separately carried out on both structural frames discussed above using the following models.

i.   The concentrated/ traditional plasticity model (hinges placed at yielded sections),

ii. The yielded block spread plasticity model (yielded blocks placed at yielded sections),

iii. The spread cracking and yielding block model (cracked blocks placed at cracked sections and yielded blocks placed at yielded sections)

In the traditional/ concentrated plasticity model of pushover analysis, whenever the moment at a point reaches yield, a hinge is placed at that point. This model assumes that its moment rotation relationship after yielding is flat as represented in Figure 3-3. However, the moment-rotation curve at a joint and moment-curvature curve for a concrete section continues to increase after yielding, albeit with much reduced slope, (Kyakula, 2010).

In the 'yielded blocks' method of pushover analysis, whenever the moment at a node reaches the yield moment of the section, the block of the beam between the yielded node and the adjacent node is replaced by "yielded block". The area and moment of inertia about the Y and Z axes of the yielded block are equal to that of the yielded cross section of the beam.
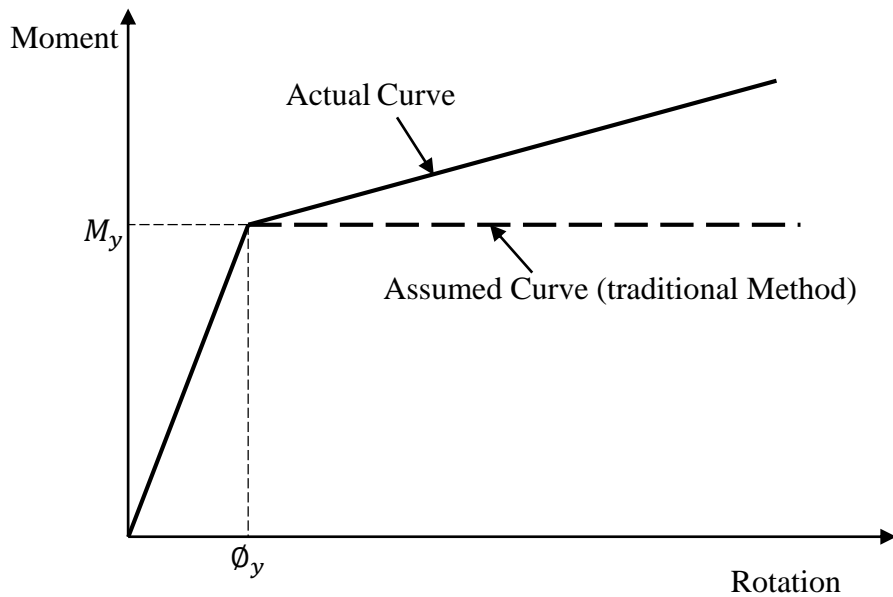
Figure 3-3: Moment-rotation curve for a reinforced concrete section

According to (Kyakula, 2010), a beam element in the yielded block spread plasticity model is made up of five sub-elements namely:

1. Elastic bending sub-element of infinite stiffness to account for linear elasticity in the beam

2. Spread plastic sub-element to account for the gradual spread of plastic deformation in the beam

3. The shear sub-element

4. The interface bond-slip sub-element

5. Elastic axial force sub-element

For the purposes of this study, we shall only consider the first two sub-elements, i.e. elastic and spread plastic sub-elements.

In this research, the effect of introducing "cracked blocks" is investigated in addition to the "yielded blocks" during the analysis of reinforced concrete structures with an aim of improving the accuracy of the load-displacement, moment-rotation, curves as well as inter-storey drift ratios.

The beam of the 'proposed spread cracking and yielding block model' shall in addition to the blocks considered in the 'yielded block spread plasticity model' include a cracked block sub-element to account for the gradual spread of cracking in the beam.

Effects of shear and interface bond slip like in the yielded block spread plasticity model are not considered in the scope of this study.
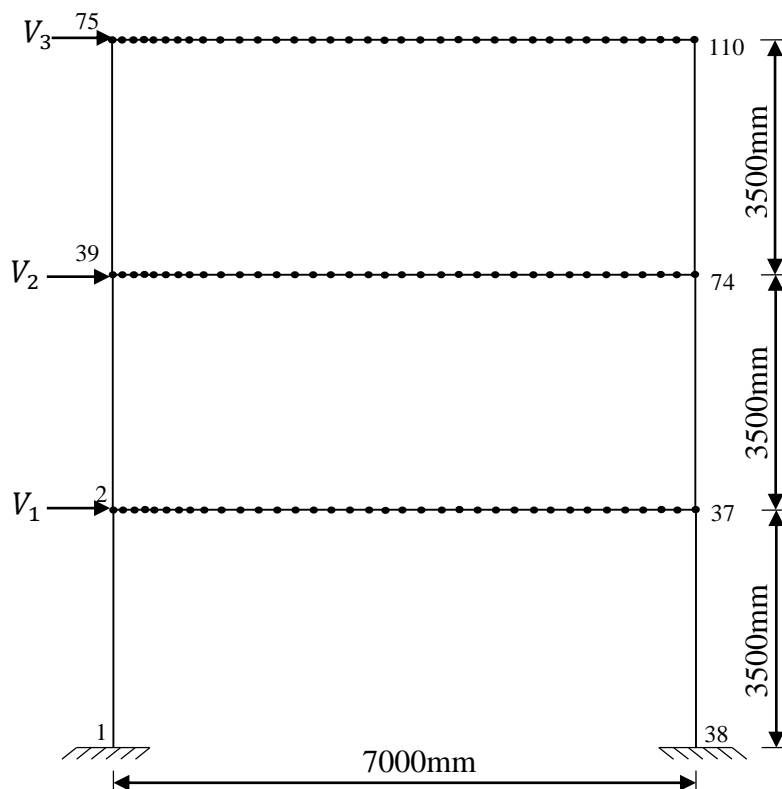
Figure 3-4: 2D modal showing the distribution of nodes in the beams of a three storey-single bay frame
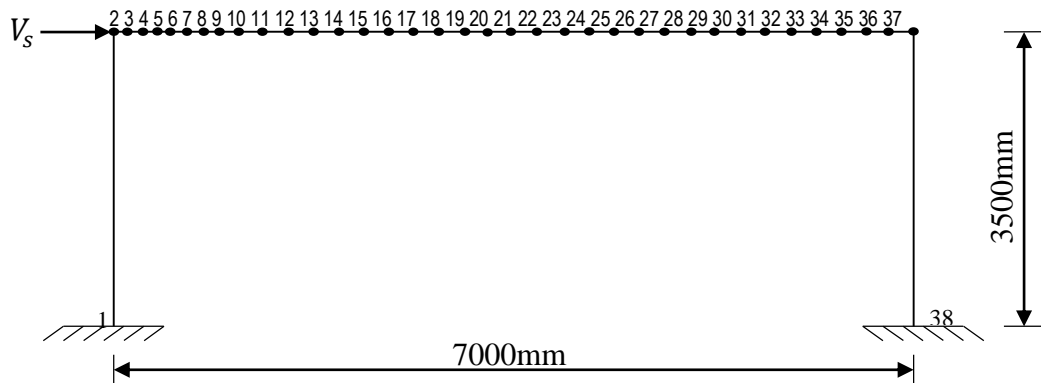
Figure 3-5: 2D model showing the distribution of nodes in the beam of a single storey-single bay frame

The procedures for carrying out push over analysis for both existing models and the proposed model. Steps 1-6 are typical for all three models.

1. The frame is represented as a two-dimensional analytical model with the use of structural modelling software (Prokon Structural Modelling Software). A sketch of the model is shown in Figure 3-4 for the three storey single bay frame and Figure 3-5 for the single storey single bay frame.

2. The beam is sub-divided into 35 elastic sub-elements each having a length of 200mm. This makes a total of 36 nodes on each beam with 2 extra nodes for the column supports. All sub-elements have rigid connections to simulate the nature of concrete. Uniform reinforcement is used throughout the length of the beam and column. The column reinforcement and section are chosen such that the column reinforcement does not reach yield moment. Kyakula & Wilkinson (2004)

24

3. The ultimate, yield and cracking moments of the critical regions of the beam are computed.

4. The structural frame is then subjected to gravity loads.

5. For the three-storey single bay frame, modal analysis is carried out to determine the modal shape for the frame and the fundamental mode is subsequently chosen to approximate the distribution of lateral loads along the height of the frame.

6. Lateral loads V_1, V_2, and V_3 are applied to floor levels 1, 2, and 3 respectively for the three storey structural frame in predetermined load patterns that follow the fundamental mode shape and represent the distribution of inertia forces or expected deflected shape of the frame as shown in Figure 3-4 whereas the single storey single bay frame is subjected to a single lateral load V_s at the floor level as shown in Figures 3-5.

7. Starting with small values, the lateral load V_s on the single storey frame and Lateral loads V_1, V_2, and V_3 for the three storey frame are increased until the yield moment for the existing models and the cracking moment for the proposed model is reached at any of the selected nodes. The moments at all selected nodes, rotations at member ends and horizontal displacements at floor level are recorded in an excel workbook for further management.

3.4.1 CONCENTRATED PLASTICITY MODEL

8. A hinge is then placed at the point where the yield moment has been reached. The modified structure is then pushed under a new set of increased lateral loads

but this time without the gravity loads. The moments at all the selected nodes are monitored at each load increment. If at any point and for any load increment the sum of the moments that have been recorded at 1st yield and those due to the load increment are found equal to the yield moment, the second hinge is formed. Again, the sum of moments for all the nodes, rotations at member ends and horizontal displacements at floor level due to the load increment and those from (7) are recorded.

9. The process of incremental lateral loading and placement of hinges at the yielded nodes is continued up until failure occurs in the frame.

3.4.2 YIELDED BLOCK SPREAD PLASTICITY MODEL

8. A yielded block is then placed between the node where the yield moment has been reached and the adjust node having the next highest moment. The modified structure is then pushed under a new set of increased lateral loads but this time without the gravity loads. The moments at all the selected nodes are monitored at each load increment. If at any point and for any load increment the sums of moment that have been recorded at 1st yield and those due to the load increment are found equal to the yield moment, the second yielded block is formed. Again, the sum of moments for all the nodes, rotations at member ends and horizontal displacements at floor level due to the load increment and those from (7) are recorded.

9. A new set of lateral loads (no gravity loads), are then applied to the modified structure (with yielded block sub-elements). The process is repeated up until any of the selected nodes reaches ultimate moment.

3.4.3 PROPOSED SPREAD CRACKING AND YIELDING BLOCK MODEL

8. The elastic sub-element between the node whose moment has equalled the cracking moment and the adjacent node with the next highest moment is then replaced with a cracked sub-element of reduced stiffness. All the gravity loads are then removed from the frame retaining only the lateral loads.

9. The modified structure is then pushed under a new set of increased lateral loads but this time without the gravity loads. The moments at all the selected nodes are monitored at each load increment. If at any node and for any load increment the sums of moments recorded in (7) and those due to the load increment are equal to the crack moment or the yield moment, a cracked sub element or a yielded block sub element is formed respectively. Again, the sums of moments for all the nodes, rotations at member ends and horizontal displacements at the floor levels due to the load increment and from (7) are recorded.

10. The moments, rotations and displacements are cumulative. The previous cumulative moment is added to the current incremental moment to obtain the current crack/yield/ultimate moment. The same applies to rotations and displacements as well.

11. The loading is further increased in small increments (no gravity loads) until the cumulative crack or yield moment is equalled at any of the elastic sub-elements or cracked sub-elements, respectively. It is assumed that any section of the beam cracks before it yields. This means that there is a transition from an elastic sub-element to a cracked sub-element and finally to a yielded block sub-element for yielding to take place.

12. A new set of lateral loads (no gravity loads), are again applied to the modified
structure (with yielded blocks and/or cracked sub-elements). The process is
repeated as other nodes reach cracking and yield moment up until any of the
selected nodes reaches ultimate moment.

S/n	Parameters and Mechanical properties	Value
1	Column size	*500 x 500 x 3500mm*
2	Beam size	*300 x 500 x 7000mm*
3	Effective flange width	*2480mm*
4	Slab thickness	*200mm*
5	Unit weight of concrete	*25kN/m³*
6	Assumed live loading	*1.5kN/m²*
7	Load combination	*1.35g_k+1.5q_k*
8	Class of concrete f_{ck}	*25kN/m²*
9	Concrete cover	*25mm*
10	Longitudinal reinforcement	*Ø16mm*
11	Stirrups	*Ø8mm*
12	Yield strength of longitudinal bars f_{yk}	*460N/mm²*
13	Yield strength of stirrups	*460N/mm²*

Table 1: Summary of model parameters and properties

Cases	To be analyzed	Output
1	Single storey, single bay R.C frame	Joint rotations, lateral displacements, base shear, and moments
2	Three storey, single bay R.C frame	Joint rotations, lateral displacements, inter-storey drift, base shear, and moments

Table 2: Summary of Analysis Cases

CHAPTER FOUR: RESULTS AND DISCUSSION

In this section, the efficacy of the proposed model is indirectly evaluated by comparing the Base shear - Displacement and Moment – Rotation curves for the proposed spread cracking and yielding block model with the corresponding curves for the concentrated and yielded block spread plasticity models.

In section 4.2, the various modified sections that have been summarised in table 1 are ably illustrated. These include the elastic, cracked and yielded block sub-elements.

4.1 SECTION MOMENTS, CURVATURES AND RESPECTIVE NEUTRAL AXIS DEPTHS

Table 3: Crack, Yield and Ultimate moments for the proposed beam

		Moment(Nmm)	Curvature	Depth of neutral axis
Cracking	*Sagging*	51,483,065	4.6×10^{-8}	139.32mm
	Hogging	138,804,095	5.61×10^{-7}	360.68mm
Yield	*Sagging*	119,156,955.89	5.67755×10^{-6}	36.8957mm
	Hogging	152,200,307.79	7.07229×10^{-6}	116.7869mm
Ultimate	*Sagging*	179,560,984.17	9.58848×10^{-6}	35.2619mm
	Hogging	261,829,126.8	1.19294×10^{-5}	115.0770mm

4.2 ELASTIC, CRACKED AND YIELDED BLOCK SUB-ELEMENTS
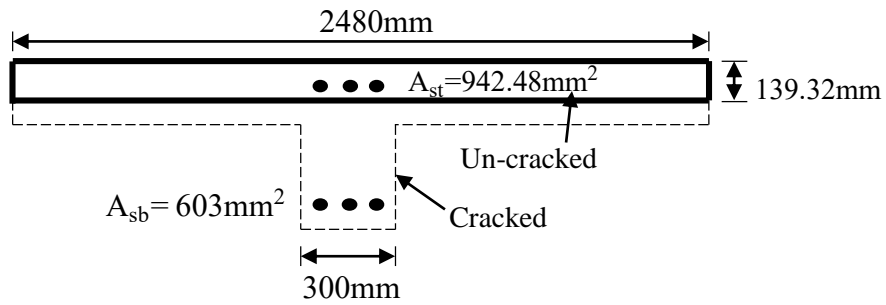
Figure 4-1: Cracked Block under sagging moment
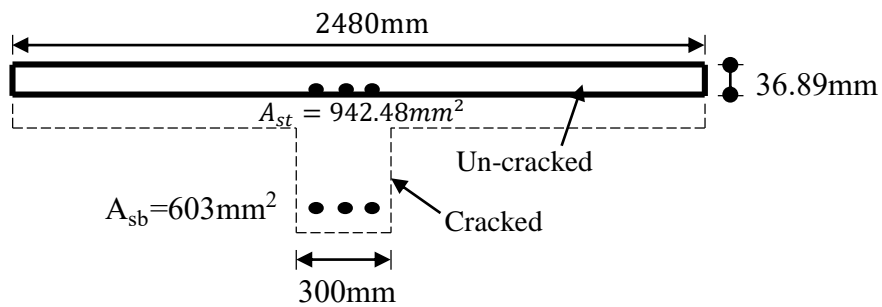
Figure 4-2: Yielded Block under sagging moment
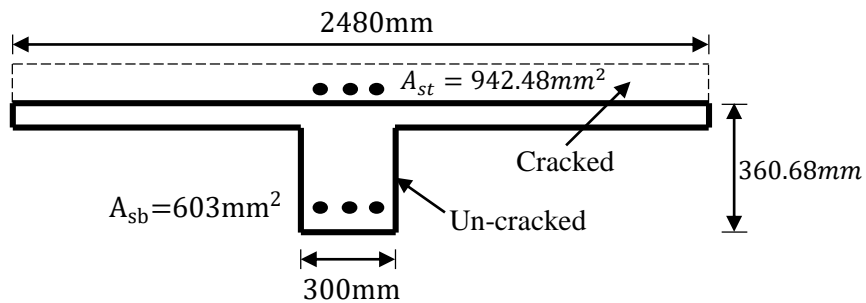
Figure 4-3: Cracked Section under hogging moment
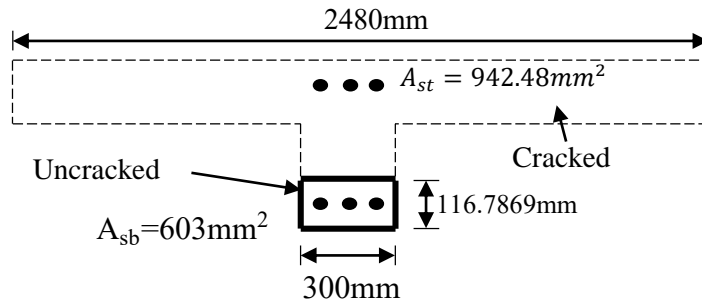
Figure 4-4: Yielded Section under hogging moment
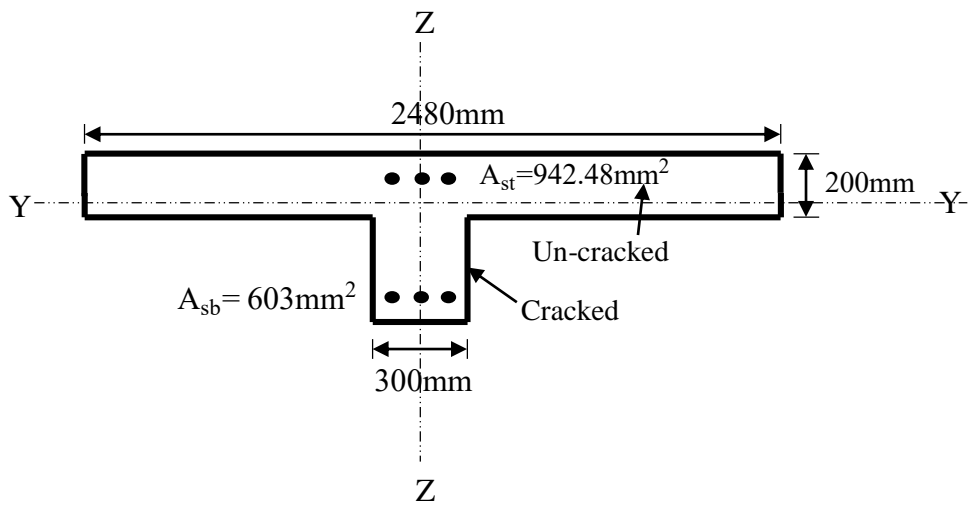
Figure 4-5: Elastic Sub-Element

31

4.3 PUSH-OVER ANALYSIS OF THE SINGLE STOREY FRAME

4.3.1 LOAD – DISPLACEMENT CURVE FOR JOINTS 2 AND 37
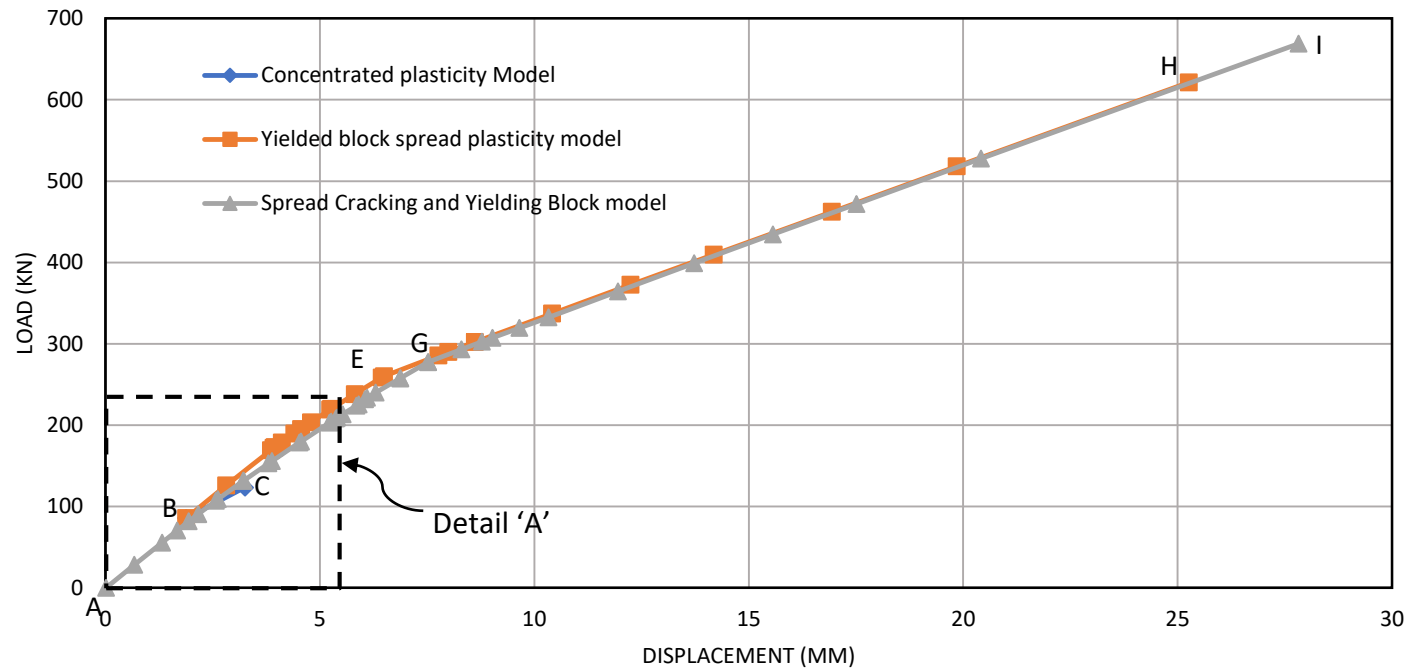
Figure 4-6: Load - Displacement Curves at Joints 2 and 37 for moments up to the attainment of the 2nd Ultimate moment along the mid-span at node 10
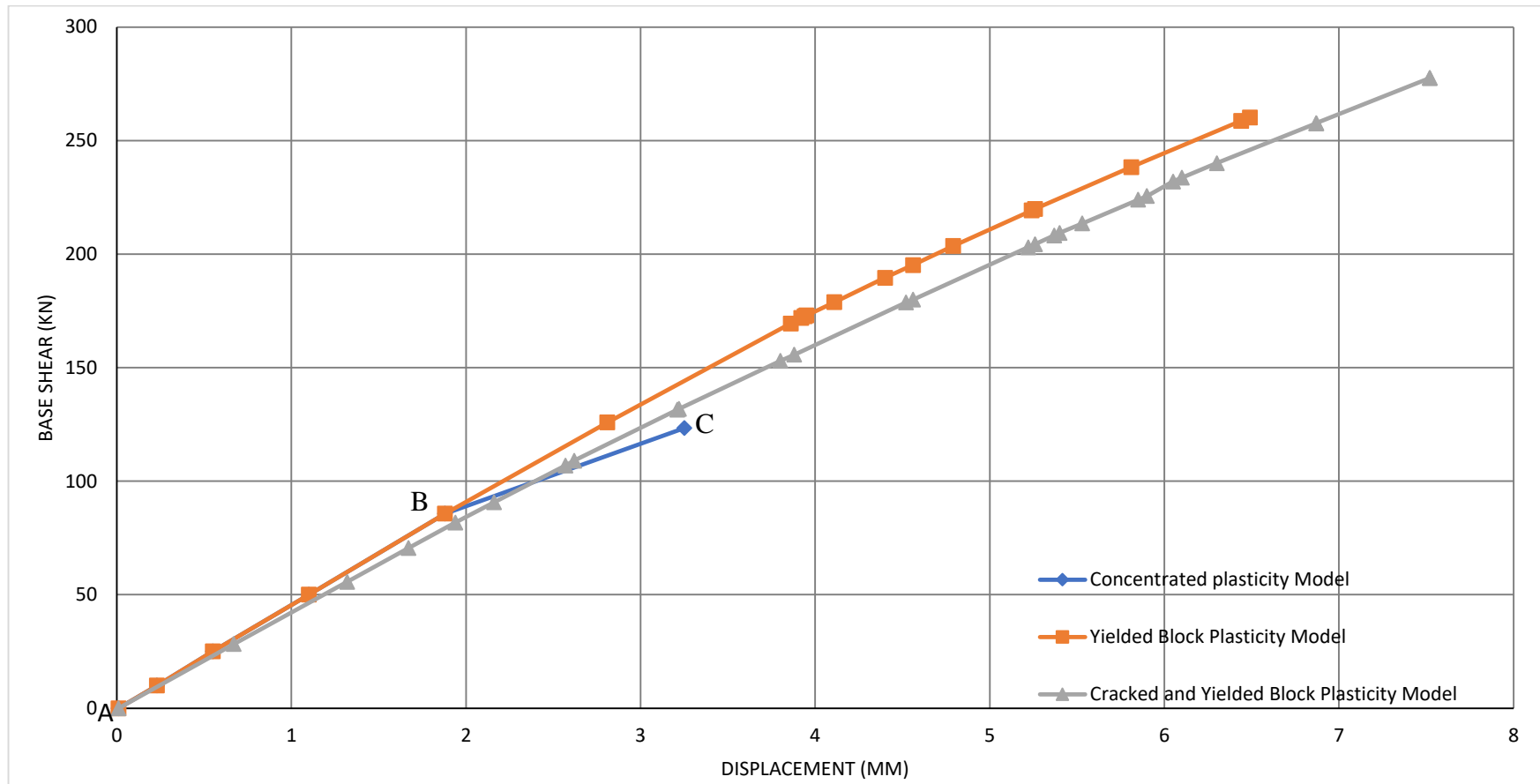
Figure 4-7: Detail 'A' for moments up to the attainment of the 1st Ultimate moment at Joints 2 and 37 for all three models

In figures 4-6 and 4-7, all models coincide at point A when the frame is subjected to only gravity loads. Between points A and B, the curves for both existing models coincide since both neglect cracking and AB is considered to be the elastic zone since it obeys Hooke's.

The curves for the existing models finally separate from each other at point B upon the initiation of yielding. The curve for the proposed model diverges from the curves of the existing models right from point A after cracking and continues to give larger deflections δ, than the existing models as can be seen in Table 2. At point B, both existing models attain 1st yield at *joint 37,* thereby underestimating the floor displacement(δ) by 7.76%. The proposed model is however observed to have an additional load-bearing and displacement capacity of 5.46% and 12.96% respectively before attaining 1st yield as compared to the existing models.

At point C, the concentrated plasticity model attains 2nd yield along the span, effectively creating a mechanism in the frame at a base shear value of 123.35kN. For the same base shear, the model overestimates the floor displacement(δ) by 8.44%, while the yielded block spread plasticity model underestimates the floor displacement(δ) by 8.14%. Further analysis of the frame using the concentrated plasticity model is not possible beyond this point. At the first ultimate moment at points E and F, the concentrated plasticity model and the yielded block spread plasticity model underestimate the floor displacement(δ) by 56.78% and 13.7% respectively.

Upon reaching the 1st ultimate moment at Joint 37, the yielded block spread plasticity and the concentrated plasticity models underestimate the base shear by 6.26% and

55.6% respectively. This shows that the concepts of spread cracking and spread plasticity greatly improve the accuracy of estimating deformations during analysis.

The yielded block spread plasticity model, branching off at point E to meet the curve for the proposed model at point F. These two models coincide up to point H where the frame under the yielded block spread plasticity model attains 2nd yield at mid-span. The curve for the proposed model continues up to point G where it attains the 2nd ultimate moment as well at mid-span. The yielded block spread plasticity model underestimates the final base shear and displacement capacity of the frame by 7.11% and 9.2% respectively. The concentrated plasticity model likewise underestimates the final base shear and displacement capacity of the frame by 81.56% and 88.5% respectively. The proposed model and the yielded block spread plasticity model generally agree beyond the point of 1st ultimate moment.

The proposed model exhibits larger final displacements(δ) than both the yielded block spread plasticity model and the concentrated plasticity model, an indication that ignoring cracking during push-over analysis underestimates deformations in building structures. The displacement behaviour at *joint 37* and *joint 2* are similar irrespective of the model applied during analysis.

Table 4: Comparative analysis of displacements and their respective margins of error for selected loads

	Concentrated Plasticity Model		Yielded Block Spread Plasticity Model		Spread cracked and yielded block Model	
Base Shear	*Displacement, δ* (mm)	*% Error*	*Displacement, δ* (mm)	*% Error*	*Displacement, δ* (mm)	*% Error*
0 kN	0	0	0	0	0	−
40 kN	0.88	7.27	0.88	7.27	0.95	−
80 kN	1.76	7.53	1.76	7.53	1.90	−
123.35 kN	3.25	8.44	2.75	8.14	3.00	−
260.17 kN	Failed	N/A	6.49	6.67	6.95	−
621.37 kN	Failed	N/A	25.26	0%	25.26	−
668.92 kN	Failed	N/A	*Failed*	N/A	27.82	−

4.3.2 MOMENT – ROTATION CURVE FOR JOINT 2
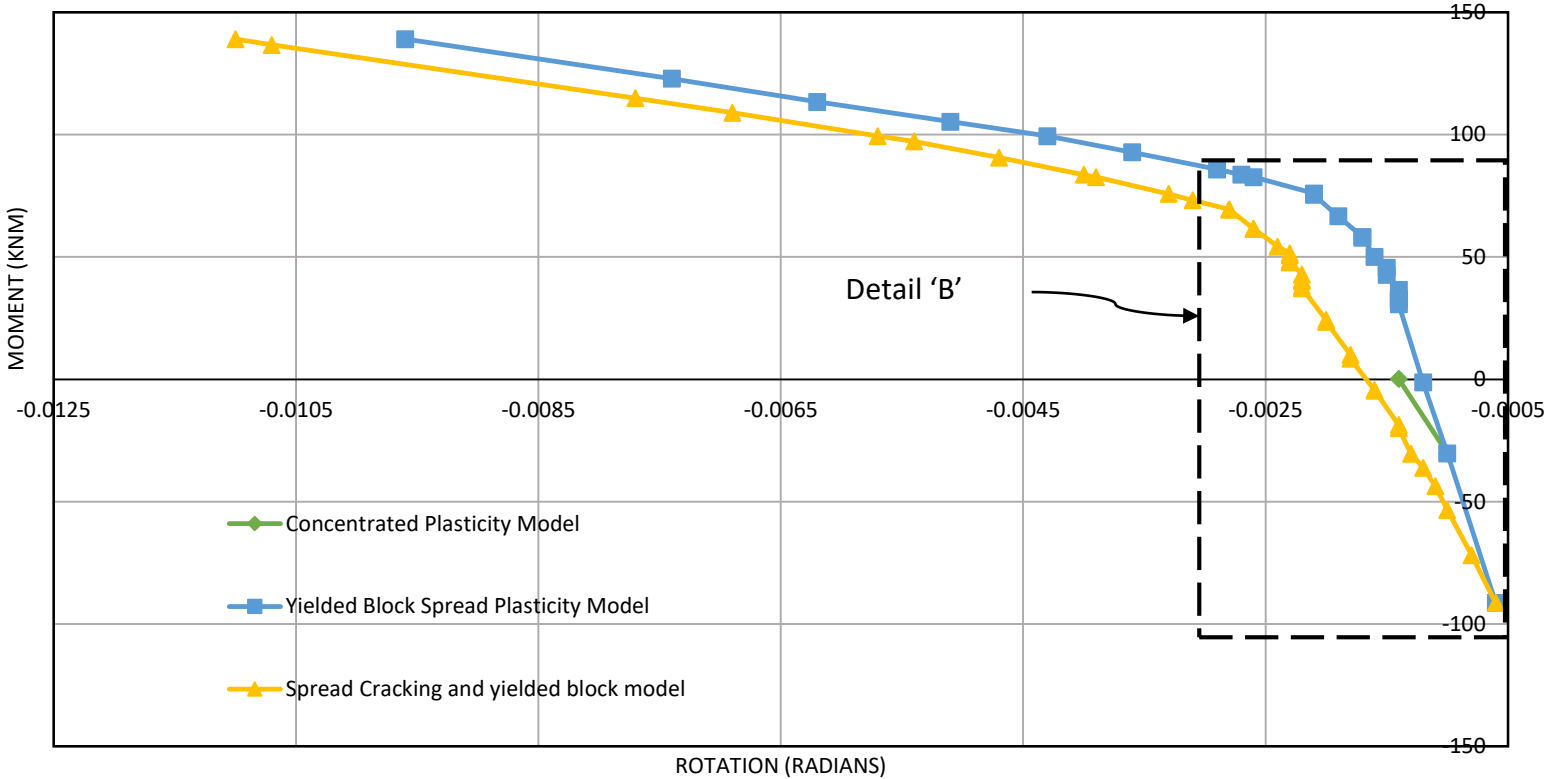
Figure 4-8: Moment - Rotation Plots at the left joint of the frame commencing from the initiation of lateral loading up to when the 2nd ultimate moment is reached at node 10 along the mid-span.
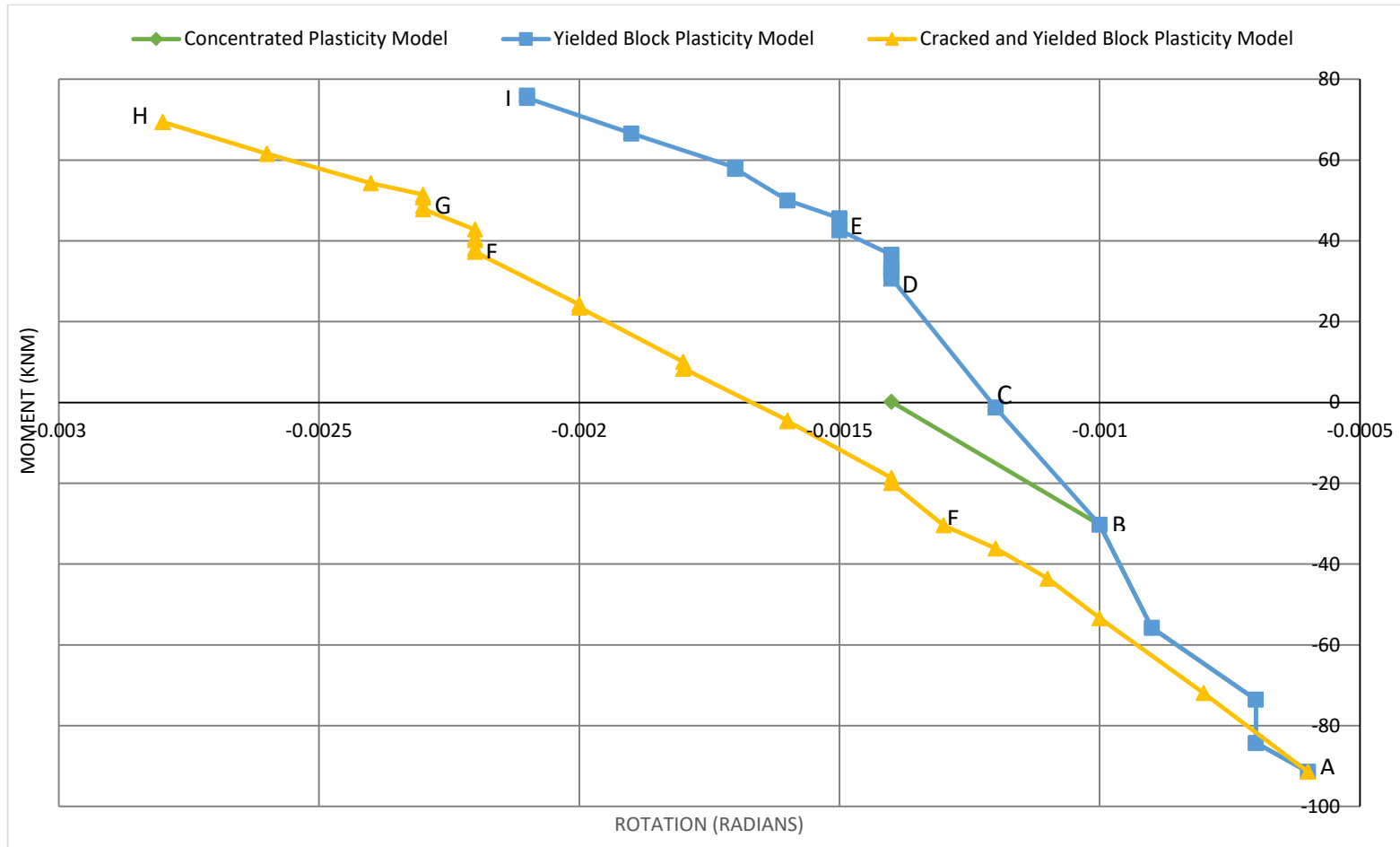
Figure 4-9: Detail 'B' showing moments up to when the 1st ultimate moment is reached at Joint 37

Figures 4-8 and 4-9, show the relationship between Moment and Rotation at *joint 2*. All models coincide at point A when only gravity loads are applied to the structure. The curves for the existing models continue to coincide between points A and B. Point B represents 1st yield at *joint 37* in both existing models at which point both models underestimate the joint rotation by 42.9%. This effect is also felt at *joint 2 b*ecause rotations are coupled. The curves of the existing models separate from each other at point B. Between points A and B, the existing models have a non-linear behaviour unlike the proposed model which exhibits an almost linear behaviour thus obeying Hooke's law of elasticity before 1st yield. Figure 4-10, is a bending moment diagram for all three models at point A while Figure 4-11 illustrates the bending moment diagram for both existing models at point B.
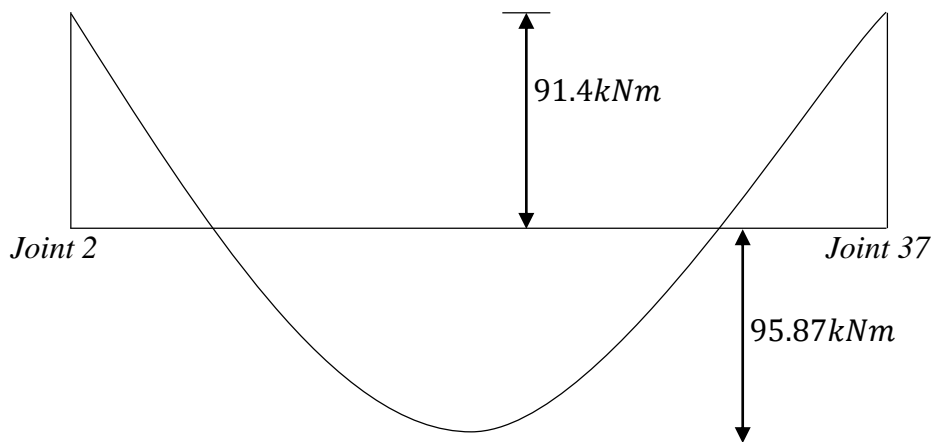
Figure 4-10: BMD at point A for all three models

Between points B and D, the yielded block spread plasticity model has a linear tendency. Point C represents yield at *joint 2*. Both the concentrated plasticity model and the yielded block spread plasticity model underestimate rotations at point C by 25.71% and 42.85% respectively. Point C represents 2nd yield in both existing models.

At this point, the yielded block spread plasticity model is less accurate than the concentrated plasticity model. Accuracy in the concentrated plasticity model increases with increase in moment while that of the yielded block spread plasticity model decreases with increase in moment. Combined bending moment diagrams at point C for all three models are illustrated in Figure 4-12 for ease of comparison.
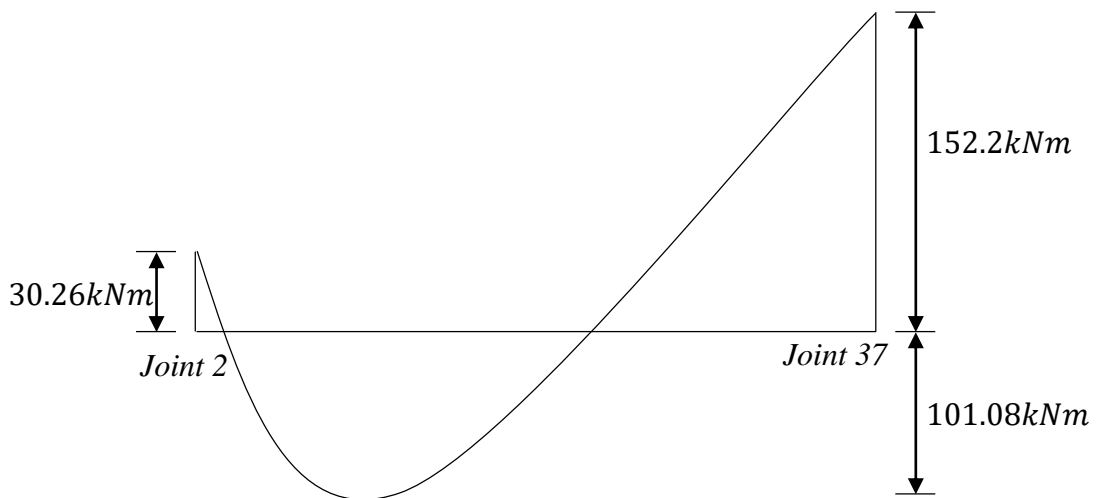
Figure 4-11: BMD at point B for both existing models

At point D, the sagging moment within the span reaches yield which is recognised by the yielded block spread plasticity model. Points between D and E represent yielding at mid-span and as such an almost constant rotation with increasing moment is observed at *joint 2*. A similar trend is observed at point F on the curve for the proposed model at the initiation of yielding at mid-span.
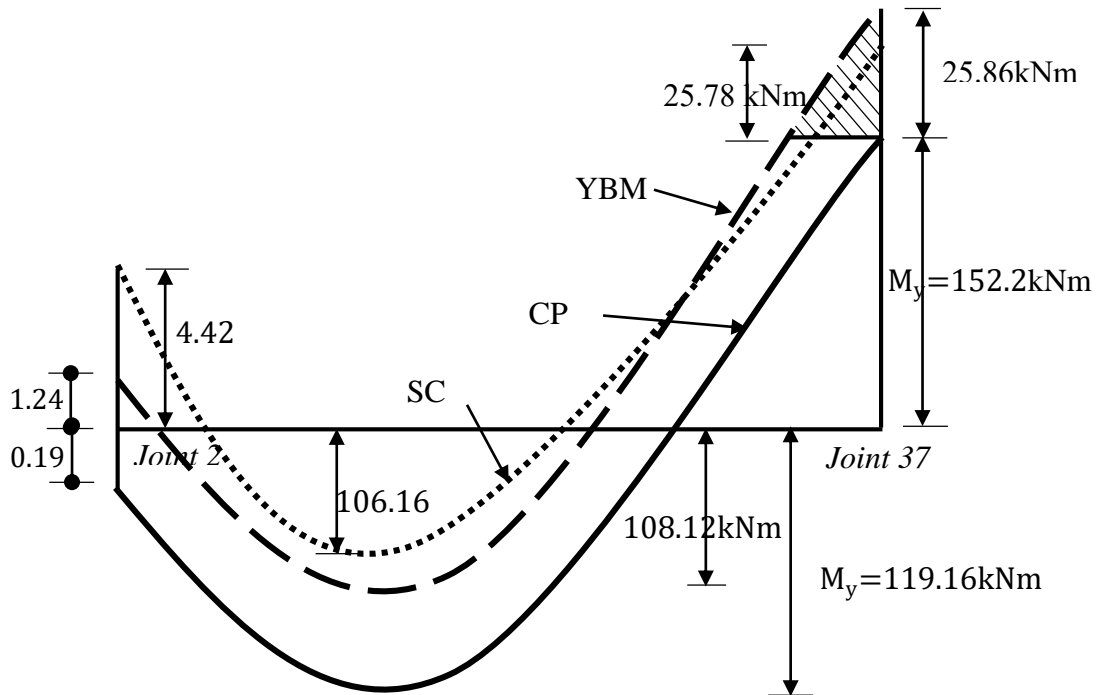
Figure 4-12: BMD at point C for the concentrated plasticity model (CPM), yielded block spread plasticity model (YBM) & the proposed spread crack and yield block model (SCM)

The proposed model for the most part has an almost perfect linear behaviour with an exception of a slight bump at point E as a result of yielding at *joint 37*, and during yielding at mid-span at points F and G. The curve of the proposed model and that of the yielded block spread plasticity model are seen to diverge away from each other right from the initiation of cracking but tend to follow a similar trend after initiation of yielding at mid-span. Final rotations are underestimated by both the concentrated plasticity and the yielded block spread plasticity models with errors in accuracy of up to 68.18% and 31.82% respectively. However, the yielded block spread plasticity model overestimates the final bending moment by 3.71% while the concentrated plasticity model underestimates the final bending moment by 43.1%.

Rotations by the concentrated plasticity model range between -0.0006 and -0.0014 while those of the yielded block spread plasticity model lie between -0.0006 and -0.0021. This increment in rotations is mainly due to the additional moment capacity allowed for in the yielded block spread plasticity model which considers moments beyond the yield moment while the concentrated plasticity model does not consider moments beyond the yield moment. These additional moments (between the yield and ultimate moment) allowed for by the yielded block spread plasticity model are responsible for the additional rotations recorded at the joint. The proposed model registers rotations ranging between -0.0006 and -0.0028 showing an increase in rotations at *joint 2* in comparison to the existing models. This can be attributed to the reduction in stiffness caused by cracking in the beam. A reduction in stiffness of the beam increases its flexibility and thus increases the beam rotations. This is a clear indication that ignoring cracking during pushover analysis overestimates the beam strength/ stiffness and thus underestimating the beam deformations.

Table 5: Comparative analysis of rotations and their margins of error for selected moments at joint 2

	Concentrated Plasticity Model		Yielded Block Spread Plasticity Model		Spread cracking and yielding block Model	
Moment	*Rotation, θ* (Rads)	*% Error*	*Rotation, θ* (Rads)	*% Error*	*Rotation, θ* (Rads)	*% Error*
-91.4 kNm	0	0	0	0	0	–
-30.27 kNm	-0.0004	42.86%	-0.0004	42.86%	-0.0007	–
0 kNm	-0.0008	27.27%	-0.0006	45.46%	-0.0011	–
40 kNm	Failed	N/A	-0.00086	46.25%	-0.0016	–
60 kNm	Failed	N/A	-0.00115	41.33%	-0.00196	–
99.41 kNm	Failed	N/A	-0.0043	24.56%	-0.0057	–
122.88 kNm	Failed	N/A	-0.0074	15.91%	-0.0088	–

4.3.3 MOMENT – ROTATION CURVE FOR JOINT 37
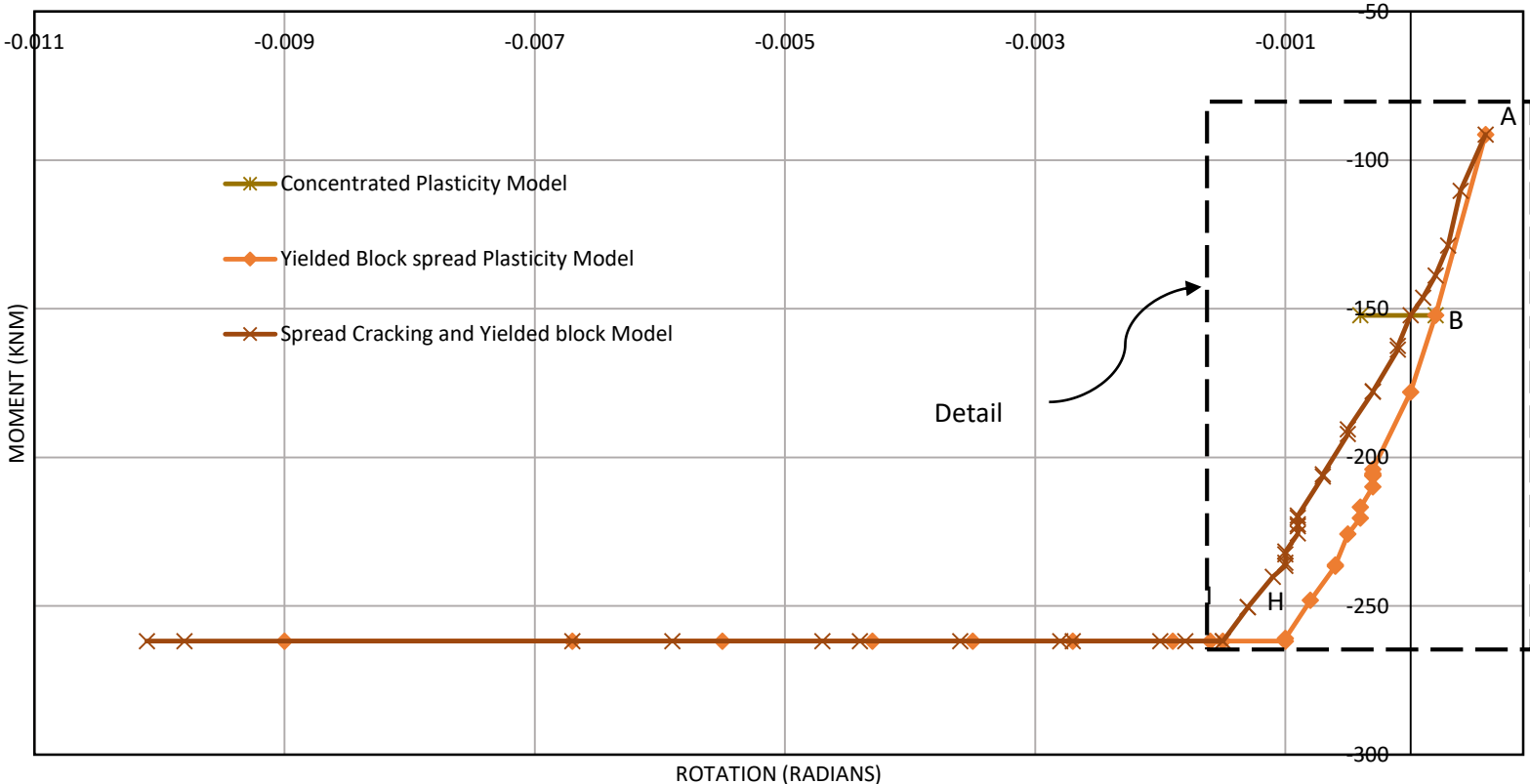
Figure 4-13: Moment – Rotation Plots at the right joint commencing from the initiation of lateral loading up to when the 2nd ultimate moment is reached at node 10 along the mid span
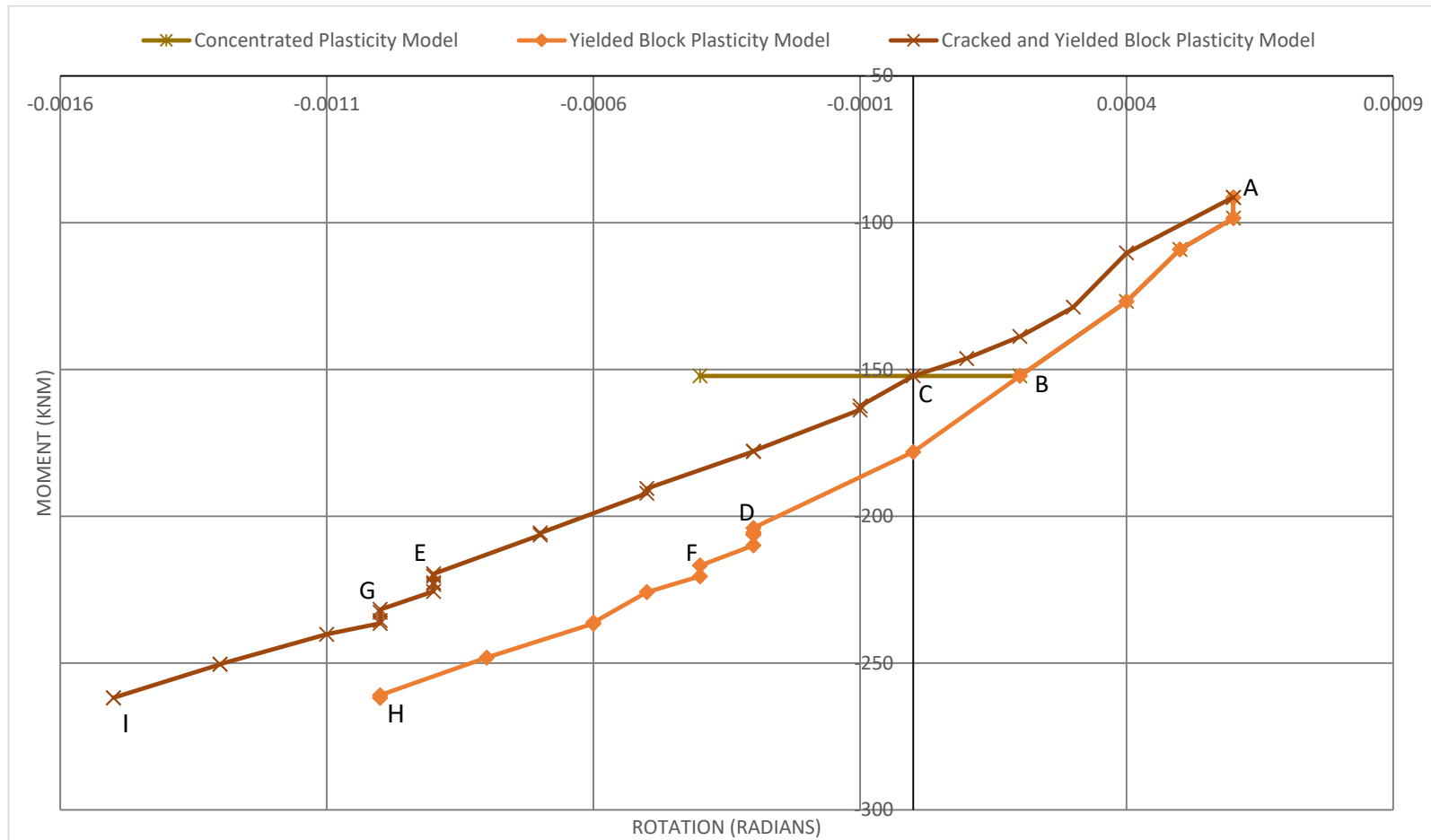
Figure 4-14: Detail 'C' at the right joint of the frame commencing from the initiation of lateral loading up to when the 1st ultimate moment is reached at Joint 37

All models coincide at point A when only gravity loads are applied as shown in figures 4-13 and 4-14. Between points A and B, both existing models coincide but diverge away from the proposed model, since both existing models ignore cracking. The existing models separate from each other beyond point B as a consequence of yielding at *joint 37*. At point B and beyond, the curve for the concentrated plasticity model flattens as the moment remains constant for increasing rotation. This occurs due to placement of a hinge at *joint 37* after reaching the yield moment. The moments for the proposed model as well as those of the yielded block spread plasticity model continue to increase with increasing rotation and also continue to gradually diverge away from each other. At point B, the yielded block spread plasticity model underestimates the joint rotation by 33.33%. Points D and E represent the initiation of yielding in the beam span for the yielded block spread plasticity model and the proposed model respectively. The moment distribution in the beams at point E and D are shown in the Figures 4-15 and 4-16 respectively.
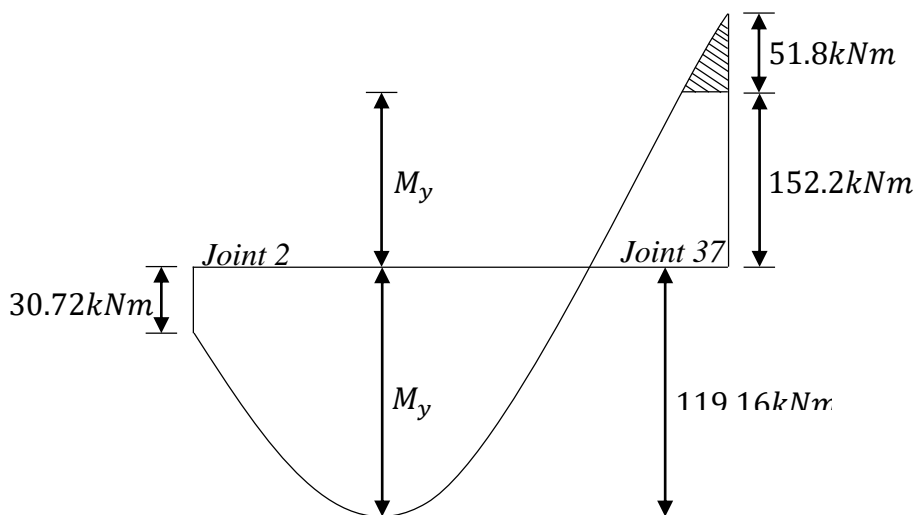
Figure 4-15: BMD at point D for the yielded block spread plasticity model at the initiation of mid-span yielding
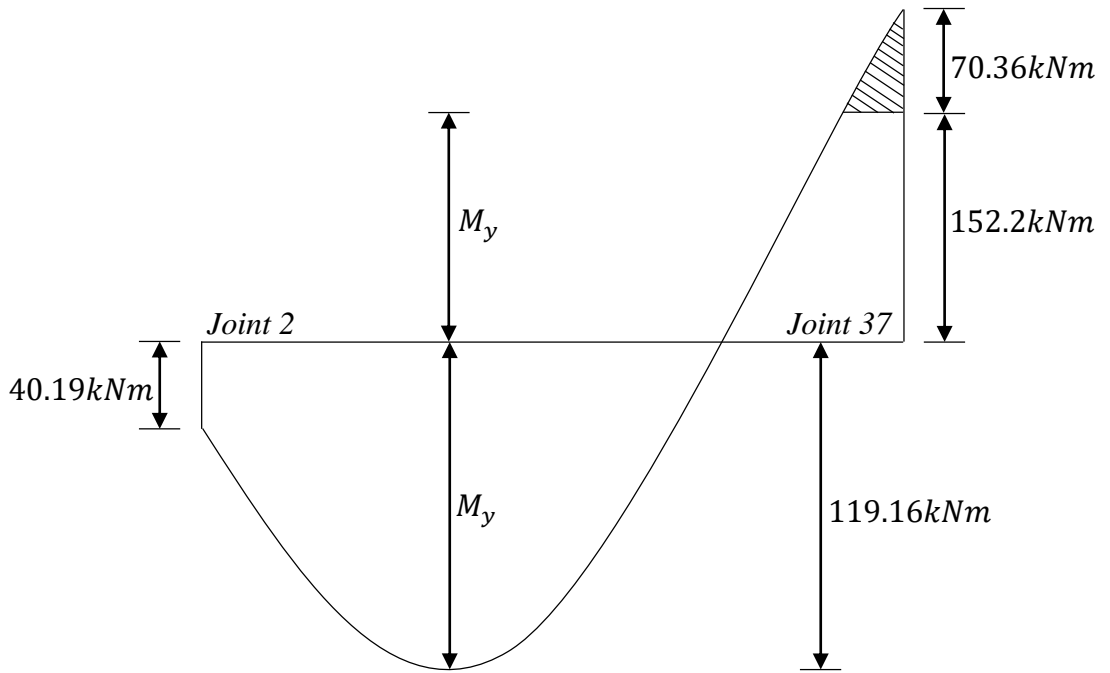
Figure 4-16: BMD at point E for the proposed model at the initiation of mid-span yielding
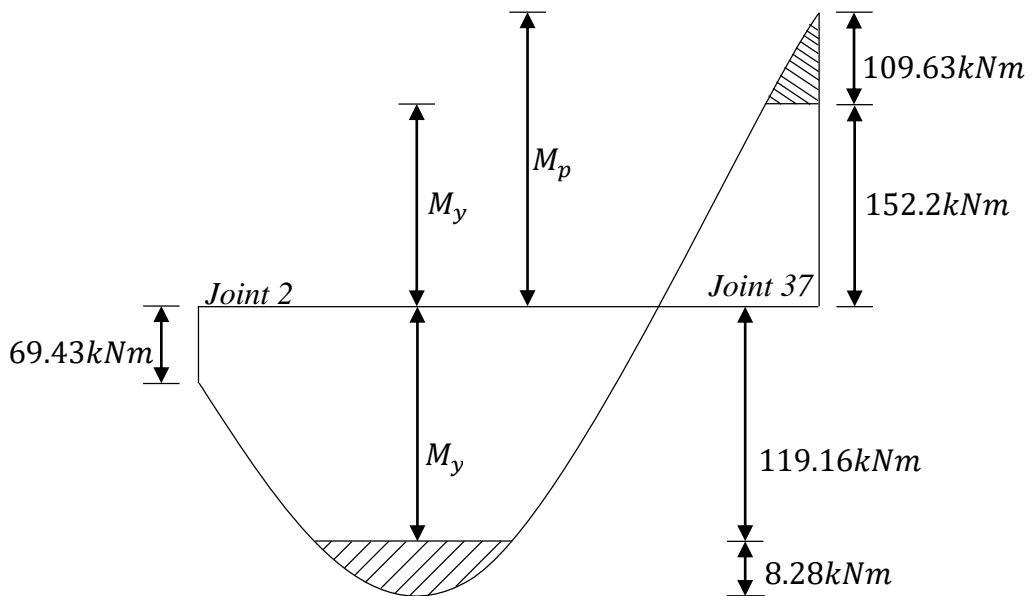
Figure 4-17: BMD at point H for the yielded block spread plasticity model

At point D, the yielded block spread plasticity model underestimates the joint rotations by 29.13%. The error in accuracy of final joint rotations reduce to 23.81% at point I

an indication that there is an increase in accuracy for the yielded block spread plasticity model as the bending moment increases. The final bending moment distribution across the beam is illustrated in Figures 4-17 and 4-18 for points I and H, respectively.
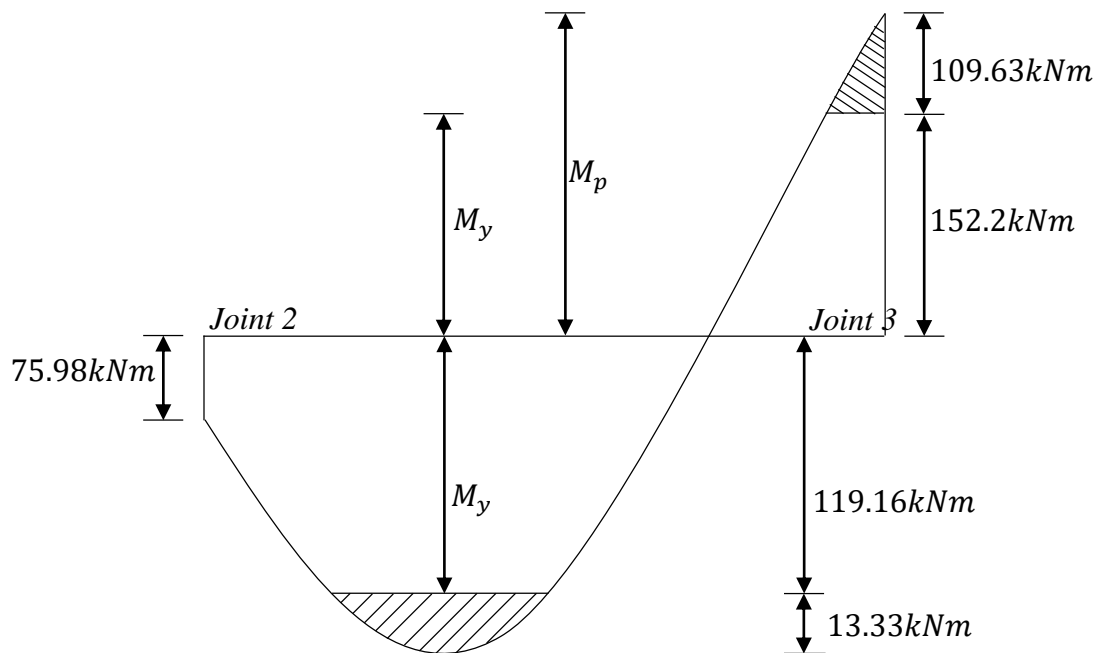
Figure 4-18: BMD at point I for the proposed model

The error in estimating the final moment at *joint 37* for the yielded block spread plasticity model and the concentrated plasticity model is -0.49% and -64.4% respectively which are less than those recorded at the opposite *joint 2*. The concentrated plasticity model registers rotations ranging between 0.0006 and -0.0004, the yielded block spread plasticity model registers rotations ranging between 0.0006 and -0.001 while the proposed spread cracking and yielding block model registers rotations ranging between 0.0006 and -0.0015.

Table 6: Comparative analysis of rotations and their margins of error for selected

moments at joint 37

	Concentrated Plasticity Model		Yielded Block Spread Plasticity Model		Spread cracked and yielded block Model	
Moment	*Rotation*	*% Error*	*Rotation*	*% Error*	*Rotation*	*% Error*
-91.4 kNm	0	0	0	0	0	−
-126.87 kNm	-0.0002	33.3%	-0.0002	33.3%	-0.0003	−
-152.2 kNm	-0.0006	0%	-0.0004	33.33%	-0.0006	−
-204 kNm	Failed	N/A	-0.0009	29.13%	-0.00127	−
-260.91 kNm	Failed	N/A	-0.0016	32.43%	-0.00208	−

4.3.4 GENERAL DISCUSSION

Analysis using the concentrated plasticity model captures results starting from the point of 1st yield. It doesn't pick any data before the point of 1st yield since the model only detects yielding/ plasticity in beams and thus not giving a clear understanding of the deformations before and between points of yield. The yielded block spread plasticity model is also activated after 1st yield. The proposed spread cracking and yielding block model further introduces a cracked sub-element into the beam to account for the gradual spread of cracking and thus offers a broader spectrum of joint rotations and displacements by identifying cracking in the beam in addition to yielding. This can be seen in Figures 4-6, 4-7 and 4-13 as the curves for the proposed model are smoother and capture more detail unlike the existing models.

For the concentrated plasticity model, *joint 37* yields first and a hinge is placed at this node. The second yield is in the span at *node 16* and a hinge is also placed at this point effectively creating a mechanism. No further analysis can be carried out beyond this point.

The yielded block spread plasticity model yields first at end *joint 37*, block *36-37* is then replaced by a yielded block sub-element of reduced stiffness. 2nd yield occurs at *Node 36* and block *36-35* is also replaced with a yielded block sub-element. This shows that plasticity in the beam spreads from the end joint towards the span unlike the concentrated plasticity model which concentrates all plasticity at a single point. The 3rd yield occurs in the span at *node14* representing a shift in the point of contra-flexure in the span as compared to that of the concentrated plasticity model. A yielded block sub-element is placed between *node14* and *node13*. Yielding thereafter is seen to

50

spread in both directions of *node 14*. A total of four(4) elastic sub-elements, i.e. *37-36*, *36-35*, *35-34*, and *34-33*, reach the yield hogging moment and thus are replaced with yielded block sub-elements. This represents a plastic zone of $0.8m$ which lies within the limit on the extent of the plastic zone length recommended by (Filippou & Issa, 1988). A total of ten (10) linear elastic sub-elements, i.e. *7-8*, *8-9*, *9-10*, *10-11*, *11-12*, *12-13*, *13-14*, *14-15*, *15-16* and *16-17*, reach the yield sagging moment in the span before the ultimate moment is reached at *node 37*. This represents a total of about 2m (approx. 28.57% of the entire span) out of the total $7m$ beam length.That means that a total of 40% (2.8m) of the beam length (*0.4L*) attains full plasticity by the time the first node (*node 37*) reaches ultimate moment. There is currently no limit on the extent of the plastic zone in the span.

It can be observed that the yielded block spread plasticity model has better accuracy during analysis as compared to the concentrated plasticity model. The concentrated plasticity model is found to be overly conservative and thus greatly underestimates the moment and rotational capacity of RC sections. This renders the concentrated plasticity model less economical than the yielded block spread plasticity model. This increment in capacity while using the yielded block spread plasticity model can be attributed to the assumption that even after yielding has occurred, the yielded section still has additional capacity unlike the concentrated plasticity model which assumes the formation of a hinge after yielding. Analysis using the yielded block spread plasticity model is terminated on reaching the ultimate moment at *joint 37*.

Figures 4-6, 4-7 and 4-13 show that the proposed model is able to detect cracking in the beam even before lateral loads are applied to the frame. *Eighteen (18)* linear elastic

sub-elements, i.e. *10-11*, *11-12*, *12-13*, *13-14*, *14-15*, *15-16*, *16-17*, *17-18*, *18-19*, *19-20*, *20-21*, *21-22*, *22-23*, *23-24*, *24-25*, *25-26*, *26-27*, *27-28*, and *28-29*, crack in the beam under sagging moment at mid-span while being subjected to only gravity loads and are subsequently replaced with cracked sub-elements of reduced stiffness. This accounts for *51.4%* of the entire beam length.

When the frame is subjected to successive point lateral loads at *joint 2*, eight (*8*) more elastic sub-elements, i.e. *2-3*, *3-4*, *4-5*, *5-6*, *6-7*, *7-8*, *8-9*, *9-10* continue to crack while spreading from the mid-span towards the end *joint 2*. A total of twenty-six (*26*) elastic sub-elements crack along the span under sagging moment, *eight (8)* of which proceed to yield. Five(*5*)elastic sub-elements, i.e. *37-36*, *36-35*, *35-34*, *34-33*, and *33-32* crack under hogging moment starting from end *joint 37* and subsequently four (*4*) of which proceed to yield, i.e. *37-36*, *36-35*, *35-34*, and *34-33*. A total of thirty two (*32*) elastic sub-elements crack and twelve (*12*) of which reach yield moment by the conclusion of the analysis giving us a cracked zone length of *6400mm* and a plastic zone length of *2400mm*. This means that *91.4%* of the beam length cracks by the time the first node (*joint 37*) attains ultimate moment. The cracked and plastic zones consist of two sections which are:

1. The section under sagging in the span and

2. The section under hogging at and near the end joints.

The total plastic zone length while using the proposed model shrinks by *14.29%* in comparison with that of the yielded block spread plasticity model.

The proposed model is computationally more demanding with a total of twenty-eight (*28*) modifications to the frame before attaining ultimate moment while the

concentrated plasticity and the yielded block spread plasticity models have a mere two (*2*) and fifteen (*15*) modifications respectively, yet the proposed model is detailed enough to give more reliable results. The accuracy of the yielded block spread plasticity model decreases with increase in moment or lateral loading. This is more so for the joint rotations as observed from the graphs.

4.4 PUSH-OVER ANALYSIS OF THE THREE STOREY FRAME

4.4.1 MOMENT-ROTATION CURVES AT JOINT 2

Figure 4-19: Moment-Rotation Curves at joint 2 (1ˢᵗ Floor, left joint) for all three models

All three models coincide at points O and A just before the proposed model diverges off to a constant rotation of *-0.0005 Rads* along AB. At point E, the concentrated plasticity model is seen to overestimate the joint rotation by up to *57.14%* and to a lesser extent the yielded block spread plasticity model overestimates the rotations by 14.29%. The curves for both the concentrated and yielded block spread plasticity models coincide between points O and D since both ignore cracking. The two curves diverge after 1st yield at *joint 74* labelled as point D. The concentrated plasticity model curve branches off to a constant moment of *0.19kNm* at point E and terminates at F. There is no further analysis beyond point F since a mechanism is formed at this point. There are two yield points that coincide at point E. One corresponding to yielding in the span on the 1st floor and the other corresponding to yielding at *joint 110 (3rd floor, right joint)*.

It can be observed that with increased moment, the error in accuracy of joint rotations for the yielded block spread plasticity model reduces to almost *0%* at point G. The yielded block spread plasticity model however overestimates the final moment by *10.17%* while the concentrated plasticity model underestimates the final joint moment by *31.63%*. The concentrated plasticity model overestimates the final joint rotation by 58.3%. The yielded block spread plasticity model on the other hand overestimates the final joint rotations by *25%*. Both the curves for the yielded block spread plasticity model and the proposed model deviate away from that of the concentrated plasticity model with increase in moment.

At *joint 2*, the concentrated plasticity model rotations range between *-0.0003* and *-0.0022 rads* while the rotations for the yielded block spread plasticity model

range between *-0.0003* and *-0.0018 rads*. The proposed model registers rotations ranging between *-0.0003* and *-0.0015 rads*. This reduction in rotations can be attributed to spread cracking which further ensures stress distribution (energy dissipation) in the beam.

Table 7: Comparative analysis of Rotations and their respective margins of error at selected moments

	Concentrated Plasticity Model		Yielded Block Spread Plasticity Model		Spread cracking and yielding block Model	
Moment	*Rotation*	*% Error*	*Rotation*	*% Error*	*Rotation*	*% Error*
-107.69 kNm	0	0	0	0	0	−
-54.54 kNm	0.00041	105%	0.00046	130%	0.0002	−
0 kNm	0.0011	57.1%	0.0008	14.3%	0.0007	−
50.1 kNm	Failed	N/A	0.0012	0	0.0012	−
66.14 kNm	Failed	N/A	0.0015	N/A	N/A	−

4.4.2 MOMENT-ROTATION CURVES AT JOINT 39
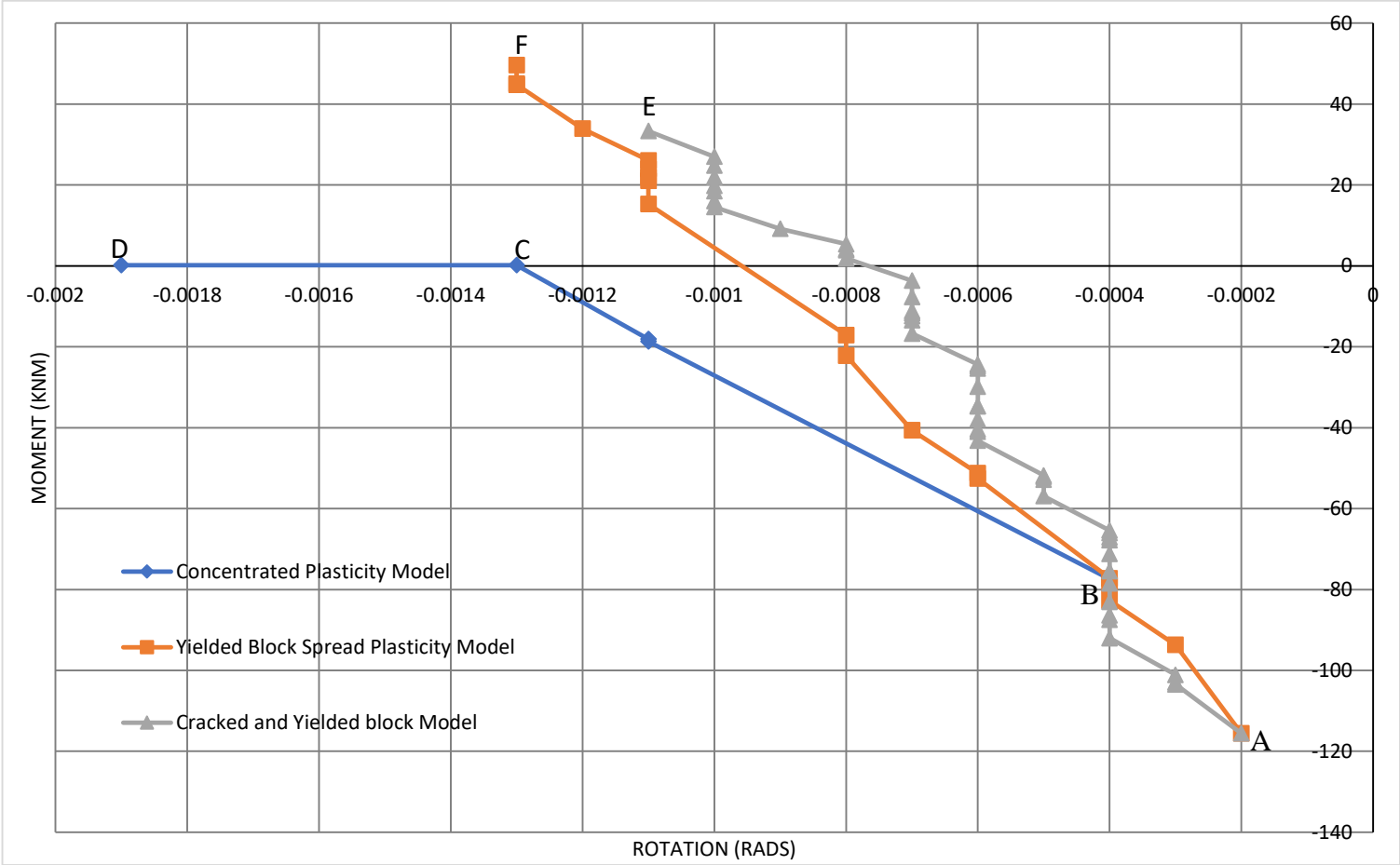
Figure 4-20: Moment-Rotation Curves at Joint 39 (2nd Floor, left joint) for all three models

All models coincide at points A and B. The models separate away from each other with increase in applied moment between points B and C. At point C, the yielded block spread plasticity and the concentrated plasticity models overestimate the end joint rotations by 33.33% and 92.98% respectively. The concentrated plasticity model flattens at a constant moment of 0.2kNm between points C and D. The model also overestimates the final joint rotation by 88.9% and at the same time underestimating the final joint moment by 22.3%. The yielded block spread plasticity model on the other hand overestimates both the final joint moment and rotation by 10.96% and 22.22% respectively.

The rotations at *joint 39 (left joint, 2nd level)* for the concentrated plasticity model range between -0.0002 and -0.0019 rads. While those of the yielded block spread plasticity model range between -0.0002 and -0.0013rads. For the proposed spread cracking and yielding block model, the rotations range between -0.0002 and -0.0011rads representing a further decline in rotations as compared to the yielded block spread plasticity model.

Table 8: Comparative analysis of Rotations and their respective margins of error at

selected moments

	Concentrated Plasticity Model		Yielded Spread Block Plasticity Model		Spread cracking and yielding block Model	
Moment	*Rotation*	*% Error*	*Rotation*	*% Error*	*Rotation*	*% Error*
-115.58 kNm	0	0	0	0	0	−
-65.39 kNm	0.00034	70%	0.0003	50%	0.0002	−
0.2 kNm	0.0011	92.98%	0.00076	33.33%	0.00057	−
33.35 kNm	Failed	N/A	0.00099	10%	0.0009	−
49.69 kNm	Failed	N/A	0.0011	N/A	Failed	N/A

4.4.3 Moment-Rotation Curves at Joint 75
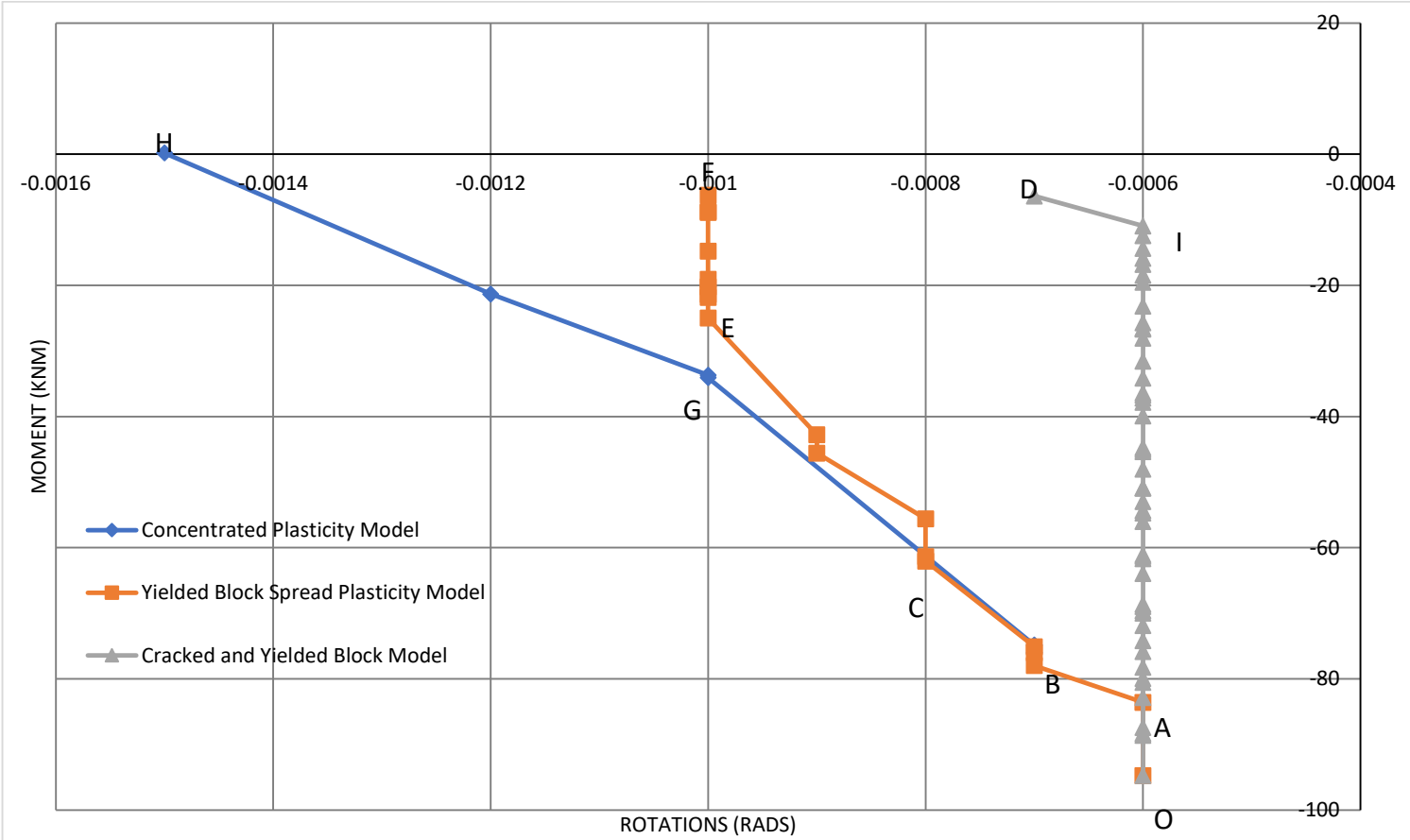
Figure 4-21: Moment-Rotation Curves at Joint 75 (3ʳᵈ Floor, left joint) for all three models

All models coincide between points O and A, as seen in figure 4-20. At point A, the existing models separate away from the proposed model and eventually also separate from each other at point B. The concentrated plasticity model and the yielded block spread plasticity model however, overestimate the final joint rotations by 800% and 300% respectively. The concentrated plasticity model overestimates the final joint moment by 7.4% while the yielded block spread plasticity model underestimates the same by 2.84%. The trend of the graph for the proposed model implies that when cracking is considered during pushover analysis, the effect of yielding and cracking in other parts of the frame doesn't affect rotations at *joint 75*. On the other hand, the existing models show that yielding elsewhere in the frame causes joint rotations at *joint 75*.

For the concentrated plasticity model, the rotations at joint 75 range between -0.0006 and-0.0015 rads, while those of the yielded block spread plasticity model range between -0.0006 and -0.001 rads. For the proposed model, rotations are very minimal as they range between -0.0006 and -0.0007 rads.

For the case of the proposed spread cracking and yielding block model, rotations are suppressed further to the extent that a constant rotation of *-0.006* is recorded for moments ranging between *-94.75kNm* and *-10.94kNm*. This can only be attributed to the effect of spread cracking in the beam. A combination of spread cracking and spread plasticity effectively ensures redistribution of stresses in the beams.

4.4.4 Moment-Rotation Curves at Joint 37

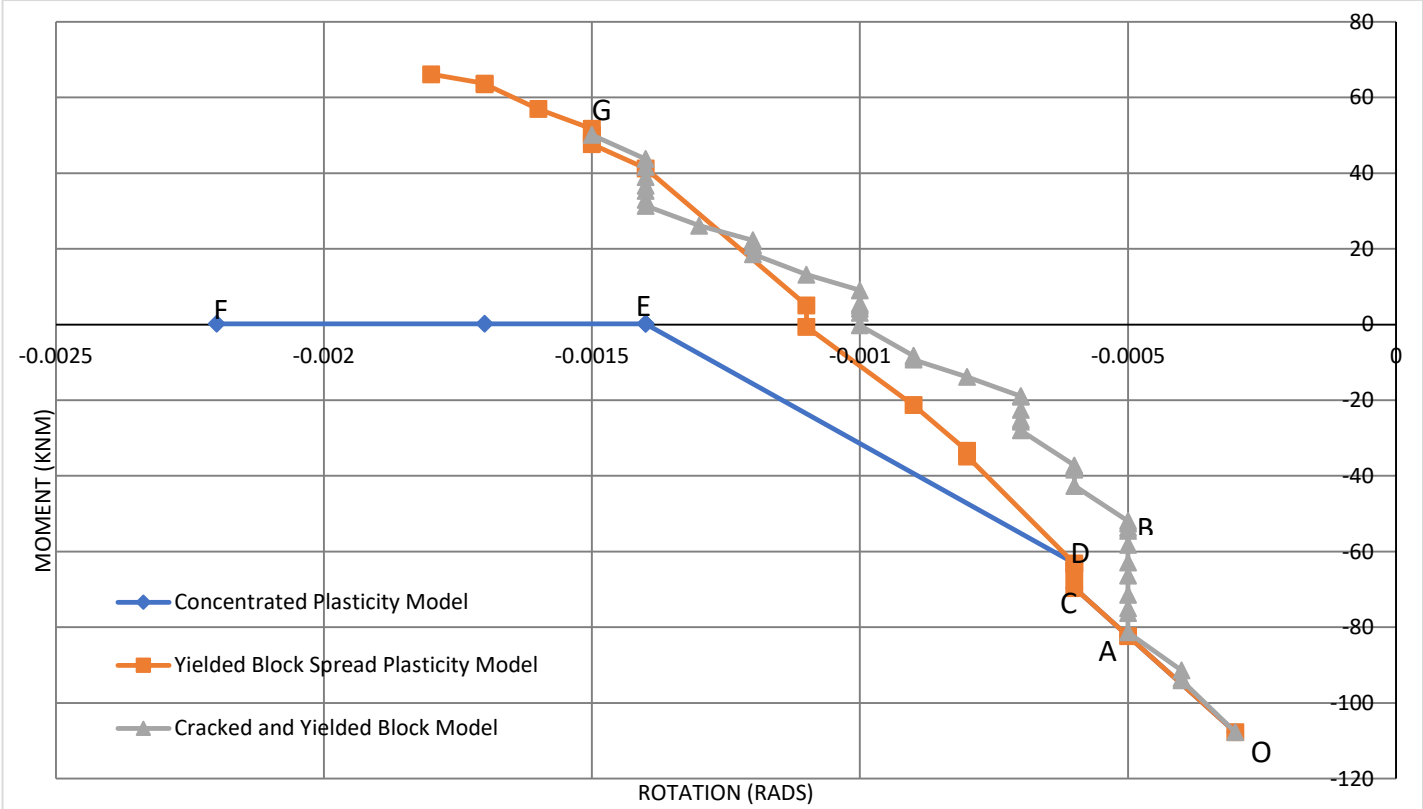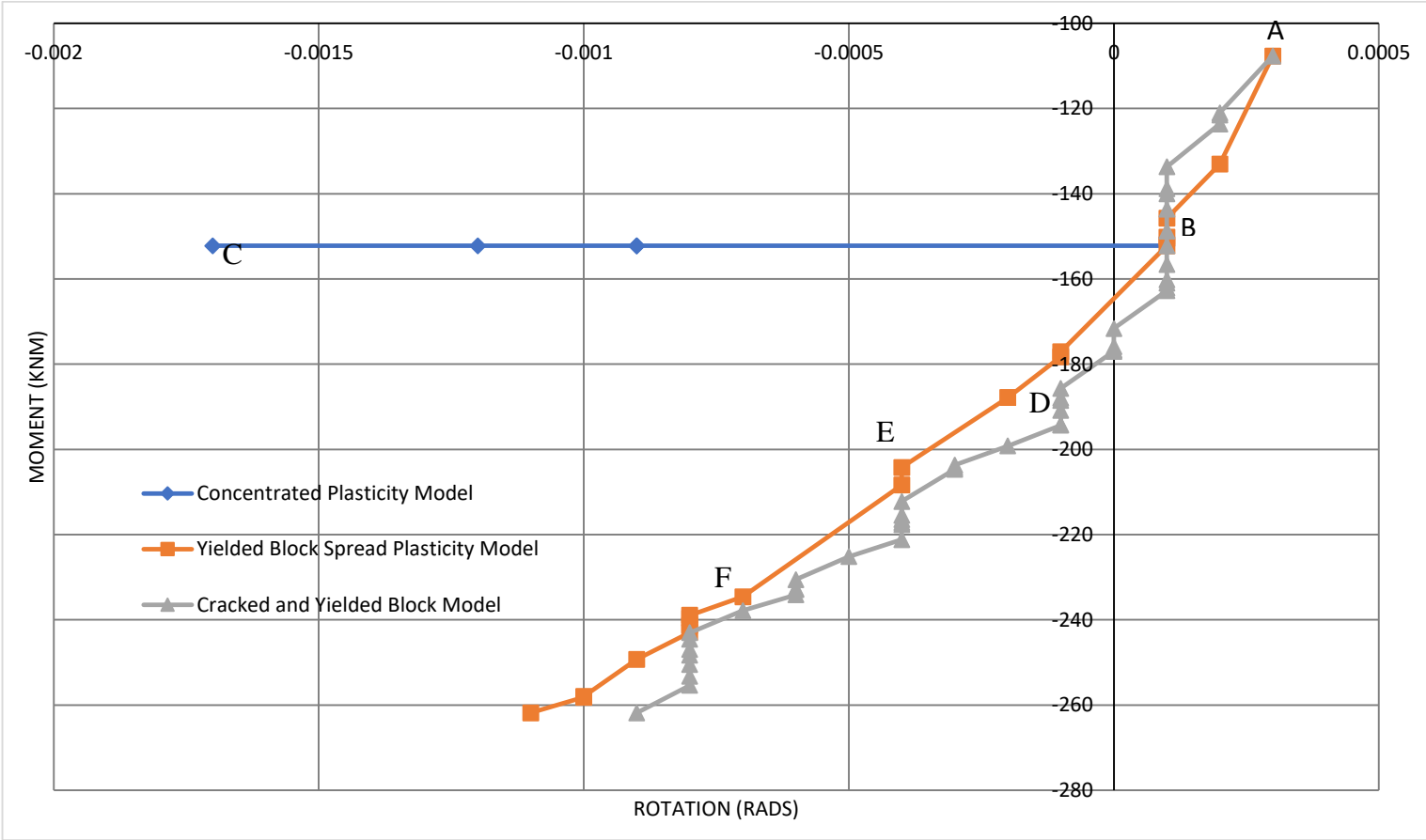*Figure 4-22: Moment-Rotation Curves at Joint 37 (1st Floor, Right hand Joint) for all three models*

All models coincide at points A and B as can be seen in figure 4-21. At point B and beyond, the yielded block spread plasticity model and the proposed model move in close proximity of each other while the concentrated plasticity model separates from the rest and flattens at a moment of *-152.2kNm*. Both the concentrated plasticity model and the yielded block spread plasticity model overestimate the final joint rotations by *66.67%* and *16.67%* respectively. On the other hand, the concentrated plasticity model underestimates the final joint moment by *71.12%*.

The rotations at *joint 37 (right hand joint, 1ˢᵗ storey)* for the concentrated plasticity model range between *0.0003* and-*0.0017 rads*. While those of the yielded block spread plasticity model range between *0.0003* and-*0.0011rads*. For the proposed spread cracking and yielding block model, the rotations range between *0.0003* and-*0.0009rads* representing a further decline in rotations.

Table 9: Comparative Analysis of Rotations and their respective margins of error at selected moments

	Concentrated Plasticity Model		Yielded Spread Model	Block Plasticity	Spread cracking and yielding block Model	
Moment	*Rotation*	*% Error*	*Rotation*	*% Error*	*Rotation*	*% Error*
-107.69 kNm	0	0%	0	0%	0	–
-133.06 kNm	-0.0001	50%	-0.0001	50%	-0.0002	–
-187.84 kNm	Failed	N/A	-0.0005	25%	-0.0004	–
-203.67kNm	Failed	N/A	-0.0007	16.67%	-0.0006	–
-234.6kNm	Failed	N/A	-0.001	11.11%	-0.0009	–

4.4.5 MOMENT-ROTATION CURVES AT JOINT 74
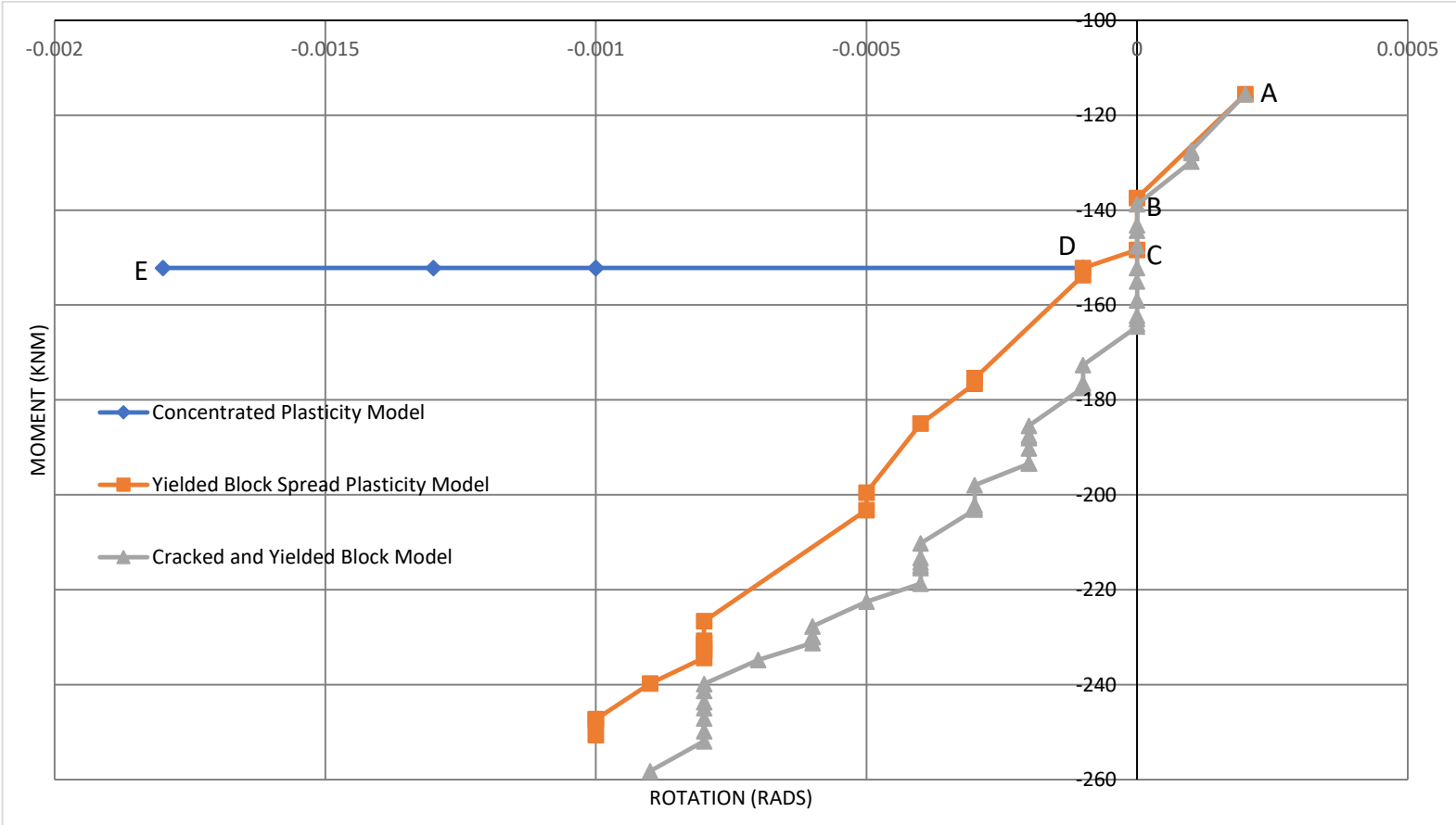
Figure 4-23: Moment-Rotation curves at Joint 74 (2nd Floor, Right hand Joint) for all three models

Point A represents rotations at *joint 74* when only gravity loads are applied to the frame. All models coincide at points A, B and C. At point C, the existing models separate from the proposed model since they don't recognise cracking until they eventually separate from each other at point D. At point D, both the existing models overestimate the joint rotation by *50%*. The yielded block spread plasticity model on average overestimates the joint rotations by *42%*. The final joint rotations for both the yielded block spread plasticity model and the concentrated plasticity model are overestimated by *9.09%* and *81.82%* respectively. The yielded block spread plasticity model and the concentrated plasticity model underestimate the final joint moments by *5.34%* and *74.34%* respectively.

The rotations at *joint 74 (right hand joint, 2ⁿᵈ storey)* for the concentrated plasticity model range between *0.0002* and *-0.0018 rads*. While those of the yielded block spread plasticity model range between *0.0002* and *-0.001rads*. For the proposed spread cracking and yielding block model, the rotations range between *0.0002* and *-0.0009rads* representing a further decline in rotations.

Table 10: Comparative Analysis of Rotations and their respective margins of error at selected moments

	Concentrated Plasticity Model		Yielded Block Spread Plasticity Model		Spread cracking and yielding block Model	
Moment	*Rotation*	*% Error*	*Rotation*	*% Error*	*Rotation*	*% Error*
-115.58 kNm	0	0%	0	0%	0	−
-152.2 kNm	-0.0003	100%	-0.0003	100%	-0.0002	−
-176.58 kNm	Failed	N/A	-0.0005	66.67%	-0.0003	−
-199.55 kNm	Failed	N/A	-0.0007	40%	-0.0005	−
-227.74 kNm	Failed	N/A	-0.001	25%	-0.0008	−
-250.65 kNm	Failed	N/A	-0.0012	20%	-0.001	−

4.4.6 MOMENT-ROTATION CURVES AT JOINT 110
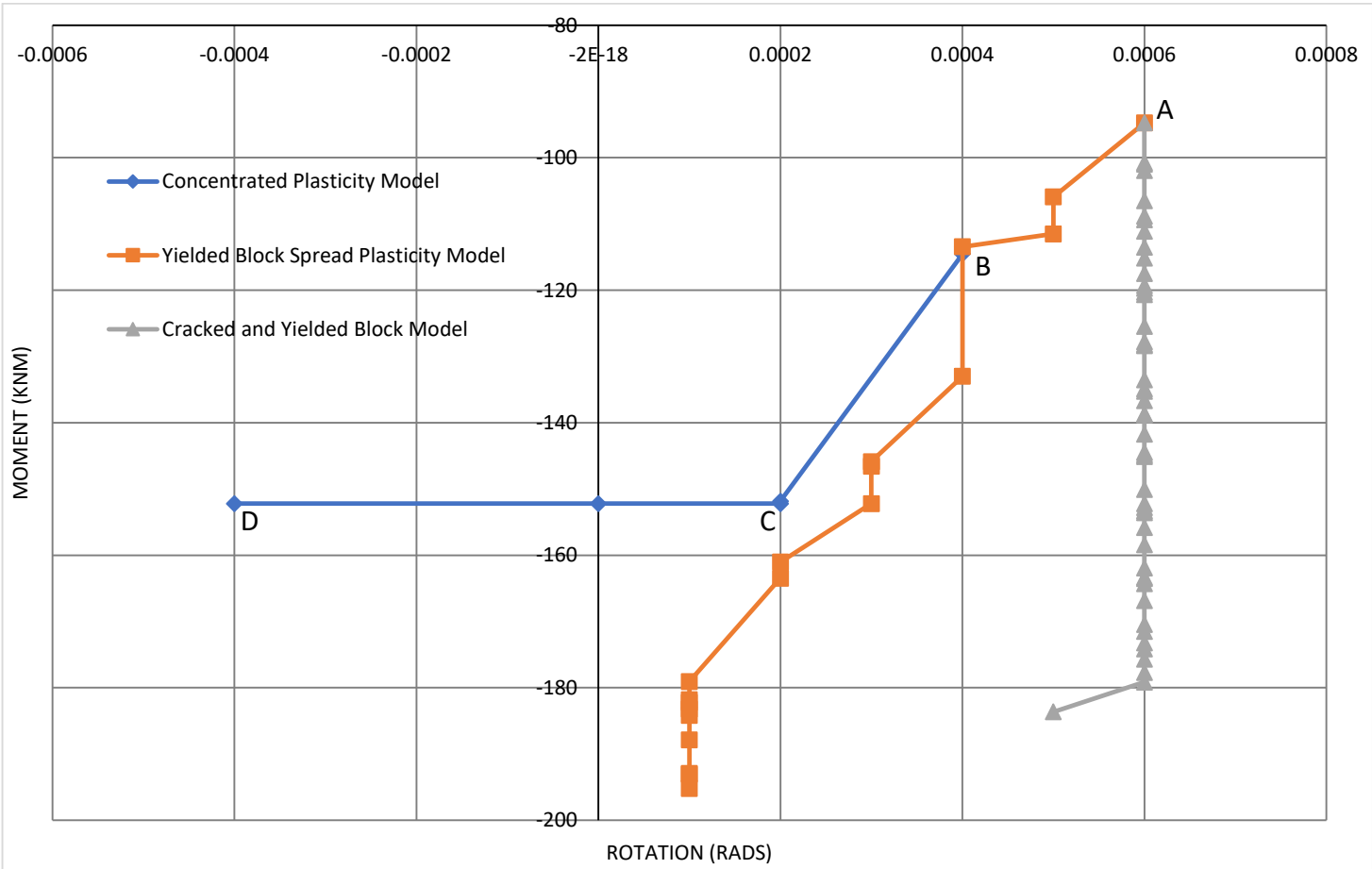
Figure 4-24: Moment-Rotation Curves at joint 110 (3rd Floor, Right hand Joint) for all three models

All models coincide at point A after the application of only gravity loads. Beyond this point, the existing models separate away from the proposed model. Both existing models coincide between points A and B. At point B, the concentrated plasticity model and the yielded block spread plasticity model separate and at point C, the concentrated plasticity model flattens to a constant moment of $-152.2 kNm$. The final joint rotations for both the yielded block spread plasticity model and the concentrated plasticity model are grossly overestimated by 80% and 180% respectively. The yielded block spread plasticity model overestimates the final joint moment by 6.3% while, the concentrated plasticity model underestimates the final joint moment by 17.12%.

The rotations at *joint 110 (right hand joint, 3rd level)* for the concentrated plasticity model range between 0.0006 and $-0.0004\ rads$. While those of the yielded block spread plasticity model range between 0.0006 and $0.0001 rads$. For the proposed spread cracking and yielding block model, the rotations range between 0.0006 and $0.0005 rads$ representing a further decline in rotations.

4.4.7 INTER-STOREY DRIFT RATIO
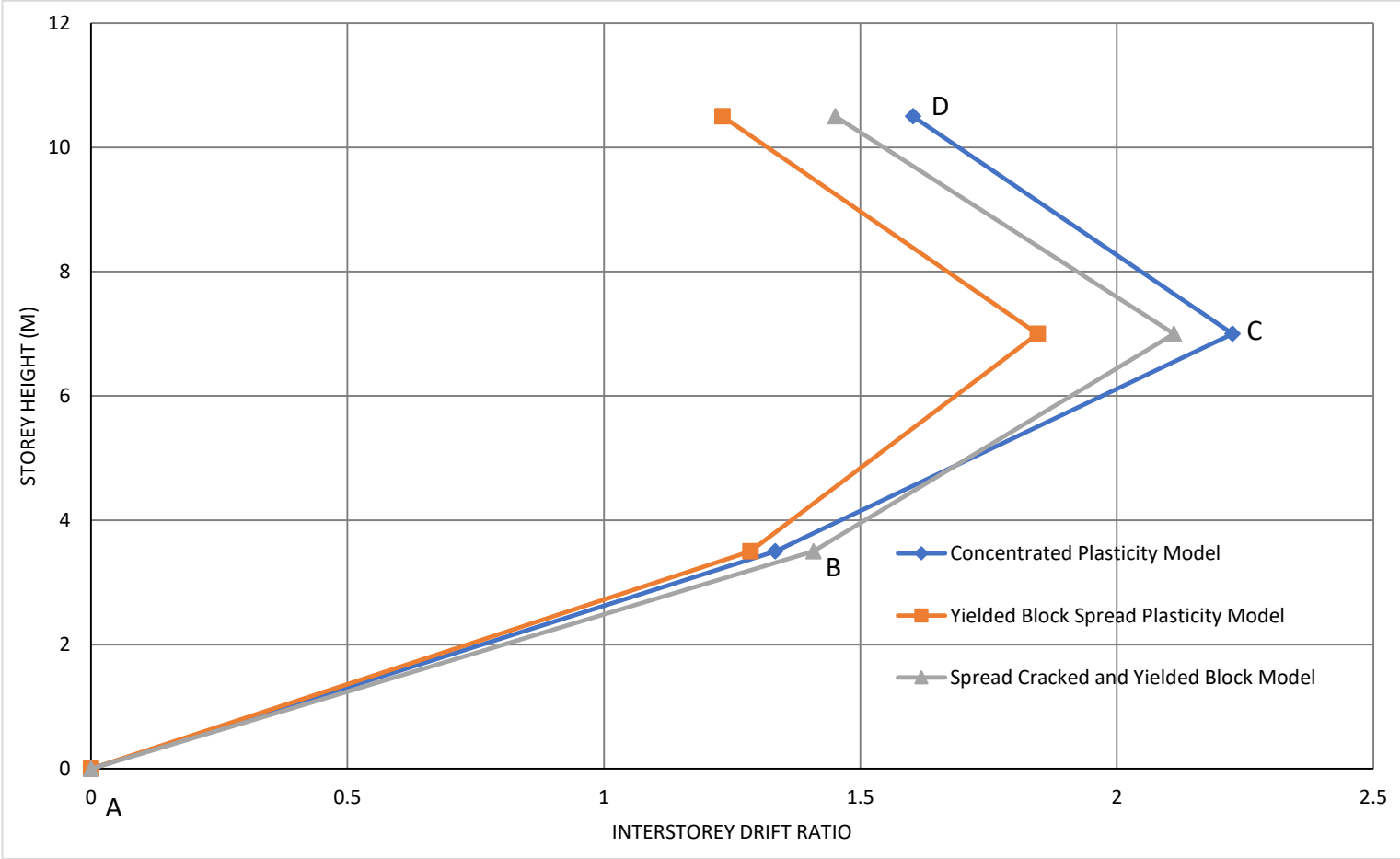
Figure 4-25: Curves of the Inter-storey drift ratio at different heights of the frame when subjected to all three models

At the 1st storey, both the concentrated plasticity model and the yielded block spread plasticity model underestimate the inter-storey drift ratio by 5.3% and 8.7% respectively. At the 2nd storey, the yielded block spread plasticity model underestimates the inter-storey drift ratio by 12.55% while on the other hand, the concentrated plasticity model overestimates the inter-storey drift ratio by 5.4%. At the 3rd storey shows that the yielded block spread plasticity model underestimates the inter-storey drift ratio by 15.16%. The concentrated plasticity model which overestimates the inter-storey drift ratio by 10.82%.

Table 11: Inter-storey drift ratios and their respective margins of error at different storey heights

	Concentrated Plasticity Model		Yielded Block Spread Plasticity Model		Spread cracking and yielding block Model	
Storey Height	*Inter-storey Drift*	*% Error*	*Inter-storey Drift*	*% Error*	*Inter-storey Drift*	*% Error*
0	0	0%	0	0%	0	–
3.5m	1.334	5.32%	1.286	8.73%	1.409	–
7m	2.226	5.45%	1.846	12.55%	2.111	–
10.5m	1.608	10.82%	1.231	15.16%	1.451	–

4.4.8 BASE SHEAR-DISPLACEMENT RELATIONSHIP AT JOINTS 2 AND 37
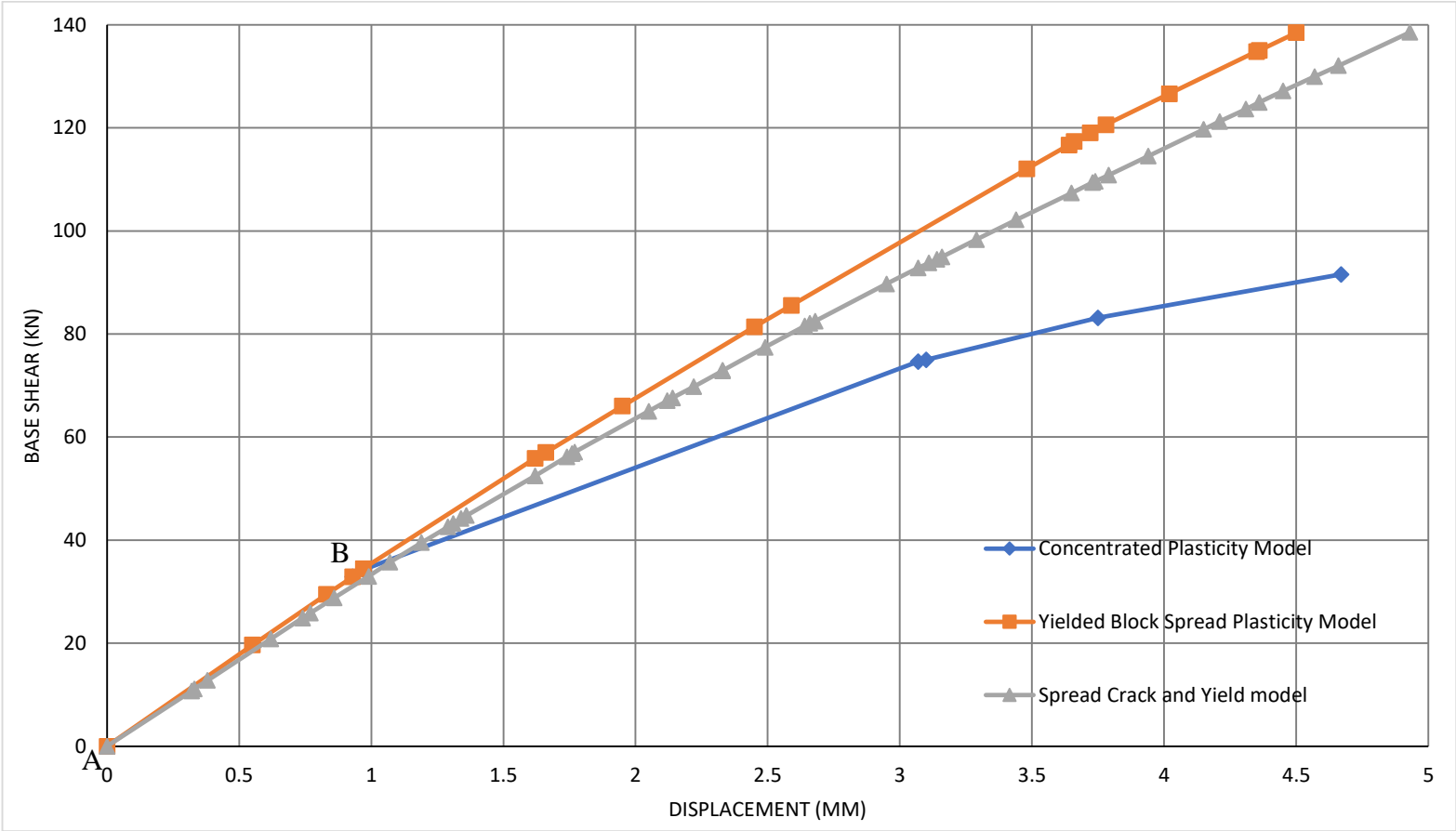
Figure 4-26: Base Shear-Displacement Curves for all three models at joints 2 and 37

Figure 4-25, shows the relationship between base shear and the floor displacement at *joints 2* and *37* on the 1st floor. All models originate at point A and the existing models separate away from that of the proposed spread cracking and yielding block model. Between points A and B, the existing models coincide but separate away from each other at and beyond point B. At this point, both existing models are seen to underestimate the floor displacement by 6.2%.

The concentrated plasticity model underestimates the final floor displacement by 5.27% while the yielded block spread plasticity model underestimates the final floor displacement by 8.72%. However, the concentrated plasticity model underestimates the final base shear by 33.9%. The final base shear for the yielded block spread plasticity model has an almost insignificant 0.06% error.

Table 12: Displacements and their respective margins of error at selected moments for all three models as observed at joints 2 and 37

	Concentrated Plasticity Model		Yielded Block Spread Plasticity Model		Spread cracking and yielding block Model	
Moment	*Displacement*	*% Error*	*Displacement*	*% Error*	*Displacement*	*% Error*
0 kNm	0	0	0	0	0	−
40 kNm	1.268	5.23%	1.138	5.56%	1.205	−
80 kNm	3.5	35.45%	2.404	6.97%	2.584	−

73

4.4.9 Base shear-Displacement Relationship at joints 39 and 74
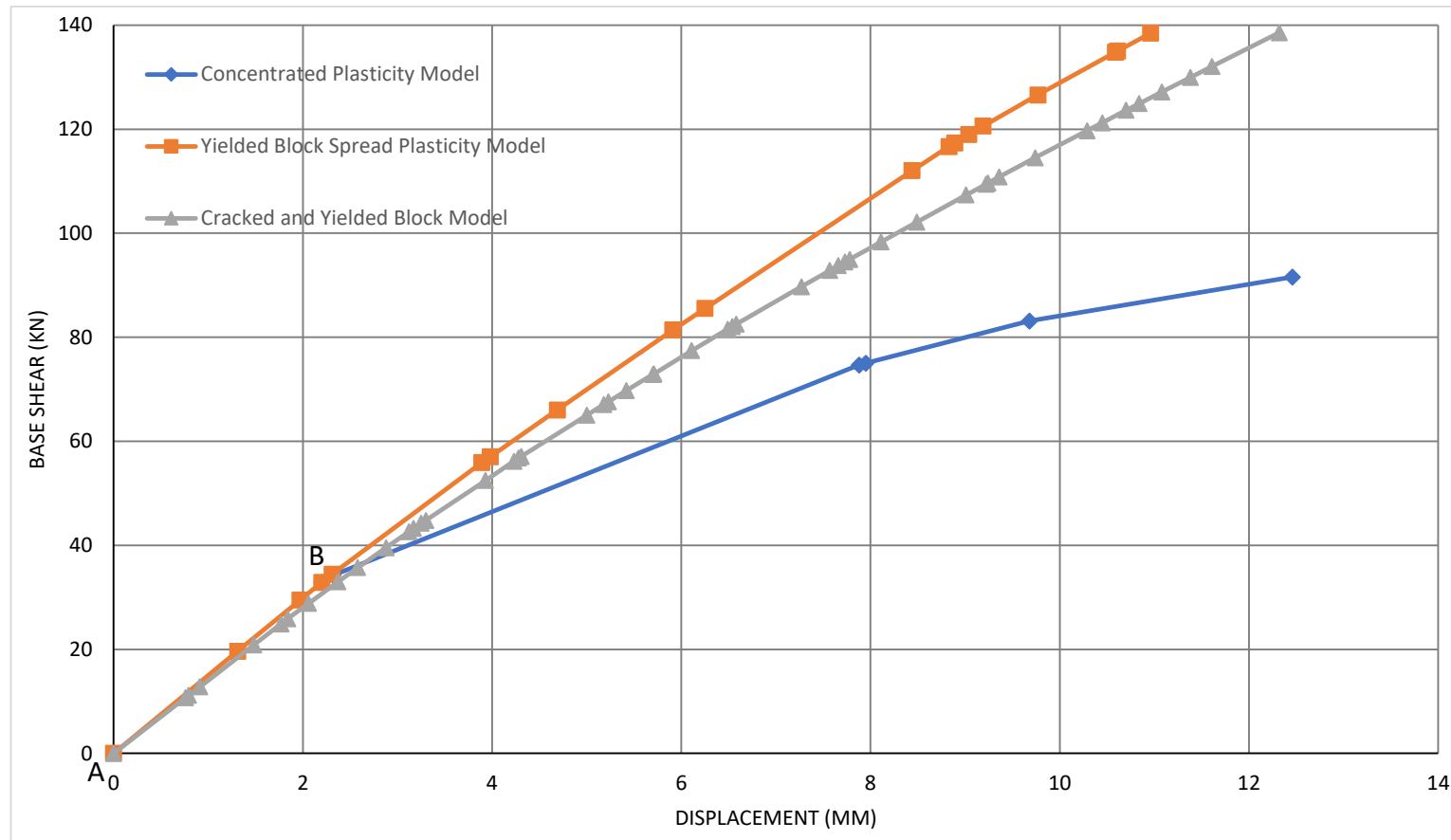
Figure 4-27: Base shear-Displacement curves at joints 39 and 74 for all three models

Figure 4-26, shows the relationship between base shear and the floor displacement at *joints 39* and *74* on the 2ⁿᵈ floor. The existing models separate from the proposed spread cracking and yielding block model immediately after the origin at point A because they ignore cracking. Yielding in the existing models is initiated at point B where the concentrated plasticity model separates away from the yielded block spread plasticity model. At this point, both existing models underestimate the floor displacement by 6.9%. The concentrated plasticity model overestimates the final floor displacement by 1.14% while the yielded block spread plasticity model underestimates the final floor displacement by 11.04%.

Whereas the concentrated plasticity model overestimates the final floor displacement, the base shear causing the displacement is overly underestimated by up to 33.9%. Errors in predicting the final base shear when using the yielded block spread plasticity model are at 0.06% and thus can be considered negligible.

Errors at *joint 74* are higher for all models as compared to those at *joint 39* save for the final floor displacement by the yielded block spread plasticity model. The errors arising out of using the concentrated plasticity model reduce across the beam from 5.3% at *joint 74* to 1.1% at *joint 39*. At the initiation of yielding in the existing models, errors in accuracy increase from 15.7% at *joint 74* to 4.44% at *joint 39*.

Below is a table showing a comparative analysis of Floor displacements and the respective errors for selected moments for the different models at *Joints 2 and 37*.

Table 13: Displacements and their respective margins of error at selected moments for all three models as observed at joints 39 and 74

	Concentrated Plasticity Model		Yielded Block Spread Plasticity Model		Spread cracking and yielding block Model	
Moment	*Displacement*	*% Error*	*Displacement*	*% Error*	*Displacement*	*% Error*
0 *kNm*	0	0	0	0	0	−
40 *kNm*	3.12	7.32%	2.729	6.12%	2.907	−
80 *kNm*	9.024	42.51%	5.799	8.42%	6.332	−

4.4.10 BASE SHEAR-DISPLACEMENT CURVES AT JOINTS 75 AND 110
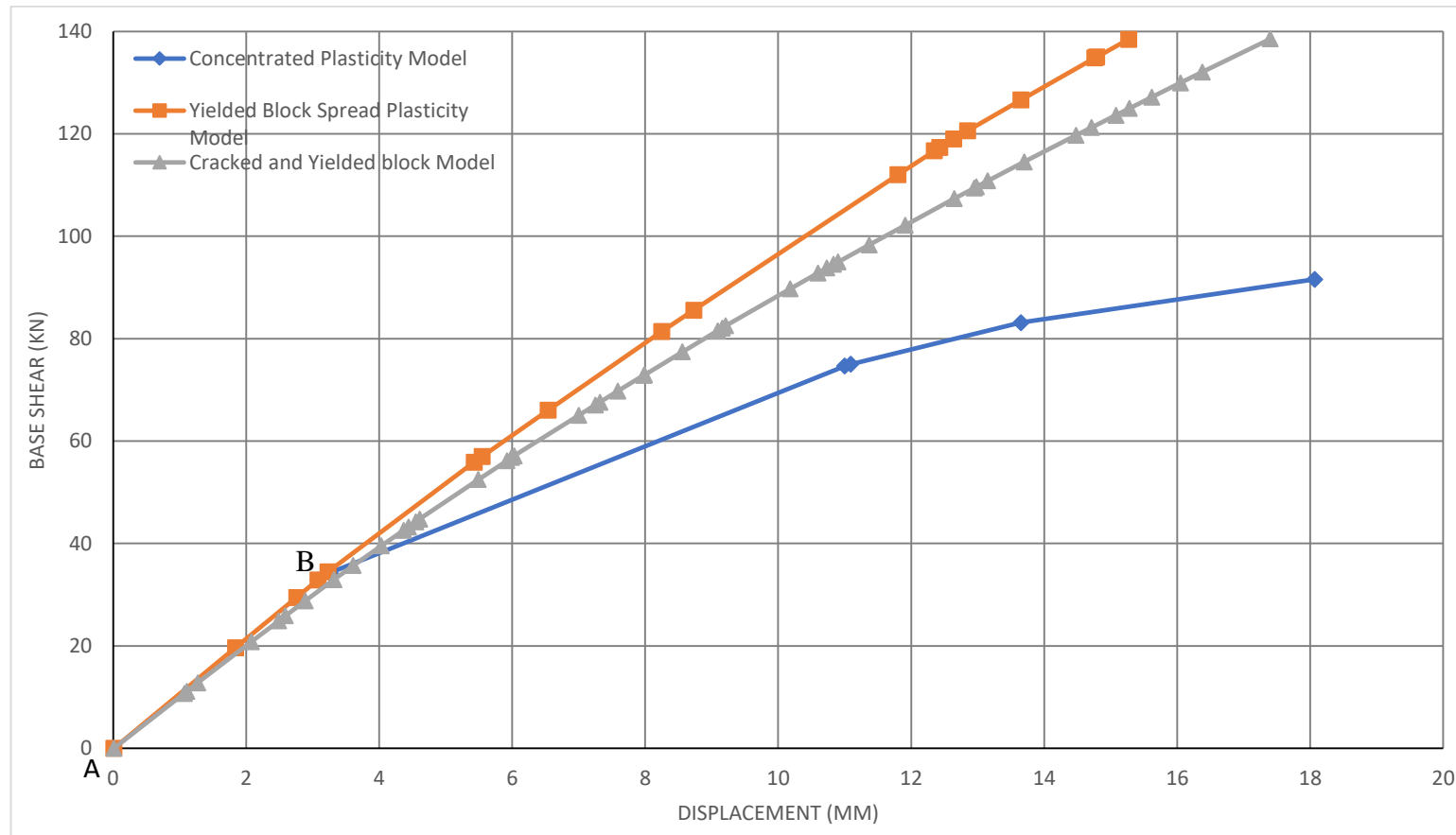
Figure 4-28: Base Shear-Displacement Curves at joints 75/110 for all three models

Figure 4-27, shows the relationship between base shear and displacement at the end joints on the 3rd floor. The existing models deviate away from the proposed model just after the origin at point A. A similar trend can be seen at the 1st and 2nd floors in Figures 4-25 and 4-26 respectively. Point B marks the initiation of yielding in both existing models. At the same point, the curve for the concentrated plasticity model separates away from that of the yielded block spread plasticity model a trend that is consistent with that of both the 1st and 2nd floors. Both existing models underestimate the floor displacement at point B by 7.18% showing a slight increment in errors as compared to the 2nd floor. The concentrated plasticity model overestimates the final floor displacement by 3.85% while underestimating the final base shear by 33.9%. The yielded block spread plasticity model underestimates the final floor displacement by 12.2% and to a much lesser extent the final base shear is underestimated by 0.06% which is consistent with findings from the two under lying floors, i.e. 1st and 2nd floor.

Table 14: Displacements and their respective margins of error at selected moments for all three models as observed at joints 75 and 110

	Concentrated Plasticity Model		Yielded Block Spread Plasticity Model		Spread cracking and yielding block Model	
Moment	*Displacement*	*% Error*	*Displacement*	*% Error*	*Displacement*	*% Error*
0 kNm	0	0	0	0	0	—
40 kNm	4.36	6.8%	3.799	6.93%	4.082	—
80 kNm	12.664	42.42%	8.093	8.99%	8.892	—

4.4.11   GENERAL DISCUSSION

In the yielded block spread plasticity model, yielding in the span occurs in the 1st storey beam. Seven blocks yield in the span accounting for about $1400mm(20\%)$ of the entire 1st storey beam length. The 2nd and 3rd storey beams yield only at the end joints under hogging moments. Four elastic blocks $(800mm)$ yield under hogging in both the 1st and 2nd storey beams and one elastic block $(200mm)$ yields in the 3rd storey beam. All three models experience 1st yield at node 74 on the 2nd storey beam. Both the yielded block spread plasticity model and the proposed model reach ultimate moment at *node 37*.

For the proposed model, there is no yielding in the span. Plasticity zones are formed at the beam ends under hogging moments. Both the 1st and 2nd storey beams each have four blocks $(800mm)$ that reach yield while the 3rd storey beam has two blocks $(400mm)$ that reach yield. Using the proposed model reduces plasticity on the 1st storey beam and increases plasticity on the 3rd storey beam. With the proposed model, beams are seen to crack extensively in both the spans and the beam ends. Twenty-four blocks $(4800mm)$ crack along the span of the 1st storey beam. This accounts for approximately 68.6% of the entire 1st storey beam length. Similarly, Twenty-two $(4400mm)$ and twenty-one blocks $(4200mm)$ crack along the spans of the 2nd and 3rd storey beams respectively. This accounts for 62.9% and 60% of the 2nd and 3rd storey beam lengths respectively. The 1st and 2nd storey beams each has five cracked blocks$(1000mm)$ while the 3rd storey beam has two cracked blocks$(400mm)$ at the beam ends accounting for $14.3\%, 14.3\%$ and 5.7% of the beam lengths on the $1^{st}, 2^{nd}$ and 3rd storeys respectively. In both the yielded block spread plasticity and the

proposed model, plasticity reduces with increase in storey height. Yielding is exhibited in both the span and at end joints at all levels of the structural frame when the concentrated plasticity model is applied to the frame.

The curve for the proposed model separates from the existing models almost immediately the push over analysis is initiated. Cracking in the beam starts to occur at mid span under gravity loads even before lateral loads are applied to the frame. Fourteen blocks $(2800mm)$, twelve blocks $(2400mm)$ and sixteen blocks $(3200mm)$ cracked at mid span in the 1st, 2nd, and 3rd storey beams respectively before the application of lateral loads representing 40%, 34.29% and 45.71% of the respective beam lengths.

The yielded block spread plasticity model generally exhibits more plasticity in the frame as compared to the proposed model. By the conclusion of the analysis of the three storey structural frame, the yielded block spread plasticity model registers up to fifteen (15) yielded blocks $(3000mm)$ in the entire frame while the proposed model only registers ten (10) yielded blocks representing a reduction in plasticity.

4.5 COMPARISON OF PROPOSED AND EXISTING MODELS WITH EXPERIMENTAL RESULTS

4.5.1 EXPERIMENTAL TESTS BY (BHABHA ATOMIC RESEARCH CENTRE, 2012)

In this section, the efficacy of the proposed model is indirectly evaluated by comparing theoretical base shear-displacement plots with experimental data in the literature. Experimental results provided by (Bhabha Atomic Research Centre, 2012) are used. A real-life RC frame structure was tested under monotonically increasing lateral pushover loads, in a parabolic pattern, till failure. The structure consisting of three stories and two bays along both orthogonal directions was gradually pushed in small increments of load and the corresponding displacements were monitored continuously, leading to the pushover curve for the structure.

(i)   Description of structure

The structure under consideration is a three-storey structure with a beam and column size of 150mm × 200mm and a slab thickness is 100mm. The average concrete strength, reinforcement yield stress and ultimate stress were 34 MPa, 478 MPa, and 665 MPa respectively.
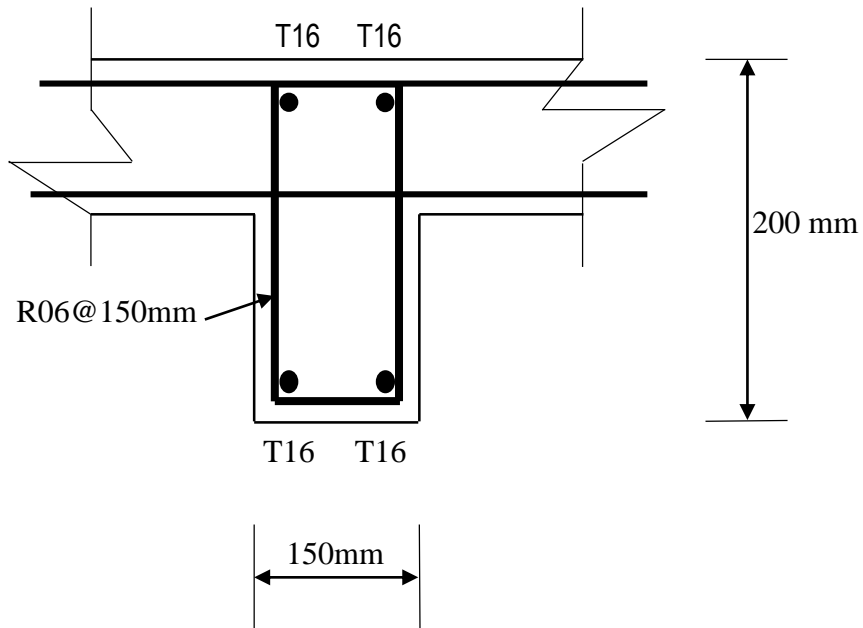
Figure 29: Beam Section
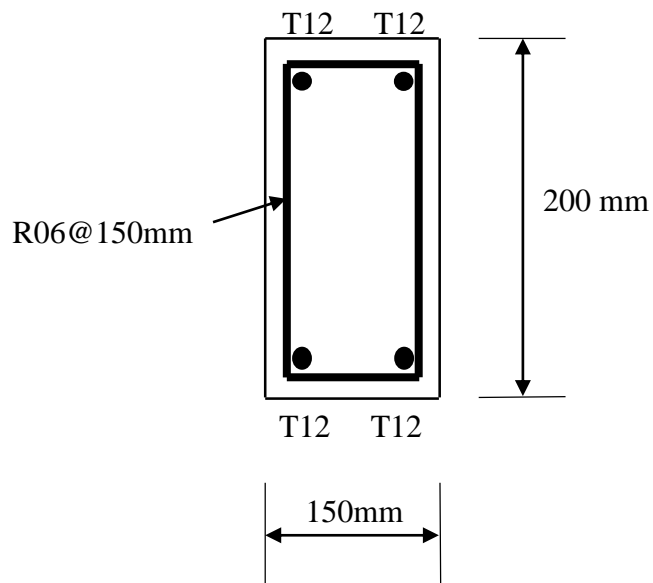
Figure 30: Column section
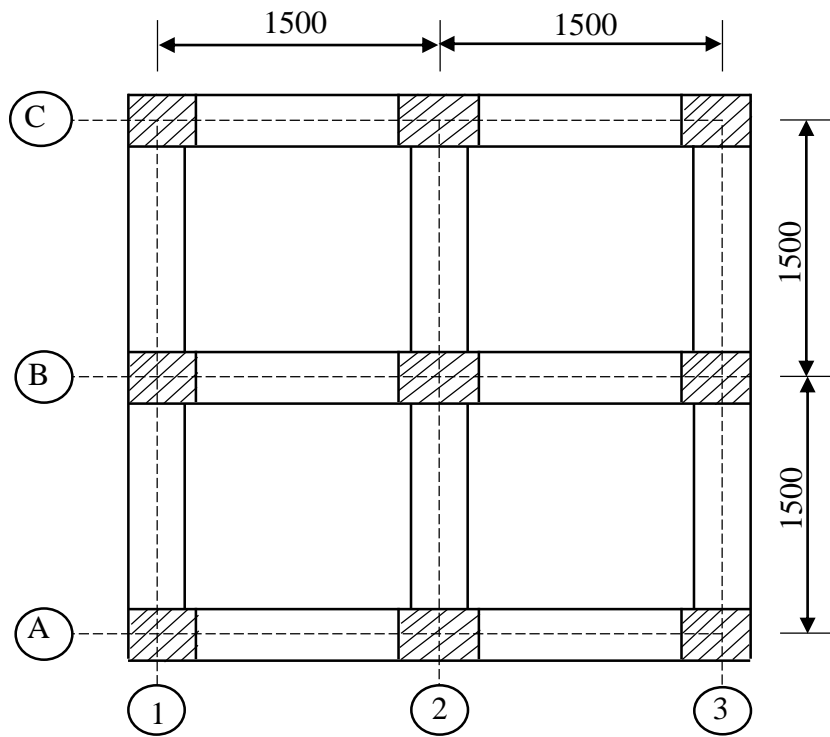
Figure 40: Column and Beam layout
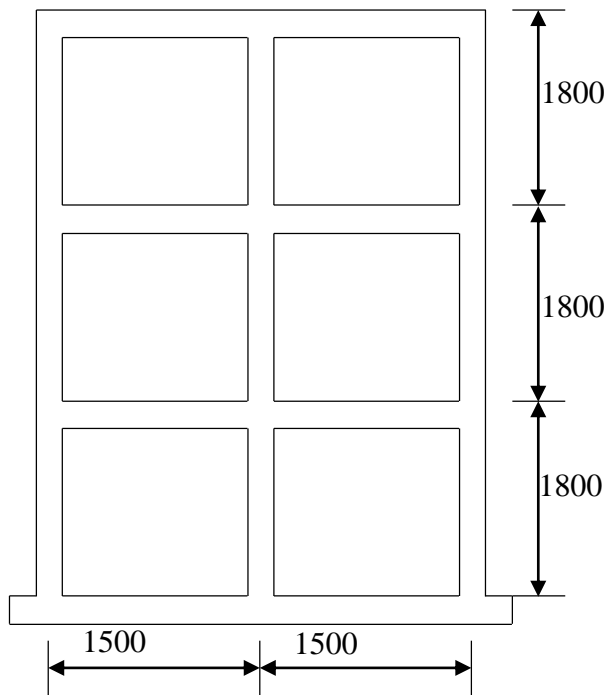
Figure 32: Sectional Elevation of the frame

Figure 27, shows the experimental setup of the structure. Additional masses of 0.54 tons were kept on each floor. Static loads were applied through hydraulic jacks at three levels of the structure in a predefined parabolic pattern with a load ratio of P, 4P, 9P for 1st floor, 2nd floor and 3rd floor respectively. Hydraulic jacks were connected to the heavy-duty reaction wall on one end and to the structure on the other end via calibrated load cell and heavy distribution beam.

The load on the structure at different floor levels was measured using load cells and the corresponding displacements were measured with the help of theodolites and Linear Variable Differential Transformers (LVDTs).

Figure 33: Experimental setup of the structure
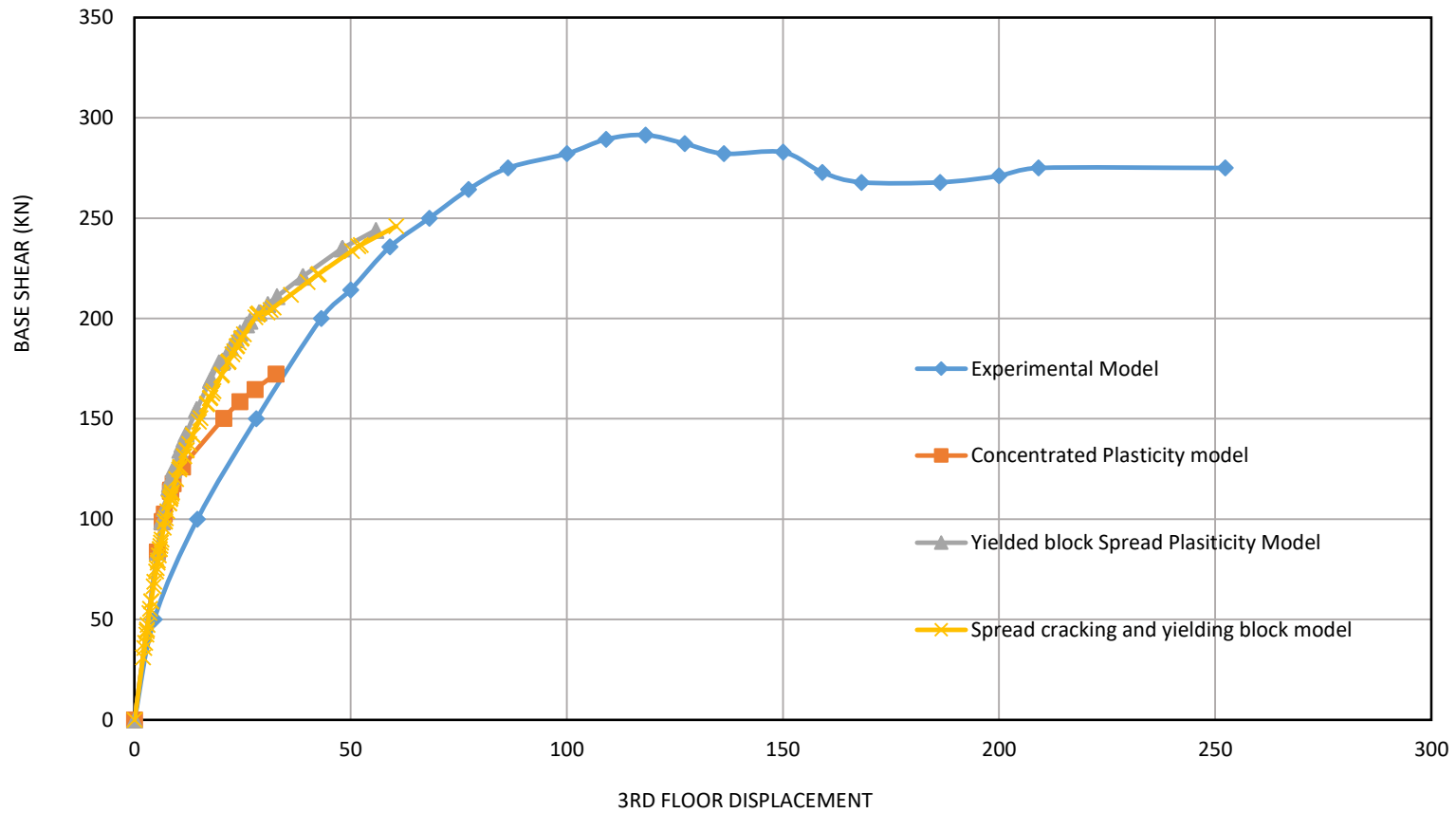
Figure 34: Base shear - displacement plot for the 3rd-floor

Theoretical and experimental base shear–displacement curves for the 3rd-floor are shown in Figure 29. Curves for the 1st and 2nd floor follow a similar trend. The base shears and displacements by each model are compared with the results from the experimental model and margins of error are computed as a measure of reliability for each of the theoretical models.

At the ultimate, the base shear is underestimated by 37.32%, 11.32%, and 10.56% by the concentrated plasticity model, the yielded block spread plasticity model and the proposed spread cracking and yielded block model respectively.

At the ultimate, the 3rd-floor displacements are grossly underestimated by 87.03%, 77.83%, and 76.01% for the concentrated plasticity model, the yielded block spread plasticity model and the proposed spread cracking and yielded block model respectively.

The errors in floor displacement observed in the theoretical models are mostly due to the assumption that the columns are assumed to remain elastic and as such undermine the flexibility induced in the structure due to column degradation at joints due to sway.

CHAPTER FIVE: CONCLUSION AND RECOMMENDATIONS

The aim of this study was to determine the effect of considering cracking during modelling on the accuracy of deflections, joint rotations, and inter-storey drift ratios in reinforced concrete structures from the initiation of loading up to peak values. It aimed at demonstrating the contribution of the proposed model and to gain understanding of its behaviour and performance. Two case studies were considered. Both cases involved subjecting structural frames to pushover analysis. The 1st case involved a single bay single storey frame while the 2nd case involved a three storey single bay frame.

5.1 CONCLUSION

5.1.1 SINGLE STOREY SINGLE BAY FRAME

It was found that the proposed model greatly improves the accuracy of estimating deformations.

A comparison between the proposed model and the yielded block spread plasticity model at *joint 2* shows that there is an increment in accuracy of the rotational, displacement, and moment capacities of 31.8%, 13.72%, and 4.07% while at *joint 37* an improvement in accuracy of the rotational, displacement, and moment capacities of 23.81%, 13.2%, and 0% were observed. The lateral load capacity of the frame also improved by 6.26%.

A comparison between the proposed model and the concentrated spread plasticity model at *joint 2* shows that there was an increment in accuracy of the rotational, displacement, and moment capacities of 63.64%, 56.86%, and 43.05% while at *joint 37* there was an improvement in accuracy of the rotational, displacement, and moment capacities of 52.38%, 56.32%, and 64.32%. The lateral load capacity of the frame also increases by 55.56%.

5.1.2 THREE STOREY SINGLE BAY FRAME

It was also found that the proposed model greatly improves the accuracy of estimating deformations.

A comparative analysis of the deformations given by both the proposed model and the yielded block spread plasticity model, indicates an improvement in the accuracy of estimating rotational capacities by 66.67% at some joints, while the accuracy of estimating moment capacities improves by 37.2% at some joints. The improvement in accuracy of estimating floor displacements, inter-storey drift ratios, and lateral load capacities of the frame is negligible.

A similar comparison of the deformations given by both the proposed model and the concentrated plasticity model, indicates an improvement in the accuracy of estimating rotational capacities by 150% at some joints, while the accuracy of estimating moment capacities improves by 102.98% at some joints. The improvement in accuracy of estimating floor displacements and inter-storey drift ratios is negligible. The accuracy of the lateral load capacity of the frame improves by 33.9%.

5.2 RECOMMENDATIONS

Cracking in the beam increases flexibility (reduces stiffness) of the beam and thus should be considered during pushover analysis of RC structures. The margins of error in the inter-storey drift ratio are seen to increase with increase in storey height.

P-delta effects, effects of shear and interface bond-slip we're not considered in this research and thus this research can be furthered in these areas.

The difference between the theoretical models and the experimental model is because the theoretical models assume that the columns do not crack or yield yet in the actual experiment the column is subject to both phenomena. The effect of cracking and yielding of the column is recommended for further research.

ANNEX

ANNEX A: COMPUTATION OF THE CRACKING MOMENTS AND CURVATURES

The cracking moment is the bending moment of a section when the concrete fibre under tensile stresses equals the modulus of rupture of the concrete. The modulus of rupture F_t is the tensile strength determined from a flexural test. Kyakula (2010)

$$F_t = 1.4 \left({f_c}/{10} \right)^{2/3}$$

Where.

f_c = Characteristic strength of concrete in compression

The strain at rupture ε_{ct} is given by.

$$\varepsilon_{ct} = {F_t}/{E_c}$$

E_c = Modulus of elasticity of concrete

$f_c = 25 MPa, E_c = 31,000 MPa$

$$F_t = 1.4x \, {25}/{10}^{2/3} = 2.58 \, N/mm^2$$

$$\varepsilon_{ct} = {2.58}/{31000} = 0.00008323$$

A.1   HOGGING CRACKING MOMENT AND CURVATURES

Depending on the beam dimensions, the reinforcement layout and amounts, the neutral axis may be in the flange or in the web. In this case, the neutral axis is in the flange as can be seen in the appendix.

Consider the T beam section shown in figure A-1 below

A_{sb} = Area of reinforcement at the bottom of the beam

A_{st} = Area of reinforcement at the top of the beam

h = Overall height of the beam

h_f = Depth of the flange

y = Depth of the neutral axis from the outer most concrete compressive fibre

ε_{cc} , ε_{cf} , ε_{ct} Refer to the strain in concrete at the outer most compressive fibre, at the in bottom of the flange and at cracking

σ_{cc}, σ_{ct} Refer to the stress in concrete at outer most compressive fibre and at cracking

b = Effective flange width

n = Ratio of the modulus of elasticity of steel to that of concrete, $n = {E_s}/{E_c}$

d_{sb} , d_{st} Refer to the effective depth to the reinforcement at the bottom and top respectively

d_b' , d_t' Refer to the cover depth to the centre of the reinforcement at the bottom and the top respectively

h_f the depth of the flange

Figure A-1: Stress and strain distribution diagram for concrete section at cracking under the action of hogging moments, with the neutral axis in the flange

It is assumed that before cracking, the stress distribution across a section is triangular as shown in the figure above

From the strain diagram we have.

$$\frac{\varepsilon_{ct}}{(h-y)} = \frac{\varepsilon_{cc}}{y} = \frac{\varepsilon_{sc}}{(y-d'_b)} = \frac{\varepsilon_{st}}{(h-y-d'_t)} = \frac{\varepsilon_{cf}}{(h_f+y-h)}$$

The neutral axis depth y is found by the first moment of area of the steel and concrete about the outermost compressive fibre by the total area of the section. This is given in the equation below.

$$y = \frac{0.5b_w h^2 + (b-b_w)h_f(h-0.5h_f) + (n-1)A_{sb}d'_b + (n-1)A_{st}(h-d'_t)}{b_w h + h_f(b-b_w) + (n-1)A_{sb} + (n-1)A_{st}}$$

$$b_w = 300mm, h = 500mm, b = 2480mm, h_f = 200mm, A_{st} = 942.48mm^2,$$

$$A_{sb} = 603mm^2, d_b' = 25 + 8 = 33mm, d_t' = 25 + 10 = 35mm,$$

$$E_s = 200,000 \ N/mm^2, E_c = 31,000 \ N/mm^2, n = {E_s}/{E_c} = {200,000}/{31,000}$$

$$= 6.45$$

y

$$= \frac{\begin{array}{c} 0.5x300x500^2 + (2480 - 300)x200x(500 - 0.5x200) + (6.45 - 1)x603x33 \\ + \\ (6.45 - 1)x942.48x(500 - 35) \end{array}}{300x500 + 200x(2480 - 300) + (6.45 - 1)x603 + (6.45 - 1)x942.48}$$

$$y = 360.68mm$$

The tensile force in concrete T_c is given by

$$T_c = 0.5b(h - y)\varepsilon_{ct}E_c$$

$$T_c = 0.5x2480x(500 - 360.68)x0.00008323x31,000$$

$$T_c = 445,507.27N$$

The tensile force in steel T_s, is given by

$$T_s = \left(\frac{n-1}{n}\right)A_{st}\left(\frac{h-y-d_t'}{h-y}\right)\varepsilon_{ct}E_s$$

$$T_s = \left(\frac{6.45-1}{6.45}\right)x942.48x\left(\frac{500-360.68-35}{500-360.68}\right)x0.00008323x200,000$$

$$T_s = 9,921.38N$$

The compressive force in steel is given by

$$C_s = \left(\frac{y - d_b'}{h - y}\right) \varepsilon_{ct} E_s A_{sb} \left(\frac{n - 1}{n}\right)$$

$$C_s = \left(\frac{360.68 - 33}{500 - 360.68}\right) x0.00008323x200,000x603x \left(\frac{6.45 - 1}{6.45}\right)$$

$$C_s = 19,938.97N$$

To simplify the calculation of the compressive force in concrete, the concrete section is divided into two parts A and B.

Part A is the central part of width b_w, and depth y equal to the depth of the neutral axis.

Part B of width $(b - b_w)$, and depth $(h_f + y - h)$, equal to the depth of the flange below the neutral axis.

The compressive force in concrete part A is given by

$$C_{CA} = 0.5 b_w y \left(\frac{y}{h - y}\right) \varepsilon_{ct} E_c$$

$$C_{CA} = 0.5x300x360.68x \left(\frac{360.68}{500 - 360.68}\right) x0.00008323x31,000$$

$$C_{CA} = 361,198.85N$$

The compressive force in concrete part B is given by

$$C_{CB} = 0.5(b - b_w)(h_f + y - h)\left(\frac{h_f + y - h}{h - y}\right) \varepsilon_{ct} E_c$$

$$C_{CB} = 0.5x(2480 - 300)x(200 + 360.68$$

$$- 500)x \left(\frac{200 + 360.68 - 500}{500 - 360.68}\right) x0.00008323x31,000$$

$$C_{CB} = 74{,}290.83N$$

The cracking moment M_{cr} is obtained by summing the moments of all these forces about the neutral axis. Thus, the cracking moment is given by

$$M_{cr} = C_{CA}\left(\frac{2}{3}y\right) + C_{CB}\left[\frac{2}{3}(h_f + y - h)\right] + C_s(y - d_b') + T_C\left[\frac{2}{3}(h - y)\right]$$
$$+ T_s(h - y - d_t')$$

$$M_{cr} = 360003.38x\left(\frac{2}{3}x360.38\right) + 73{,}435.6x\left[\frac{2}{3}(200 + 360.38 - 500)\right]$$

$$+ 26524.198x(360.38 - 33) + 446694.81\left[\frac{2}{3}(500 - 360.38)\right]$$

$$+ 13244.124x(500 - 360.38 - 35)$$

$$M_{cr} = 138{,}804{,}095Nmm = 138.8kNm$$

At the onset of cracking, the moment of inertia considered is the gross moment of inertia I_g. This is given by.

$$I_g = \frac{b_w h^3}{12} + b_w h(0.5h - y)^2 + \frac{(b - b_w)h_f^3}{12} + (b - b_w)h_f\left(h - y - 0.5h_f\right)^2$$
$$+ (n - 1)A_{sb}(y - d_b')^2 + (n - 1)A_{st}(h - y - d_t')^2$$

$$I_g = \frac{300x500^3}{12} + 300x500x(0.5x500 - 360.38)^2 + \frac{(2480 - 300)x200^3}{12}$$

$$+ (2480 - 300)x200x(500 - 360.38 - 0.5x200)^2$$

$$+ (6.45 - 1)x603x(360.38 - 33)^2$$

$$+ (6.45 - 1)x942.48x(500 - 360.38 - 35)^2$$

$$I_g = 7{,}498{,}814{,}987mm^4$$

The cracking curvature $\emptyset_{cr}$ is given by.

$$\emptyset_{cr} = \frac{M_{cr}}{I_g E_c} = \frac{138,804,095}{7,498,814,987 x 31,000} = 0.000000597$$

A.2 SAGGING CRACKING MOMENT AND CURVATURE

Consider the section shown the figure A-2 below, with the terms as defined in figure A-1.
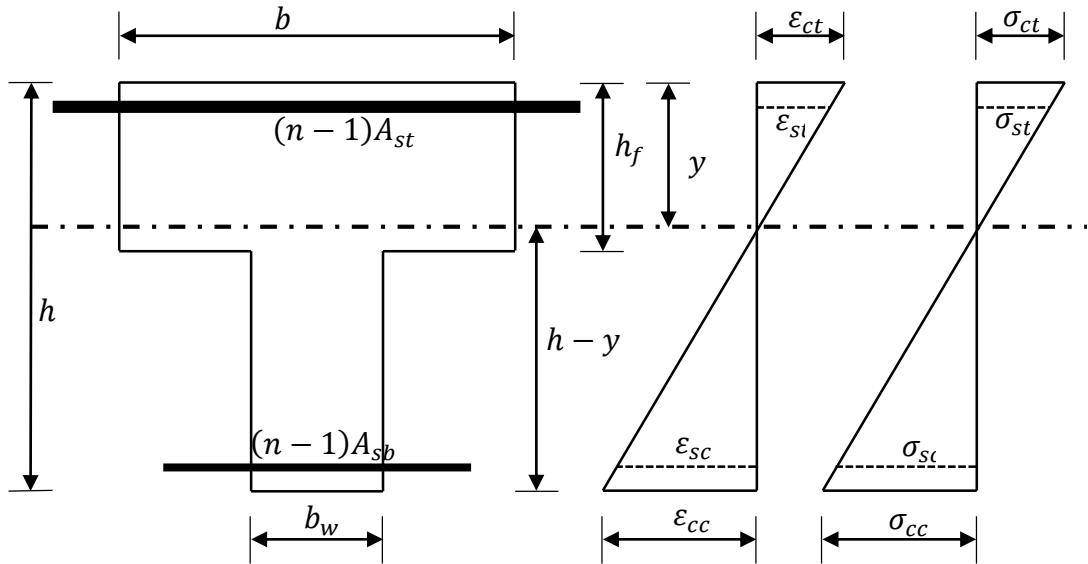
Figure A-2: Stress and strain distribution diagram for concrete section at cracking under the action of sagging moments, with the neutral axis in the flange

The strains are given by:

$$\frac{\varepsilon_{ct}}{h-y} = \frac{\varepsilon_{cc}}{y} = \frac{\varepsilon_{sb}}{h-y-d_b'} = \frac{\varepsilon_{st}}{y-d_t'} = \frac{\varepsilon_{cf}}{h_f - y}$$

The depth y of the neutral axis is found by dividing the first moments of the concrete and the steel areas taken about the outermost compressive fibre by the area of the section.

$$y = \frac{0.5b_w h^2 + 0.5(b - b_w)h_f^2 + (n - 1)A_{sb}(h - d_b') + (n - 1)A_{st}d_t'}{b_w h + (b - b_w)h_f + (n - 1)A_{sb} + (n - 1)A_{st}}$$

$$y = \frac{\begin{array}{c}0.5x300x500^2 + 0.5(2480 - 300)x200^2 + (6.45 - 1)x603x(500 - 33) + \\ (6.45 - 1)x942.48x35\end{array}}{300x500 + (2480 - 300)x200 + (6.45 - 1)x603 + (6.45 - 1)x942.48}$$

$$y = 139.32mm$$

The compressive force in concrete is given by

$$C_c = 0.5by\left(\frac{y}{h - y}\right)\varepsilon_{ct}E_c$$

$$C_c = 0.5x2480x139.32x\left(\frac{139.32}{500 - 139.32}\right)x0.00008323x31{,}000$$

$$C_c = 172{,}085N$$

The compressive force in the reinforcement is given by

$$C_s = \left(\frac{n - 1}{n}\right)A_{st}\left(\frac{y - d_t'}{h - y}\right)\varepsilon_{ct}E_s$$

$$C_s = \left(\frac{6.45 - 1}{6.45}\right)x942.48x\left(\frac{139.32 - 35}{500 - 139.32}\right)x0.00008323x200{,}000$$

$$C_s = 3{,}832N$$

The tension force in the steel reinforcement is given by

$$T_s = \left[\frac{n - 1}{n}\right]A_{sb}\left(\frac{h - y - d_b'}{h - y}\right)\varepsilon_{ct}E_c$$

$$T_s = \left[\frac{6.45 - 1}{6.45}\right]x603x\left(\frac{500 - 139.32 - 33}{500 - 139.32}\right)x0.00008323x31{,}000$$

$T_s = 1,194N$

The tension force in concrete is calculated in two parts; A and B. Part A consists of the tensile force that acts on the web of width b_w and depth $(h - y)$. Part B consists of the tension force that acts on the parts of the flange under tension. It acts on the flange parts of width $(b - b_w)$ and depth $(h_f - y)$.

Tensile force on part A of concrete in tension is given by

$T_{CA} = 0.5 b_w (h - y) \varepsilon_{ct} E_c$

$T_{CA} = 0.5 x 300 x (500 - 139.32) x 0.00008323 x 31,000$

$T_{CA} = 139,520N$

The tensile force on part B of concrete in tension is given by

$$T_{CB} = 0.5(b - b_w)(h_f - y)\left(\frac{h_f - y}{h - y}\right) \varepsilon_{ct} E_c$$

$$T_{CB} = 0.5(2480 - 300) x (200 - 139.32) x \left(\frac{200 - 139.32}{500 - 139.32}\right) x 0.00008323 x 31,000$$

$T_{CB} = 28,696N$

The cracking moment M_{cr} is found by calculating moments of the forces about the neutral axis.

$$M_{cr} = C_c \left(\frac{2}{3}y\right) + C_s(y - d_t') + T_s(h - y - d_b') + T_{CA}\left[\frac{2}{3}(h - y)\right]$$
$$+ T_{CB}\left[\frac{2}{3}(h_f - y)\right]$$

$$M_{cr} = 173{,}060.46x \left(\frac{2}{3}x139.32 \right) + 5{,}131.1x(139.32 - 35)$$

$$+ 1{,}592.8x(500 - 139.32 - 33) + 139{,}474.09 \left[\frac{2}{3}(500 - 139.32) \right]$$

$$+ 28{,}450.74 \left[\frac{2}{3}(200 - 139.32) \right]$$

$$M_{cr} = 51{,}483{,}065 Nmm = 51.48 kNm$$

At the onset of cracking, the moment of inertia considered is the gross moment of inertia I_g. This is given by.

$$I_g = \frac{b_w h^3}{12} + b_w h(0.5h - y)^2 + \frac{(b - b_w)h_f^3}{12} + (b - b_w)h_f \left(y - 0.5h_f \right)^2$$

$$+ (n - 1)A_{sb}(h - y - d_b')^2 + (n - 1)A_{st}(y - d_t')^2$$

$$I_g = \frac{300x500^3}{12} + 300x500x(0.5x500 - 139.32)^2 + \frac{(2480 - 300)x200^3}{12}$$

$$+ (2480 - 300)x200x(139.32 - 0.5x200)^2$$

$$+ (6.45 - 1)x603x(500 - 139.32 - 33)^2$$

$$+ (6.45 - 1)x942.48x(139.32 - 35)^2$$

$$I_g = 7{,}498{,}814{,}987 mm^4$$

The cracking curvature $\emptyset_{cr}$ is given by.

$$\emptyset_{cr} = \frac{M_{cr}}{I_g E_c} = \frac{51{,}483{,}065}{7{,}498{,}814{,}987x31{,}000} = 0.0000002215$$

Table 15: Summary of section moments and curvatures

		Moment(Nmm)	Curvature	Depth of neutral axis
Cracking	*Sagging*	51,483,065	$4.6x10^{-8}$	$139.32mm$
	Hogging	138,804,095	$5.61x10^{-7}$	$360.68mm$
Yield	*Sagging*	119,156,955.89	$5.67755x10^{-6}$	$36.8957mm$
	Hogging	152,200,307.79	$7.07229x10^{-6}$	$116.7869mm$
Ultimate	*Sagging*	179,560,984.17	$9.58848x10^{-6}$	$35.2619mm$
	Hogging	261,829,126.8	$1.19294x10^{-5}$	$115.0770mm$

ANNEX B: STRESS – STRAIN RELATIONSHIP FOR BOTH STEEL AND CONFINED CONCRETE

B.1   STRESS -STRAIN CURVE FOR CONCRETE

The Park, Priestly and Gill (1982) model shall be used to represent the behaviour of confined concrete because it is based on adequate number of experimental data and it is simple (Kyakula, 2010). The model of the stress-strain relationship consists of an ascending parabolic branch, the descending linear branch and a constant stress linear portion as shown in figure A-3.
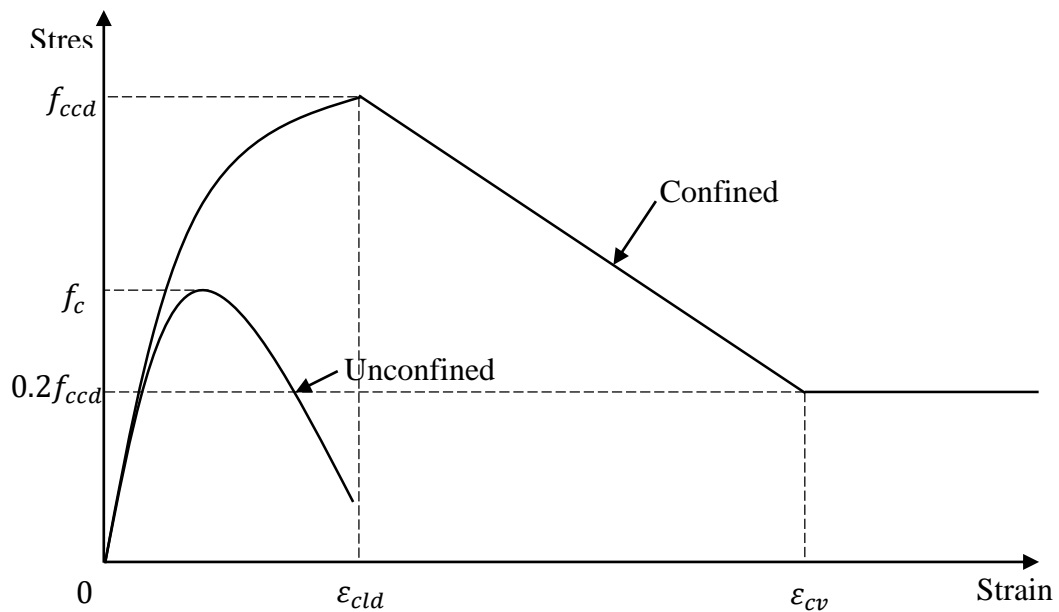
Figure A-3: Stress-strain diagram for confined concrete

The ascending branch of stress-strain curve is Hognestad's parabola, given by

$$\sigma_{cc} = f_{ccd} \left[\frac{2\varepsilon_{cc}}{\varepsilon_{cld}} - \left(\frac{\varepsilon_{cc}}{\varepsilon_{cld}} \right)^2 \right]$$

Where

f_{ccd} is the maximum dynamic stress of confined concrete

ε_{cld} is the strain corresponding to maximum stress

σ_{cc} is the compressive stress in concrete corresponding to a compressive strain ε_{cc}.

The descending branch of confined concrete under dynamic loading is given by:

$$\sigma_{cc} = f_{ccd}[1 - Z(\varepsilon_{cc} - \varepsilon_{cld})] \tag{a}$$

Where

$$Z = \frac{0.5}{\varepsilon_{cc50} - \varepsilon_{cld}}$$

ε_{cc50} is the strain corresponding to 50% f_{ccd} and is given by

$$\varepsilon_{cc50} = \frac{3 + 0.29f_c}{145f_c - 1000} + 0.75\rho_w \left(\frac{b_c}{s}\right)^{\frac{1}{2}}$$

ρ_w - the volumetric ratio of hoops defined with respect to the outside perimeter of hoops

s - the spacing of the hoops

b_c - the size of the square confined core measured to the centroid of the peripheral hoop. For a beam section, where the hoops are normally rectangular, it is proposed to assume a square section with the same perimeter of hoops.

The volumetric ratio ρ_w is given by Equation (2.4),

$$\rho_w = 0.5(\rho_{sx} + \rho_{sy})$$

Where

$$\rho_{sx} = \frac{5.41A_b}{h_c s} \quad , \quad \rho_{sy} = \frac{3.41A_b}{b_c s}$$

$$A_b = \frac{\pi \emptyset^2}{4} = \frac{\pi \times 8^2}{4} = 50.3mm^2$$

$$h_c = h - 2xcover - \emptyset = 500 - 2x25 - 8 = 442mm$$

$$b_c = b_w - 2xcover - \emptyset = 300 - 2x25 - 8 = 242mm$$

$$s = 200mm$$

$$\rho_{sx} = \frac{5.41x50.3}{442x200} = 0.003$$

$$\rho_{sy} = \frac{3.41x50.3}{242x200} = 0.0035$$

$$\rho_w = 0.5(\rho_{sx} + \rho_{sy}) = 0.5x(0.003 + 0.0035) = 0.00325$$

$$\varepsilon_{cc50} = \frac{3 + 0.29f_c}{145f_c - 1000} + 0.75\rho_w \left(\frac{b_c}{s}\right)^{\frac{1}{2}}$$

$$\varepsilon_{cc50} = \frac{3 + 0.29x25}{145x25 - 1000} + 0.75x0.00325x \left(\frac{242}{200}\right)^{\frac{1}{2}}$$

$$\varepsilon_{cc50} = 0.0066$$

Confinement index K, is given by Equation (2.1)

$$K = 1 + \partial \left(\rho_w \frac{f_{yw}}{f_c}\right)^b = 1 + 1.0x \left(0.00325x\frac{250}{25}\right)^{0.75} = 1.077$$

From equation (2.3)

$$E_{co} = 2.15x10^4 \left(\frac{25}{10}\right)^{\frac{1}{3}} = 29179.99$$

From equation (2.2)

$$\varepsilon_{cl} = \frac{2x25}{29179.99} = 0.0017$$

$$\varepsilon_{ccl} = K^2\varepsilon_{cl} = 1.077^2x0.0017 = 0.002$$

$$\bar{\varepsilon}_{cd} = \frac{0.01 + 0.02}{2} = 0.015$$

From equation (2.11)

$$\varepsilon_{cld} = 0.002x \left(\frac{0.015}{3x10^{-5}}\right)^{0.02} = 0.0023$$

$$f_{cc} = Kf_c = 1.077x25 = 26.925$$

From equation (2.10)

$$a_s = \left(\frac{1}{5 + 0.9x26.925}\right) = 0.035$$

From equation (2.9)

$$f_{ccd} = 26.925x \left(\frac{0.02}{3x10^{-5}}\right)^{1.026x0.035} = 33.63$$

From equation (2.4)

$$Z = \frac{0.5}{\varepsilon_{cc50} - \varepsilon_{cld}} = \frac{0.5}{0.0066 - 0.0023} = 116.28$$

The ultimate strain of concrete ε_{cu}, is defined based on the $0.85f_c$, along the descending branch of the stress-strain curve. Where f_c is the strength of unconfined concrete

$$\varepsilon_{cu} = \varepsilon_{cld} + \frac{K - 0.85}{ZK}$$

$$\varepsilon_{cu} = 0.0023 + \frac{1.077 - 0.85}{116.28x1.077} = 0.0041$$

The constant stress branch of the stress-strain relationship is given by

$$\sigma_{cc} = 0.2f_{ccd} \qquad\qquad\qquad (b)$$

$$\sigma_{cc} = 0.2x33.63 = 6.726\,N/mm^2$$

The strain ε_{cv} at which the constant stress branch starts is found by setting $\varepsilon_{cv} = \varepsilon_{cc}$ in equation and equating equation (a) and (b) and solving for ε_{cv} is given by;

$$\varepsilon_{cv} = \frac{0.8}{Z} + \varepsilon_{cld} = \frac{0.8}{116.28} + 0.0023 = 0.0092$$

B.2 THE STRESS- STRAIN RELATIONSHIP FOR STEEL

The stress strain relationship for steel is shown in Figure A-4.

In the Figure A-4:

ε_y - the yield strain

ε_{sh} - the strain at the end of the plastic region plateau or start of the strain hardening

ε_{su} - the ultimate strain
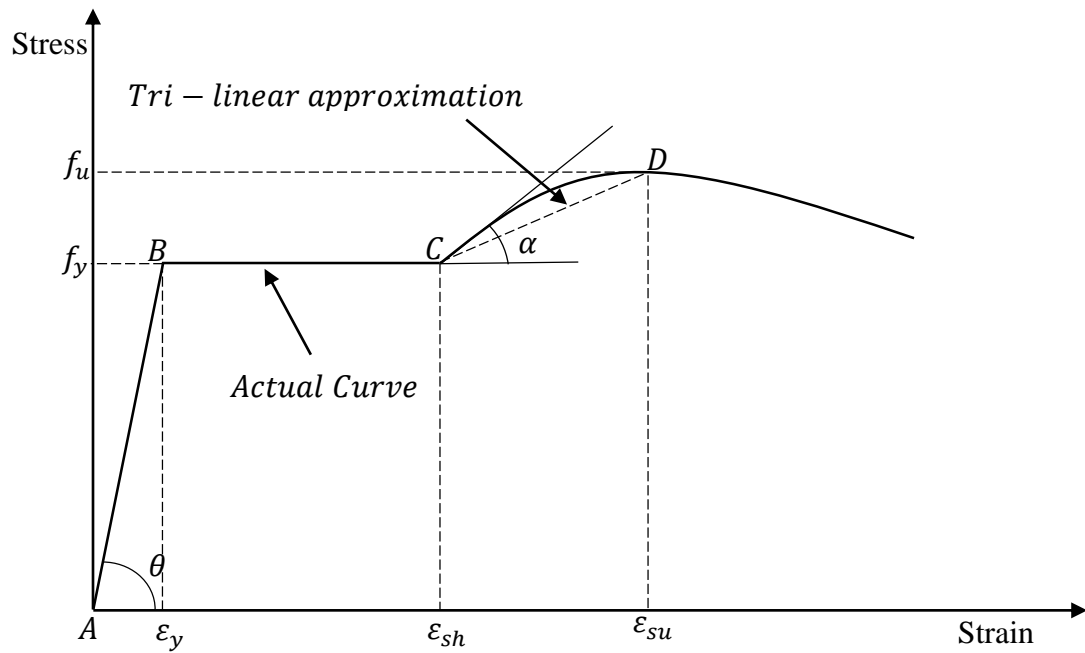
Figure A-4: Stress- Strain Curve for steel reinforcement

f_y - the yield stress

f_u - the ultimate stress

The curve consists of an elastic region AB, whose slope $Tan\theta = E_s$, the modulus of elasticity of steel. A plastic region BC, stretching from ε_y to ε_{sh} follows. Lastly, a strain hardening region CD. A tri-linear approximation is used in this research. Unloading and reloading before and after yielding follows a path parallel to the elastic curve.

ANNEX C: YIELD AND ULTIMATE MOMENTS WITH THE CORRESPONDING CURVATURES

C.1 INTRODUCTION

The rectangular stress block used for calculating the moment in most codes is a simplification of the assumption that the behaviour of concrete is represented by a parabolic stress-strain relationship up to a strain ε_{co}, then the strain increases with a constant stress up to an ultimate strain of 0.0035,Kyakula (2010).

According to Kyakula (2010), the rectangular stress block is not considered accurate for analysis of a confined concrete section under dynamic loading because:

a) Confinement and the dynamic loading increase the concrete strain

b) Confinement and dynamic loading also increase the concrete stress

c) The rectangular stress block assumes that at the time of yielding of the tension reinforcement, the concrete has reached its ultimate stress. This may not be the case, depending on the section dimensions, concrete strength, and area of tension reinforcement.

d) After the ultimate stress has been reached, the stress reduces uniformly as the strain increases, then becomes constant at 20% of the maximum stress.

Thus, the stress-strain relationship shown in Figure A-5 is used to calculate the yield and ultimate moments and their corresponding curvatures.

The moment curvature relationships are calculated for both the sagging and hogging bending moments, considering whether the neutral axis is in the web or flange and

whether the strain at the outer most concrete fibre has exceeded ε_{cld}, ε_{cv}, given in Figure A-5.

In the following section, formulae for various forces, moments, and curvatures acting on a section shall be simply stated, the derivation of which can be sourced from Kyakula (2010).

C.2 SAGGING MOMENTS AND CURVATURES

(i) Compressive force in concrete when the neutral axis is in the flange

The strain and stress distribution diagrams across the section under sagging moments with neutral axis in the flange is shown in Figure A-5.
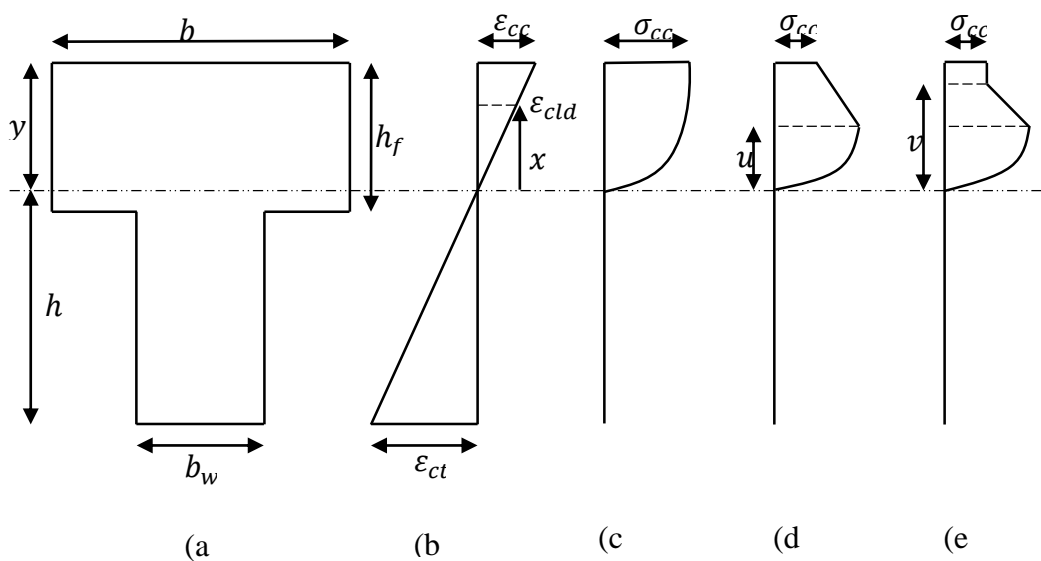
Figure A-5: Strain and stress distribution after cracking for a section under sagging moment with the neutral axis in the flange

b is the flange width

b_w is the web width

h the overall depth of the section

h_f is the flange depth

ε_{ct} Refers to the tensile strain

ε_{cc} Refers to the maximum compressive strain

σ_{cld} Refers to the maximum stress

σ_{cc} Refers to the compressive stress in the outer most layer of concrete

ε_{cld} Refers to the strain corresponding to the maximum stress

y Refers to the depth of the neutral axis

The stress-strain relationship is as shown in Figure A-5. The stress diagram changes under increasing strain as shown in Figure 6-5 (c), (d) and (e). the strain diagram is shown in Figure A-5 (b).

The stress diagram (c) corresponds to a case where the maximum compressive strain in concrete ε_{cc}, is less than the strain ε_{cld}, corresponding to the maximum stress.

Stress diagram (d) corresponds to a case where the maximum compressive strain in concrete ε_{cc} , is greater than the strain ε_{cld} , corresponding to the maximum stress, but less than the strain ε_{cv} at which the stress becomes constant.

Stress diagram (e) corresponds to the case where the maximum compressive strain in concrete ε_{cc} , is greater than the strain ε_{cv} , at which the stress becomes constant.

(ii)   Determination of the neutral axis y at yield:

The neutral axis is the point where the compressive and tensile forces are equal. For a given yield strain in steel, the neutral axis is obtained as follows:

The compressive force C is obtained by adding the compressive force C_c in concrete to the compressive force C_s in steel.

$$C = C_c + C_s$$

The tensile force in concrete at yield or ultimate stress shall be neglected because it is small compared to the other forces. Only the tensile force T_s in steel is to be considered.

Starting at a depth y_1 equal to the depth of the compression steel from the outer most compressive fibre, forces C_c, C_s and T_s shall be computed. The tensile force shall then be subtracted from the compressive force to get a difference ΔTC_1.

$$\Delta TC_1 = C - T_s$$

The value of y_1 shall then be increased by a small amount Δy to give a new depth y_2 as shown in equation (3.26).

For the value of y_2, the forces C_c, C_s and T_s shall be computed. Typical values for Δy shall be $0.0001m$ as was considered by (Kyakula, 2010).

The tensile force shall again be subtracted from the compressive forces to get a tolerance ΔTC_2 and the previous value of y_2 and ΔTC_2 renamed y_1 and ΔTC_1 respectively.

$$y_2 = y_1 + \Delta y \tag{3.26}$$

$$\Delta TC_2 = C - T_s \tag{3.27}$$

$$y_1 = y_{2(previous)}$$

$$\Delta TC_1 = \Delta TC_{2(previous)}$$

The process is to be continued up to a depth equal to half the overall depth. $y_2 = 0.5h$

Figure 0-6: Difference ΔTC between compressive and tensile force for incremental depth Δy at the neutral axis

Except of a single increment of Δy, if the tensile force is not equal to the compressive force, the product $(\Delta TC_1.\Delta TC_2)$ is always positive because both ΔTC_1 and ΔTC_2 are either positive or negative. When the tensile force is equal to the compressive force the product $(\Delta TC_1.\Delta TC_2)$ is zero. The exception occurs when depth y_1 is less and y_2 is greater than the neutral axis depth y. Then ΔTC_2 and ΔTC_1 have opposite signs and the product $(\Delta TC_1.\Delta TC_2)$ is negative. Therefore, the neutral axis depth is found by tracing the point at which the difference between the tensile and compressive forces changes signs. This is done by interpolation as shown in equation (3.28).

$$y = y_2 - \Delta y \left(\frac{\Delta TC_2}{\Delta TC_2 - \Delta TC_1} \right) \tag{3.28}$$

The computations were carried out in excel spread sheets and the summary below for the neutral axis was extracted.

By interpolation

36.8	4,587,476.32
y	0
36.9	-206,691.49

$$y = y_2 - \Delta y \left(\frac{\Delta TC_2}{\Delta TC_2 - \Delta TC_1}\right) = 36.9 - 0.1x \left(\frac{-206691.49}{-206691.49 - 4587476.32}\right)$$

$$= 36.896mm$$

(iii)   Compressive forces in concrete at yield

The yield moment and curvature are assumed to be the point at which the reinforcement under tension reaches yield strain.

At yield, the tensile strain in steel ε_{st} is 0.0023 for $f_y = 460\,N/mm^2$ steel. According to Kyakula (2010), the corresponding strain at the outer most compressive fibre in concrete ε_{cc} is given by:

$$\varepsilon_{cc} = \left(\frac{y}{d-y}\right)\varepsilon_{st}$$

$$y = 36.896mm,$$

$$d = h - cover - \frac{1}{2}\emptyset = 500 - 25 - 8 = 442mm$$

$$\varepsilon_{cc} = \left(\frac{36.896}{442 - 36.896}\right)x0.0023 = 0.00021 < \varepsilon_{cld} = 0.0023$$

Considering case (c), that is the strain does not exceed that corresponding to the maximum stress, then the compressive force is given by:

$$C_c = byf_{ccd}\left[\frac{\varepsilon_{cc}}{\varepsilon_{cld}} - \frac{1}{3}\left(\frac{\varepsilon_{cc}}{\varepsilon_{cld}}\right)^2\right] \qquad (3.3)$$

$$b = 2480mm, y = 36.896mm, f_{ccd} = 33.63\,N/mm^2, \varepsilon_{cc} = 0.00021,$$

$$\varepsilon_{cld} = 0.0023$$

$$C_c = 2480x36.896x33.63x\left[\frac{0.00021}{0.0023} - \frac{1}{3}\left(\frac{0.00021}{0.0023}\right)^2\right] = 275,834.93N$$

The depth of the point of action $\bar{y}$, of the compressive force in concrete C_c, from the neutral axis is given by:

$$C_c\bar{y} = by^2 f_{ccd}\left[\frac{2}{3}\left(\frac{\varepsilon_{cc}}{\varepsilon_{cld}}\right) - \frac{1}{4}\left(\frac{\varepsilon_{cc}}{\varepsilon_{cld}}\right)^2\right] \qquad (3.6)$$

$$C_c\bar{y} = 2480x36.896^2x33.63x\left[\frac{2}{3}\left(\frac{0.00021}{0.0023}\right) - \frac{1}{4}\left(\frac{0.00021}{0.0023}\right)^2\right]$$

$$= 6,757,621.53Nmm$$

$$\bar{y} = \frac{C_c\bar{y}}{C_c}$$

$$\bar{y} = \frac{6,757,621.53}{275,834.93} = 24.5mm$$

(iv)   Tensile and compressive force in reinforcement

When the reinforcement under tension (bottom reinforcement) reaches yield strain ε_y, the tensile force in concrete is zero, since concrete will have cracked, (Kyakula, 2010)

The tensile force in the reinforcement T_s is given by:

113

$$T_s = f_y A_{sb}$$

Where

$$f_y = 460\ N/mm^2, \qquad A_{sb} = 603mm^2$$

$$T_s = 460x603 = 277{,}380N$$

If at or after yielding of the tensile steel, the compression steel has not reached the yield strain, the compressive force in the reinforcement under compression at the top is obtained by considering the strain relationships from the strain diagram.

$$\frac{\varepsilon_{sy}}{h - y - d'_b} = \frac{\varepsilon_{st}}{y - d'_t}$$

d'_b, d'_t the cover to the centreline of the bottom and top reinforcement respectively

ε_{st} the strain in the top reinforcement

The force in the compression reinforcement is given by:

$$C_s = \left(\frac{n - 1}{n}\right) A_{st} \left(\frac{y - d'_t}{h - y - d'_b}\right) \varepsilon_y E_s$$

$n = 6.452, A_{st} = 942.48mm^2, y = 36.896mm, d'_t = 35mm, d'_b = 33mm, \varepsilon_y$

$$= 0.0023,$$

$$E_s = 200000\ N/mm^2, h = 500mm$$

$$C_s = \left(\frac{6.452 - 1}{6.452}\right) x942.48x \left(\frac{36.896 - 35}{500 - 36.896 - 33}\right) x0.0023x200000 = 1614.94N$$

114

(v)   *Neutral axis at ultimate moment*

The neutral axis at ultimate shall be found the same way as outlined for the neutral axis at yield moment except that an Ultimate stress $f_u = 690.8\,N/mm^2$ and steel strains ranging from 0.0024 to 0.15 shall be considered. The yield strain for $f_y = 460\,N/mm^2$ is 0.0023. The neutral axis depth shall be determined based on the following:

a) The neutral axis depth shall be greater than the depth to the compression reinforcement

b) The neutral axis depth shall be smaller than that of the yield moment

c) The ultimate moment shall be greater than the yield moment

d) The ultimate curvature shall be greater than the yield curvature.

The highest moment to satisfy conditions (a) to (d) shall be the ultimate moment and its corresponding curvature and neutral axis depth as the ultimate curvature and neutral axis depth at ultimate moment.

The computations were carried out in excel spread sheets and the summary below for the neutral axis was extracted.

By interpolation

35.2	1,909,719.96
y	0
35.3	-1,176,236.34

$$y = y_2 - \Delta y \left(\frac{\Delta T C_2}{\Delta T C_2 - \Delta T C_1} \right) = 35.3 - 0.1x \left(\frac{-1276354.45}{-1276354.45 - 2323660.04} \right)$$

$$y = 35.262mm$$

At ultimate stress, the tensile strain in steel ε_{st} ranging from 0.0024 to 0.15 shall be considered for $f_u = 690.8\,N/mm^2$ steel. According to Kyakula (2010), the corresponding strain at the outer most compressive fibre in concrete ε_{cc} is given by:

$$\varepsilon_{cc} = \left(\frac{y}{d - y} \right) \varepsilon_{st}$$

$$y = 35.262mm,$$

$$d = h - cover - \frac{1}{2}\emptyset = 500 - 25 - 8 = 442mm$$

$$\varepsilon_{cc} = \left(\frac{35.262}{442 - 35.262} \right) x0.039 = 0.00034 < \varepsilon_{cld} = 0.00225$$

Considering case (c), that is the strain does not exceed that corresponding to the maximum stress, then the compressive force is given by:

$$C_c = byf_{ccd} \left[\frac{\varepsilon_{cc}}{\varepsilon_{cld}} - \frac{1}{3} \left(\frac{\varepsilon_{cc}}{\varepsilon_{cld}} \right)^2 \right] \tag{3.3}$$

$$b = 2480mm, y = 35.262mm, f_{ccd} = 33.63\,N/mm^2, \varepsilon_{cc} = 0.014, \varepsilon_{cld} = 0.0023,$$

$$C_c = 2480x35.262x33.63x \left[\frac{0.00034}{0.00225} - \frac{1}{3} \left(\frac{0.00034}{0.00225} \right)^2 \right] = 417,141.67N$$

The depth of the point of action $\bar{y}$, of the compressive force in concrete C_c, from the neutral axis is given by:

$$C_c \bar{y} = by^2 f_{ccd} \left[\frac{2}{3} \left(\frac{\varepsilon_{cc}}{\varepsilon_{cld}} \right) - \frac{1}{4} \left(\frac{\varepsilon_{cc}}{\varepsilon_{cld}} \right)^2 \right]$$

(3.6)

$$C_c \bar{y} = 2480 x 35.262^2 x 33.63 x \left[\frac{2}{3} \left(\frac{0.00034}{0.00225} \right) - \frac{1}{4} \left(\frac{0.00034}{0.00225} \right)^2 \right] = 9,743,588.92 Nm$$

$$\bar{y} = \frac{C_c \bar{y}}{C_c}$$

$$\bar{y} = \frac{9,741,588.92}{417,141.67} = 23.35 mm$$

(vii)   Tensile and compressive force in reinforcement

When the reinforcement under tension (bottom reinforcement) reaches yield strain ε_y, the tensile force in concrete is zero, since concrete will have cracked, (Kyakula, 2010)

The tensile force in the reinforcement T_s is given by:

$$T_s = f_u A_{sb}$$

Where

$$f_u = 690.8 \, N/mm^2, \qquad A_{sb} = 603 mm^2$$

$$T_s = 690.8 x 603 = 416,552.4 N$$

If at or after yielding of the tensile steel, the compression steel has not reached the yield strain, the compressive force in the reinforcement under compression at the top is obtained by considering the strain relationships from the strain diagram.

$$\frac{\varepsilon_{sy}}{h - y - d_b'} = \frac{\varepsilon_{st}}{y - d_t'}$$

d_b', d_t' the cover to the centreline of the bottom and top reinforcement respectively

ε_{st} the strain in the top reinforcement

The force in the compression reinforcement is given by:

$$C_s = \left(\frac{n-1}{n}\right) A_{st} \left(\frac{y - d_t'}{h - y - d_b'}\right) \varepsilon_u E_s$$

$n = 6.452, A_{st} = 942.48mm^2, y = 35.262mm, d_t' = 35mm, d_b' = 33mm, \varepsilon_u$

$$= 0.0039,$$

$E_s = 200000 \, N/mm^2, h = 500mm$

$$C_s = \left(\frac{6.452-1}{6.452}\right) x942.48x \left(\frac{35.262-35}{500-35.262-33}\right) x0.0039x200000 = 376.80N$$

(viii)   Determination of the section moment capacity

The yield and ultimate moments are to be computed by taking moments about the centreline of the tensile steel reinforcement. The lever arm Z_c, to the compressive force in concrete and that to the compressive steel Z_s are given by:

$$Z_c = d_{sb} - y + \bar{y}$$

$$Z_s = d_{sb} - d_t'$$

Equating the compressive and the tensile forces gives the neutral axis depth y.

The moment is given by:

$$M = C_c Z_c + C_s Z_s$$

The yield moment of the section is the moment corresponding to the yield strain in the tensile reinforcement. On the other hand, the determination of the ultimate moment

involves comparing the moment for the current strain value satisfying the four conditions for the ultimate moment with the current ultimate moment.

Yield moment

$$Z_c = d_{sb} - y + \bar{y} = 442 - 36.896 + 24.5 = 429.604mm$$

$$Z_s = d_{sb} - d'_t = 442 - 35 = 407mm$$

$$M_y = C_c Z_c + C_s Z_s = 275{,}834.93 x 429.604 + 1614.66 x 407$$

$$= 119{,}156{,}955.89 Nmm$$

Ultimate moment

$$Z_c = d_{sb} - y + \bar{y} = 442 - 35.262 + 23.35 = 430.088mm$$

$$Z_s = d_{sb} - d'_t = 442 - 35 = 407mm$$

$$M_u = C_c Z_c + C_s Z_s = 417{,}141.67 x 430.088 + 376.8 x 407 = 179{,}560{,}984.17 Nmm$$

(ix)   Determination of curvature

The curvature at yield $\emptyset_y$, and ultimate strain $\emptyset_u$, are respectively given by:

$$\emptyset_y = \frac{\varepsilon_{ccy}}{y}$$

$$\emptyset_u = \frac{\varepsilon_{ccu}}{y}$$

Where,

ε_{ccy} and ε_{ccu} are the concrete strains at the outer most compressive fibre at yield and ultimate moments respectively. Given the value of the tensile steel strain ε_{st} the concrete strain at the outer most compressive fibre is given by:

$$\varepsilon_{cc} = \left(\frac{y}{d-y}\right)\varepsilon_{st}$$

Yield curvature

$$\emptyset_y = \frac{\varepsilon_{ccy}}{y} = \frac{0.000209477}{36.896} = 5.67755x10^{-6}$$

Ultimate curvature

$$\emptyset_u = \frac{\varepsilon_{ccu}}{y} = \frac{0.000338108}{35.262} = 9.58848x10^{-6}$$

C.3 HOGGING MOMENTS AND CURVATURES

The strain and stress diagrams across the section under the action of hogging moments with the neutral axis in the web are shown in Figure A-7.
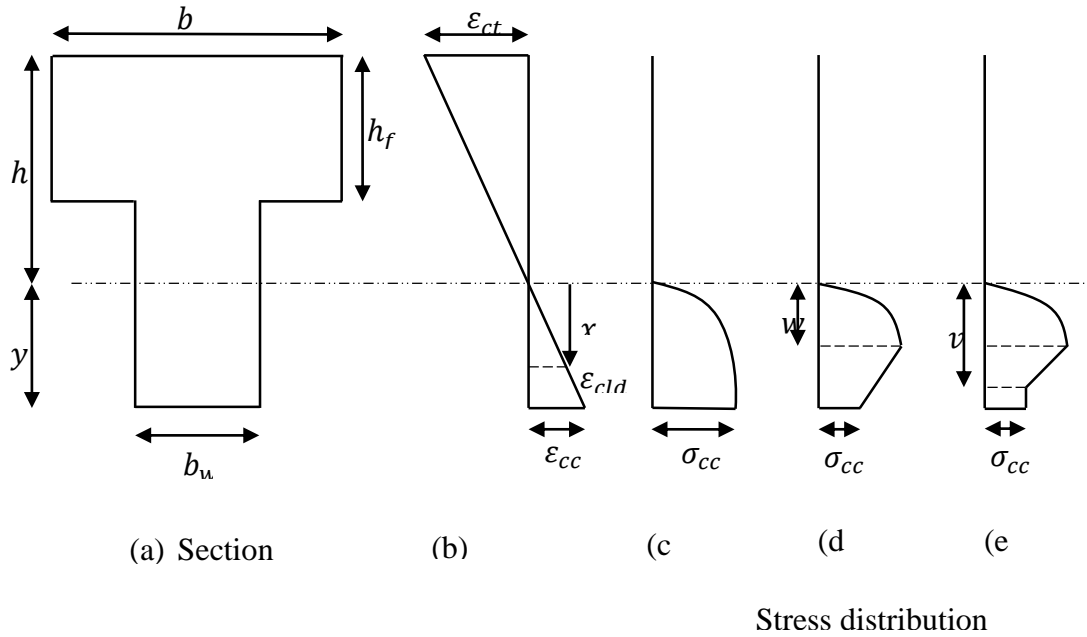
Figure A-7: Strain and stress distribution for a section under hogging moment with the neutral axis in the web

In the Figure A-7:

b refers to the flange width

b_w refers to the web width

h refers to the overall depth of the section

h_f refers to the flange depth

$\varepsilon_{ct}, \varepsilon_{cc}, \sigma_{cld}, \sigma_{cc}$ Refer to the tensile strain, maximum compressive strain, maximum stress, and compressive stress in the outer most layer of concrete, respectively.

ε_{cld} the strain corresponding to the maximum stress

y the depth of the neutral axis

Stress diagram (c) corresponds to a case where the maximum compressive strain in concrete ε_{cc}, is less than the strain ε_{cld}, corresponding to the maximum stress.

Stress diagram (d) corresponds to a case where the maximum compressive strain in concrete ε_{cc}, is greater than the strain ε_{cld}, corresponding to the maximum stress, but less than the strain ε_{cv} at which the stress becomes constant.

(x)   Determination of the neutral axis y at yield:

The neutral axis is the point where the compressive and tensile forces are equal. For a given yield strain in steel, the neutral axis is obtained as follows:

The compressive force C is obtained by adding the compressive force C_c in concrete to the compressive force C_s in steel.

$$C = C_c + C_s$$

The tensile force in concrete at yield or ultimate stress shall be neglected because it is small compared to the other forces. Only the tensile force T_s in steel is to be considered.

Starting at a depth y_1 equal to the depth of the compression steel from the outer most compressive fibre, forces C_c , C_s and T_s shall be computed. The tensile force shall then be subtracted from the compressive force to get a difference ΔTC_1.

$$\Delta TC_1 = C - T_s$$

The value of y_1 shall then be increased by a small amount Δy to give a new depth y_2 as shown in equation (3.26).

For the value of y_2, the forces C_c, C_s and T_s shall be computed. Typical values for Δy shall be $0.0001m$ as was considered by (Kyakula, 2010).

The tensile force shall again be subtracted from the compressive forces to get a tolerance ΔTC_2 and the previous value of y_2 and ΔTC_2 renamed y_1 and ΔTC_1 respectively.

$$y_2 = y_1 + \Delta y \tag{3.26}$$

$$\Delta TC_2 = C - T_s \tag{3.27}$$

$$y_1 = y_{2(previous)}$$

$$\Delta TC_1 = \Delta TC_{2(previous)}$$

The process is to be continued up to a depth equal to half the overall depth. $y_2 = 0.5h$

Except of a single increment of Δy, if the tensile force is not equal to the compressive force, the product $(\Delta TC_1 . \Delta TC_2)$ is always positive because both ΔTC_1 and ΔTC_2 are either positive or negative. When the tensile force is equal to the compressive force the product $(\Delta TC_1 . \Delta TC_2)$ is zero. The exception occurs when depth y_1 is less and y_2 is greater than the neutral axis depth y. Then ΔTC_2 and ΔTC_1 have opposite signs and the product $(\Delta TC_1 . \Delta TC_2)$ is negative. Therefore, the neutral axis depth is found by tracing the point at which the difference between the tensile and compressive forces changes signs. This is done by interpolation as shown in equation (3.28) and illustrated in Figure 3-16.

$$y = y_2 - \Delta y \left(\frac{\Delta TC_2}{\Delta TC_2 - \Delta TC_1} \right) \tag{3.28}$$

123
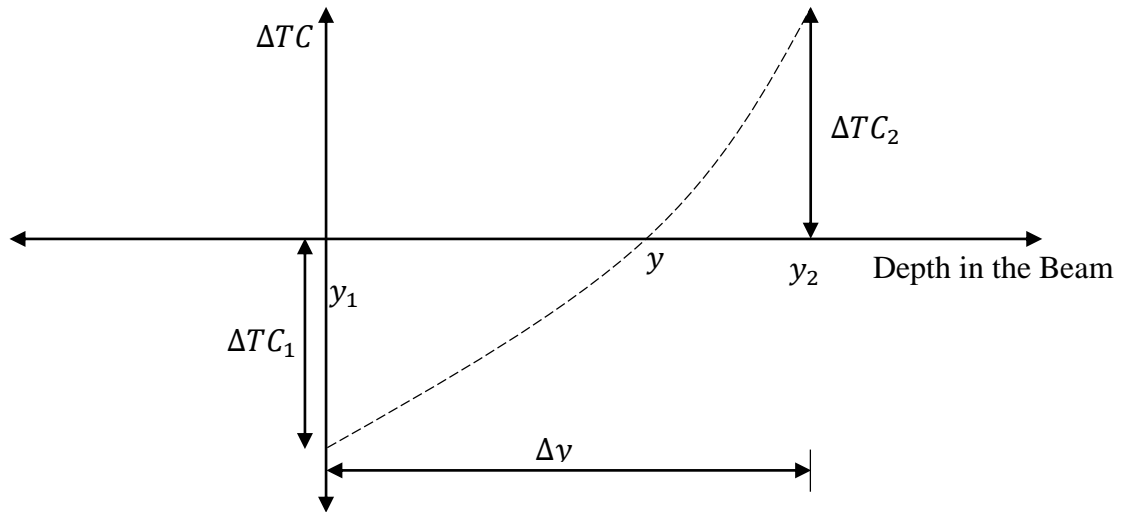
Figure A-9: Difference ΔTC between compressive and tensile force for incremental depth Δy at the neutral axis

The computations were carried out in excel spread sheets and the summary below for the neutral axis was extracted.

By interpolation

116.7	789,666.38
y	0
116.8	-118,610.06

$$y = y_2 - \Delta y \left(\frac{\Delta TC_2}{\Delta TC_2 - \Delta TC_1}\right) = 116.8 - 0.1x \left(\frac{-118610.06}{-118610.06 - 789666.38}\right)$$

$$= 116.79 mm$$

(xi)   Compressive forces in concrete at yield

The yield moment and curvature are assumed to be the point at which the reinforcement under tension reaches yield strain

124

At yield, the tensile strain in steel ε_{st} is 0.0023 for $f_y = 460 \, N/mm^2$ steel. According to Kyakula (2010), the corresponding strain at the outer most compressive fibre in concrete ε_{cc} is given by:

$$\varepsilon_{cc} = \left(\frac{y}{d-y}\right)\varepsilon_{st}$$

$y = 116.79mm,$

$d = h - cover - \frac{1}{2}\emptyset = 500 - 25 - 8 = 442mm$

$$\varepsilon_{cc} = \left(\frac{116.79}{442 - 116.79}\right)x0.0023 = 0.000826 < \varepsilon_{cld} = 0.0023$$

Considering case (c), when the stress does not exceed that corresponding to maximum stress, the compressive force in concrete is given by

$$C_c = b_w y f_{ccd}\left[\frac{\varepsilon_{cc}}{\varepsilon_{cld}} - \frac{1}{3}\left(\frac{\varepsilon_{cc}}{\varepsilon_{cld}}\right)^2\right] \tag{3.31}$$

$b_w = 300mm, y = 116.79mm, f_{ccd} = 33.63 \, N/mm^2, \varepsilon_{cc} = 0.000826, \varepsilon_{cld}$
$$= 0.0023,$$

$$C_c = 300x116.79x33.63x\left[\frac{0.000826}{0.0023} - \frac{1}{3}\left(\frac{0.000826}{0.0023}\right)^2\right] = 377,245N$$

The depth of the point of action $\bar{y}$, of the compressive force in concrete C_c, from the neutral axis is determined as follows:

Considering case (c), where the stress does not exceed that corresponding to the maximum stress,

$$C_c\bar{y} = b_w y^2 f_{ccd}\left[\frac{2}{3}\left(\frac{\varepsilon_{cc}}{\varepsilon_{cld}}\right) - \frac{1}{4}\left(\frac{\varepsilon_{cc}}{\varepsilon_{cld}}\right)^2\right] \tag{3.34}$$

$$C_c\bar{y} = 300x116.79x33.63x\left[\frac{2}{3}\left(\frac{0.00826}{0.0023}\right) - \frac{1}{4}\left(\frac{0.00826}{0.0023}\right)^2\right] = 28,860,431.8 Nmm$$

$$\bar{y} = \frac{C_c\bar{y}}{C_c} = \frac{28,860,431.8}{377,245.13} = 76.50mm$$

(xii)   Neutral axis at ultimate moment

The computations were carried out in excel spread sheets and the summary below for the neutral axis was extracted.

By interpolation

115	1,038,122.55
y	0
115.1	-309,773.57

$$y = y_2 - \Delta y\left(\frac{\Delta TC_2}{\Delta TC_2 - \Delta TC_1}\right) = 115.1 - 0.1x\left(\frac{-309773.57}{-309773.57 - 1038122.55}\right)$$

$$= 115.08mm$$

(xiii)   Compressive forces in concrete at yield

The yield moment and curvature are assumed to be the point at which the reinforcement under tension reaches yield strain

At ultimate stress, the tensile strain in steel ε_{st} ranging from 0.0024 to 0.15 shall be considered for $f_u = 690.8\ N/mm^2$ steel. According to Kyakula (2010), the corresponding strain at the outer most compressive fibre in concrete ε_{cc} is given by:

126

$$\varepsilon_{cc} = \left(\frac{y}{d-y}\right)\varepsilon_{st}$$

$$y = 115.08mm,$$

$$d = h - cover - {}^1\!/_2\,\emptyset = 500 - 25 - 8 = 442mm$$

$$\varepsilon_{cc} = \left(\frac{115.08}{442 - 115.08}\right)x0.0023 = 0.001373 < \varepsilon_{cld} = 0.0023$$

Considering case (c), when the stress doesn't exceed that corresponding to maximum stress, the compressive force in concrete is given by

$$C_c = b_w y f_{ccd}\left[\frac{\varepsilon_{cc}}{\varepsilon_{cld}} - \frac{1}{3}\left(\frac{\varepsilon_{cc}}{\varepsilon_{cld}}\right)^2\right] \tag{3.31}$$

$b_w = 300mm, y = 115.08mm, f_{ccd} = 33.63\,N/mm^2, \varepsilon_{cc} = 0.001373, \varepsilon_{cld}$

$$= 0.0023,$$

$$C_c = 300x115.08x33.63x\left[\frac{0.001373}{0.0023} - \frac{1}{3}\left(\frac{0.001373}{0.0023}\right)^2\right] = 560,888.18N$$

The depth of the point of action $\bar{y}$, of the compressive force in concrete C_c, from the neutral axis is determined as follows:

Considering case (c), where the stress does not exceed that corresponding to the maximum stress,

$$C_c\bar{y} = b_w y^2 f_{ccd}\left[\frac{2}{3}\left(\frac{\varepsilon_{cc}}{\varepsilon_{cld}}\right) - \frac{1}{4}\left(\frac{\varepsilon_{cc}}{\varepsilon_{cld}}\right)^2\right] \tag{3.34}$$

$$C_c\bar{y} = 300x115.08x33.63x\left[\frac{2}{3}\left(\frac{0.001373}{0.0023}\right) - \frac{1}{4}\left(\frac{0.001373}{0.0023}\right)^2\right]$$

$$= 41,659,326.92Nmm$$

$$\bar{y} = \frac{C_c \bar{y}}{C_c} = \frac{41,659,326.92}{560,888.18} = 74.274mm$$

(xiv)   Tensile and compressive force in reinforcement

When the reinforcement under tension (bottom reinforcement) reaches yield strain ε_y , the tensile force in concrete is zero, since concrete will have cracked, (Kyakula, 2010)

The tensile force in the reinforcement T_s is given by:

$$T_s = f_u A_{sb}$$

Where

$$f_u = 690.8 \, N/mm^2, \qquad A_{sb} = 603mm^2$$

$$T_s = 690.8x603 = 416,552.4N$$

If at or after yielding of the tensile steel, the compression steel has not reached the yield strain, the compressive force in the reinforcement under compression at the top is obtained by considering the strain relationships from the strain diagram.

$$\frac{\varepsilon_{sy}}{h - y - d'_b} = \frac{\varepsilon_{st}}{y - d'_t}$$

d'_b, d'_t the cover to the centreline of the bottom and top reinforcement respectively

ε_{st} the strain in the top reinforcement

The force in the compression reinforcement is given by:

$$C_s = \left(\frac{n-1}{n}\right) A_{st} \left(\frac{y - d'_b}{h - y - d'_t}\right) \varepsilon_u E_s$$

128

$$n = 6.452, A_{st} = 603mm^2, y = 35.262mm, d'_t = 35mm, d'_b = 33mm, \varepsilon_u$$

$$= 0.0039,$$

$$E_s = 200000 \, N/mm^2, h = 500mm$$

$$C_s = \left(\frac{6.452 - 1}{6.452}\right) x603x \left(\frac{115.08 - 33}{500 - 115.08 - 35}\right) x0.0039x200000 = 90,433.41N$$

(xv) *Determination of the section moment capacity*

The yield and ultimate moments are to be computed by taking moments about the centreline of the tensile steel reinforcement. The lever arm Z_c, to the compressive force in concrete and that to the compressive steel Z_s are given by:

$$Z_c = d_{sb} - y + \bar{y}$$

$$Z_s = d_{sb} - d'_t$$

Equating the compressive and the tensile forces gives the neutral axis depth y.

The moment is given by:

$$M = C_c Z_c + C_s Z_s$$

The yield moment of the section is the moment corresponding to the yield strain in the tensile reinforcement. On the other hand, the determination of the ultimate moment involves comparing the moment for the current strain value satisfying the four conditions for the ultimate moment with the current ultimate moment.

Yield moment

$$Z_c = d_{sb} - y + \bar{y} = 442 - 116.79 + 76.5 = 401.71mm$$

$$Z_s = d_{sb} - d'_t = 442 - 35 = 407mm$$

$$M_y = C_c Z_c + C_s Z_s = 377{,}245.13 x 401.71 + 1614.66 x 407$$

$$= 152{,}200{,}307.79 Nmm$$

Ultimate moment

$$Z_c = d_{sb} - y + \bar{y} = 442 - 115.08 + 74.27 = 401.19mm$$

$$Z_s = d_{sb} - d'_t = 442 - 35 = 407mm$$

$$M_u = C_c Z_c + C_s Z_s = 560888.18 x 401.19 + 90433.41 x 407$$

$$= 261{,}829{,}126.8 Nmm$$

(xvi)   *Determination of curvature*

The curvature at yield $\emptyset_y$, and ultimate strain $\emptyset_u$, are respectively given by:

$$\emptyset_y = \frac{\varepsilon_{ccy}}{y}$$

$$\emptyset_u = \frac{\varepsilon_{ccu}}{y}$$

Where

ε_{ccy} and ε_{ccu} are the concrete strains at the outer most compressive fibre at yield and ultimate moments, respectively. Given the value of the tensile steel strain ε_{st} the concrete strain at the outer most compressive fibre is given by:

$$\varepsilon_{cc} = \left(\frac{y}{d-y}\right)\varepsilon_{st}$$

Yield curvature

$$\emptyset_y = \frac{\varepsilon_{ccy}}{y} = \frac{0.000825951}{116.787} = 7.07229 x 10^{-6}$$

130

Ultimate curvature

$$\emptyset_u = \frac{\varepsilon_{ccu}}{y} = \frac{0.0013728}{115.077} = 1.19294x10^{-5}$$

C.4 SUMMARY OF SECTION MOMENTS AND CURVATURES

		Moment(Nmm)	Curvature	Depth of neutral axis
Cracking	*Sagging*	51,483,065	$4.6x10^{-8}$	139.32mm
	Hogging	138,804,095	$5.61x10^{-7}$	360.68mm
Yield	*Sagging*	119,156,955.89	$5.67755x10^{-6}$	36.8957mm
	Hogging	152,200,307.79	$7.07229x10^{-6}$	116.7869mm
Ultimate	*Sagging*	179,560,984.17	$9.58848x10^{-6}$	35.2619mm
	Hogging	261,829,126.8	$1.19294x10^{-5}$	115.0770mm

C.5 SECTION PROPERTIES

Figure A-10: Cracked Block under Sagging moment

Moment of inertia for the cracked block under sagging moment

$$I_{cr} = \frac{by^3}{3} + (n-1)A_{st}(y-d'_t)^2 + (n-1)A_{sb}(h-y-d'_b)$$

$$I_{cr} = 2480x\left(\frac{139.32^3}{3}\right) + (6.452-1)x942.48x(139.32-35)^2$$

$$+ (6.452-1)x603x(500-139.32-33)^2$$

$$I_{cr} = 2,644,398,299.2mm^4$$

Area of section

$$A_s = by + (n-1)A_{sb} + (n-1)A_{st}$$

$$= 2480x139.32 + (6.452 - 1)x603 + (6.452 - 1)x942.48 = 353,939.557mm^2$$
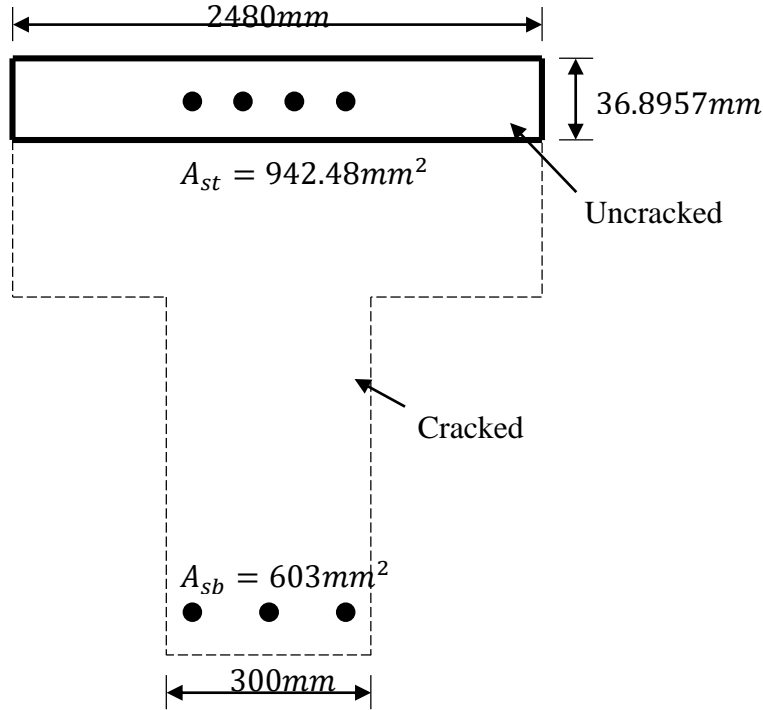
Figure A-11: Yielded Block under sagging moment

Moment of inertia for the Yielded block under sagging moment

$$I_y = \frac{by^3}{3} + (n-1)A_{st}(y-d'_t)^2 + (n-1)A_{sb}(h-y-d'_b)$$

$$I_y = 2480x\left(\frac{36.8957^3}{3}\right) + (6.452 - 1)x942.48x(36.8957 - 35)^2$$

$$+ (6.452 - 1)x603x(500 - 36.8957 - 33)^2$$

$$I_y = 609,307,828.40mm^4$$

Area of section

$$A_s = by + (n-1)A_{sb} + (n-1)A_{st}$$

$$= 2480x36.8957 + (6.452 - 1)x603 + (6.452 - 1)x942.48 = 99,927.293mm^2$$
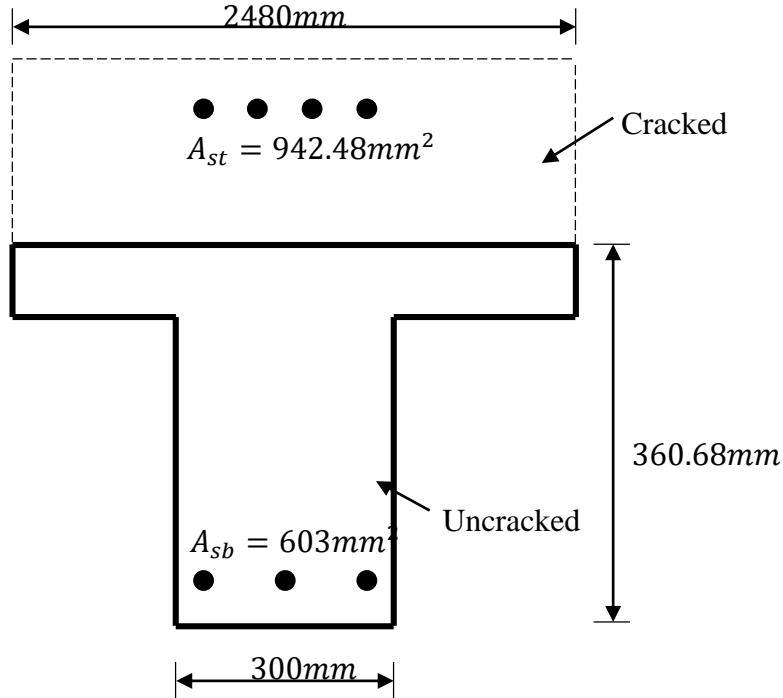
Figure A-12: Cracked Section under hogging moment

Moment of inertia for the cracked block under hogging moment

$$I_{cr(hog)} = \frac{b(y - h + h_f)^3}{3} + b_w(h - h_f)x\left(\frac{2y + h_f - h}{2}\right)^2$$

$$+ (n - 1)A_{st}(h - y - d_t')^2 + (n - 1)A_{sb}(y - d_b')^2$$

$$I_{cr(hog)} = \frac{2480x(360.68 - 500 + 200)^3}{3}$$

$$+ 300x(500 - 200)x\left(\frac{2x360.68 + 200 - 500}{2}\right)^2$$

$$+ (6.452 - 1)x942.48x(500 - 360.68 - 35)^2$$

$$+ (6.452 - 1)x603x(360.68 - 33)^2 = 4,588,363,841.5682mm^4$$

Area of section

$$A_s = b(y - h + h_f) + b_w(h - h_f) + (n - 1)A_{sb} + (n - 1)A_{st}$$

$$= 2480x(360.68 - 500 + 200) + 300x(500 - 200)$$

$$+ (6.452 - 1)x(603 + 942.48) = 248,912.357mm^2$$
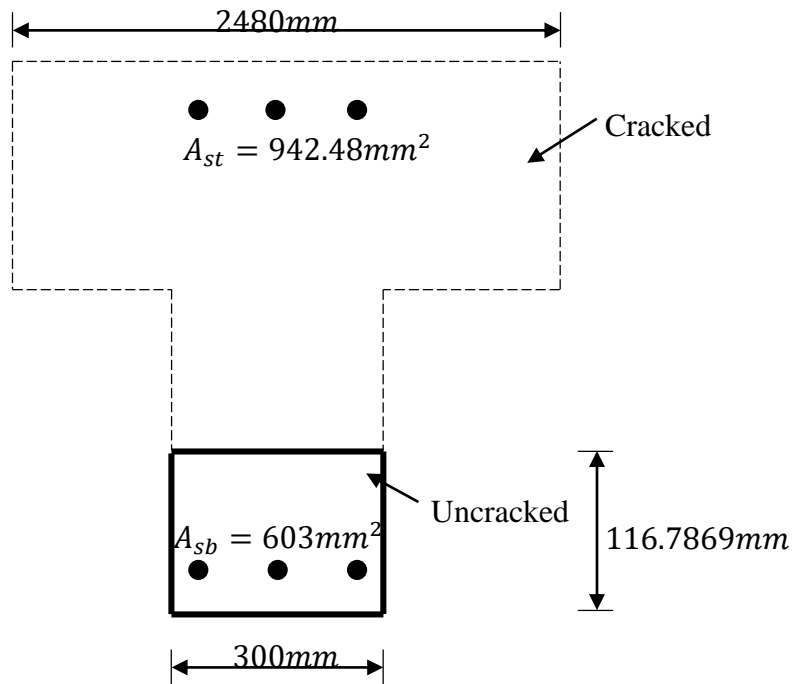
Figure 0-13: Yielded Section under hogging moment

Moment of inertia for the Yielded block under hogging moment

Depth of the neutral axis $y = 116.7869mm$

$$I_y = \frac{by^3}{3} + (n - 1)A_{st}(h - y - d_t')^2 + (n - 1)A_{sb}(y - d_b')$$

$$I_y = 2480x\left(\frac{116.7869^3}{3}\right) + (6.452 - 1)x942.48x(500 - 116.7869 - 35)^2$$

$$+ (6.452 - 1)x603x(116.7869 - 33)^2$$

135

$$I_y = 1,962,901,482.1964 mm^4$$

Area of section

$$A_s = b_w y + (n-1)A_{sb} + (n-1)A_{st}$$

$$= 300x116.7869 + (6.452 - 1)x603 + (6.452 - 1)x942.48 = 43,462.027 mm^2$$
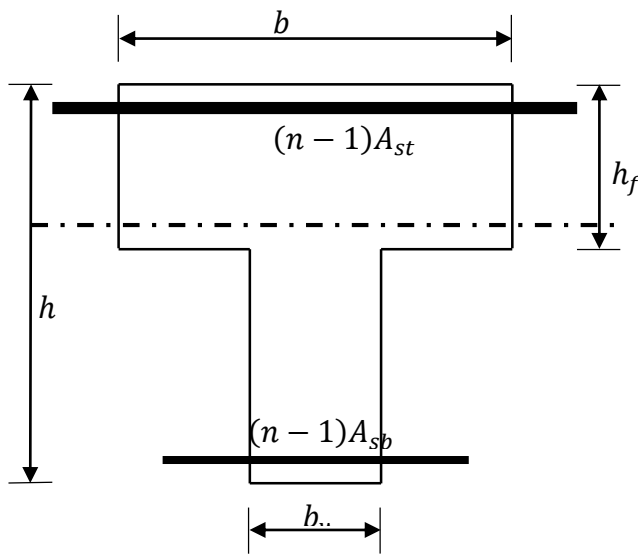
Figure A-14: Elastic Un-cracked Section

Gross moment of inertia

$$I_g = \frac{b_w h^3}{12} + b_w h(0.5h - y)^2 + \frac{(b - b_w)h_f^3}{12} + (b - b_w)h_f(y - 0.5h_f)^2$$

$$+ (n-1)A_{sb}(h - y - d_b')^2 + (n-1)A_{st}(y - d_t')^2$$

$$I_g = \frac{300x500^3}{12} + 300x500x(0.5x500 - 139.32)^2 + \frac{(2480 - 300)x200^3}{12}$$

$$+ (2480 - 300)x200x(139.32 - 0.5x200)^2$$

$$+ (6.45 - 1)x603x(500 - 139.32 - 33)^2$$

$$+ (6.45 - 1)x942.48x(139.32 - 35)^2$$

$$I_g = 7{,}498{,}814{,}987 mm^4$$

Gross Area of section

$$A_s = bh_f + b_w(h - h_f) + (n - 1)A_{sb} + (n - 1)A_{st}$$

$$= 2480x200 + 300x(500 - 200) + (6.452 - 1)x(603 + 942.48)$$

$$= 594{,}425.957 mm^2$$

ANNEX D: CRACKING MOMENTS AND CURVATURES

The cracking moment is the bending moment of a section when the concrete fibre under tensile stresses equals the modulus of rupture of the concrete. The modulus of rupture F_t is the tensile strength determined from a flexural test. (Kyakula, 2010)

$$F_t = 1.4 \left(\frac{f_c}{10} \right)^{2/3}$$

Where:

f_c = Characteristic strength of concrete in compression

The strain at rupture ε_{ct} is given by:

$$\varepsilon_{ct} = \frac{F_t}{E_c}$$

E_c = Modulus of elasticity of concrete

D.1 HOGGING CRACKING MOMENT AND CURVATURES

Depending on the beam dimensions, the reinforcement layout and amounts, the neutral axis may be in the flange or in the web. In this case, the neutral axis is in the flange as can be seen in the appendix.

D.1.1 Neutral axis in the flange

Consider the T beam section shown in figure A-15 below

A_{sb} = Area of reinforcement at the bottom of the beam

A_{st} = Area of reinforcement at the top of the beam

h = Overall height of the beam

h_f = Depth of the flange

y = Depth of the neutral axis from the outer most concrete compressive fibre

ε_{cc}, ε_{cf}, ε_{ct} Refer to the strain in concrete at the outer most compressive fibre, at the in bottom of the flange and at cracking

σ_{cc}, σ_{ct} Refer to the stress in concrete at outer most compressive fibre and at cracking

b = Effective flange width

n = Ratio of the modulus of elasticity of steel to that of concrete, $n = \dfrac{E_s}{E_c}$

d_{sb}, d_{st} Refer to the effective depth to the reinforcement at the bottom and top respectively

d'_b, d'_t Refer to the cover depth to the centre of the reinforcement at the bottom and the top respectively

h_f the depth of the flange

It is assumed that before cracking, the stress distribution across a section is triangular as shown in figure A-15.

From the strain diagram we have.

$$\frac{\varepsilon_{ct}}{(h-y)} = \frac{\varepsilon_{cc}}{y} = \frac{\varepsilon_{sc}}{(y-d'_b)} = \frac{\varepsilon_{st}}{(h-y-d'_t)} = \frac{\varepsilon_{cf}}{(h_f+y-h)}$$
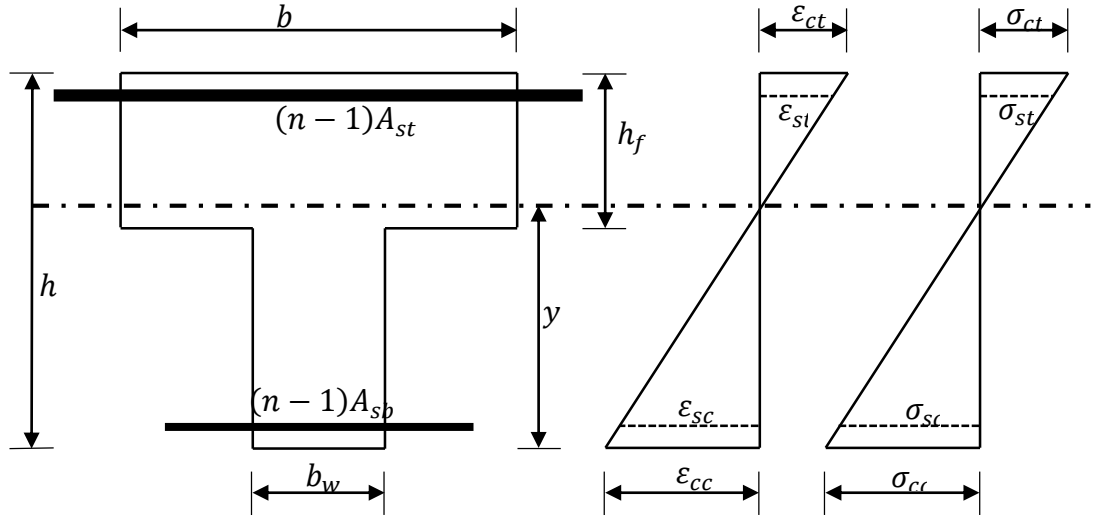
Figure A-15: Stress and strain distribution diagram for concrete section at cracking under the action of hogging moments, with the neutral axis in the flange

The neutral axis depth y is found by the first moment of area of the steel and concrete about the outermost compressive fibre by the total area of the section. This is given in the equation below.

$$y = \frac{0.5b_w h^2 + (b - b_w)h_f\left(h - 0.5h_f\right) + (n - 1)A_{sb}d'_b + (n - 1)A_{st}(h - d'_t)}{b_w h + h_f(b - b_w) + (n - 1)A_{sb} + (n - 1)A_{st}}$$

The tensile force in concrete T_c is given by.

$$T_c = 0.5b(h - y)\varepsilon_{ct}E_c$$

The tensile force in steel T_s, is given by

$$T_s = \left(\frac{n - 1}{n}\right) A_{st} \left(\frac{h - y - d'_t}{h - y}\right)\varepsilon_{ct}E_s$$

The compressive force in steel is given by

$$C_s = \left(\frac{y - d'_b}{h - y}\right) \varepsilon_{ct} E_s A_{sb} \left(\frac{n - 1}{n}\right)$$

To simplify the calculation of the compressive force in concrete, the concrete section is divided into two parts A and B.

Part A is the central part of width b_w, and depth y equal to the depth of the neutral axis.

Part B of width $(b - b_w)$, and depth $(h_f + y - h)$, equal to the depth of the flange below the neutral axis.

The compressive force in concrete part A is given by

$$C_{CA} = 0.5 b_w y \left(\frac{y}{h - y}\right) \varepsilon_{ct} E_c$$

The compressive force in concrete part B is given by

$$C_{CB} = 0.5(b - b_w)(h_f + y - h)\left(\frac{h_f + y - h}{h - y}\right) \varepsilon_{ct} E_c$$

The cracking moment M_{cr} is obtained by summing the moments of all these forces about the neutral axis. Thus, the cracking moment is given by

$$M_{cr} = C_{CA}\left(\frac{2}{3}y\right) + C_{CB}\left[\frac{2}{3}(h_f + y - h)\right] + C_s(y - d'_b) + T_C\left[\frac{2}{3}(h - y)\right]$$
$$+ T_s(h - y - d'_t)$$

At the onset of cracking, the moment of inertia considered is the gross moment of inertia I_g. This is given by

$$I_g = \frac{b_w h^3}{12} + b_w h (0.5h - y)^2 + \frac{(b - b_w) h_f^3}{12} + (b - b_w) h_f \left(h - y - 0.5 h_f \right)^2$$

$$+ (n - 1) A_{sb} (y - d_b')^2 + (n - 1) A_{st} (y - d_t')^2$$

The cracking curvature $\emptyset_{cr}$ is given by

$$\emptyset_{cr} = \frac{M_{cr}}{I_g E_c}$$

D.1.2 Neutral axis in the web

Consider a T beam section shown in Figure A-16 below:

The terms have the same meaning as assigned them in Figure A-1.
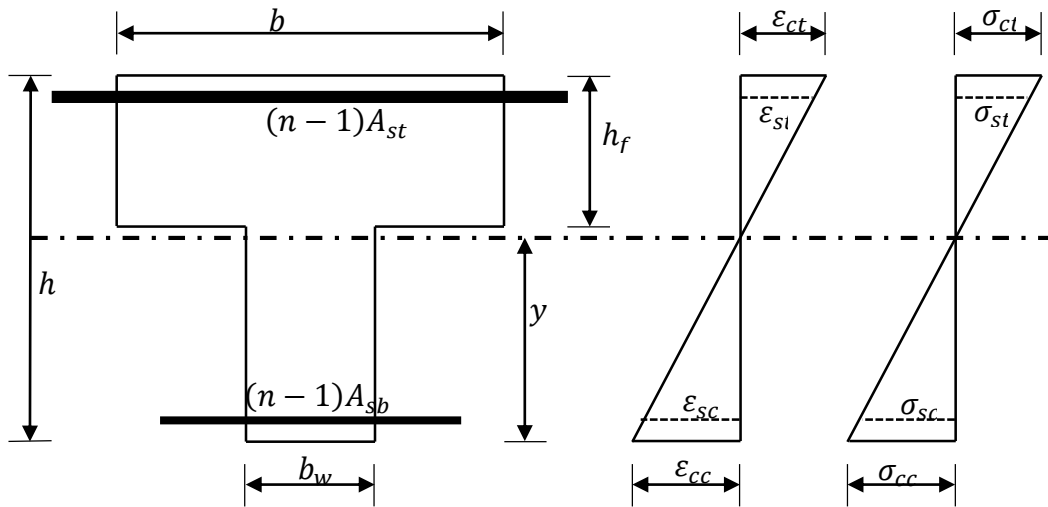
Figure A-16: Stress and strain distribution diagram for concrete section at cracking under the action of hogging moments, with the neutral axis in the web

Equation below is obtained by considering the strain diagram

$$\frac{\varepsilon_{ct}}{(h - y)} = \frac{\varepsilon_{cc}}{y} = \frac{\varepsilon_{sc}}{(y - d_b')} = \frac{\varepsilon_{st}}{(h - y - d_t')} = \frac{\varepsilon_{cf}}{\left(h_f + y - h \right)}$$

The compressive force in concrete is given by:

142

$$C_c = 0.5 b_w y \left(\frac{y}{h-y} \right) \varepsilon_{ct} E_c$$

The compressive force in steel is given by:

$$C_s = \left(\frac{n-1}{n} \right) A_{sb} \left(\frac{y - d_b'}{h-y} \right) \varepsilon_{ct} E_s$$

The tensile force in steel is given by:

$$T_s = \left(\frac{n-1}{n} \right) A_{st} \left(\frac{h - y - d_t'}{h-y} \right) \varepsilon_{ct} E_s$$

To simplify the task of finding tensile force in concrete, the part of concrete stress diagram above the neutral axis is divided as shown in Figure 6-16 below.

Stress distribution in concrete in tension is as shown in stress diagram A. this caters for the area A of the beam with width b_w. Stress distribution B is equal to the stress at the depth of the flange. Stress distribution C is the difference between the tensile stress diagram A and the rectangular tensile stress diagram representing the stress at the bottom of the flange.
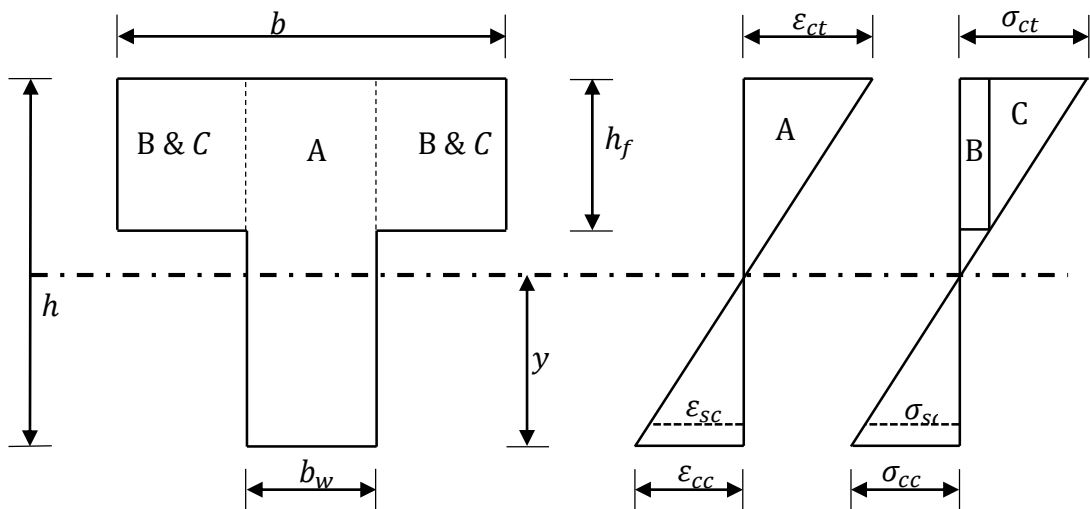
Figure A-17: Stress diagram for calculating the tensile force in concrete

Part of the tensile force in concrete T_{CA} acting on part A in figure A-17 is given by:

$$T_{CA} = 0.5b_w(h - y)\varepsilon_{ct}E_c$$

Part of the tensile force in concrete T_{CB} acting on flanges with a constant strain marked B in Figure A-17 is given by:

$$T_{CB} = (b - b_w)h_f\left(\frac{h - y - h_f}{h - y}\right)\varepsilon_{ct}E_c$$

Part of the tensile force in concrete T_{CC} acting on the flange with strain diagram marked C is given by:

$$T_{CC} = 0.5(b - b_w)h_f\left(\frac{h_f}{h - y}\right)\varepsilon_{ct}E_c$$

The total tensile force in concrete is given by:

$$T_C = T_{CA} + T_{CB} + T_{CC}$$

The depth y of the neutral axis is given by:

$$y = \frac{0.5b_wh^2 + (b - b_w)h_f\left(h - 0.5h_f\right) + (n - 1)A_{sb}d'_b + (n - 1)A_{st}(h - d'_t)}{b_wh + h_f(b - b_w) + (n - 1)A_{sb} + (n - 1)A_{st}}$$

The cracking moment M_{cr} is found by taking moments of the above forces about the neutral axis. It is given in the equation below.

$$M_{cr} = C_c\left(\frac{2}{3}y\right) + C_s(y - d'_b) + T_s(h - y - d'_t) + T_{CA}\left[\frac{2}{3}(h - y)\right]$$

$$+ T_{CB}(h - y - 0.5h_f) + T_{cc}\left(h - y - \frac{1}{3}h_f\right)$$

144

At the onset of cracking, the moment of inertia considered is the gross moment of inertia I_g. This is given by:

$$I_g = \frac{b_w h^3}{12} + b_w h(0.5h - y)^2 + \frac{(b - b_w)h_f^3}{12} + (b - b_w)h_f\left(h - y - 0.5h_f\right)^2$$
$$+ (n - 1)A_{sb}(y - d_b')^2 + (n - 1)A_{st}(y - d_t')^2$$

The cracking curvature $\emptyset_{cr}$ is given by:

$$\emptyset_{cr} = \frac{M_{cr}}{I_g E_c}$$

D.2   SAGGING CRACKING MOMENT AND CURVATURE

D.2.1   Neutral axis in the flange

Consider the section shown the figure A-18 below, with the terms as defined in figure A-15.
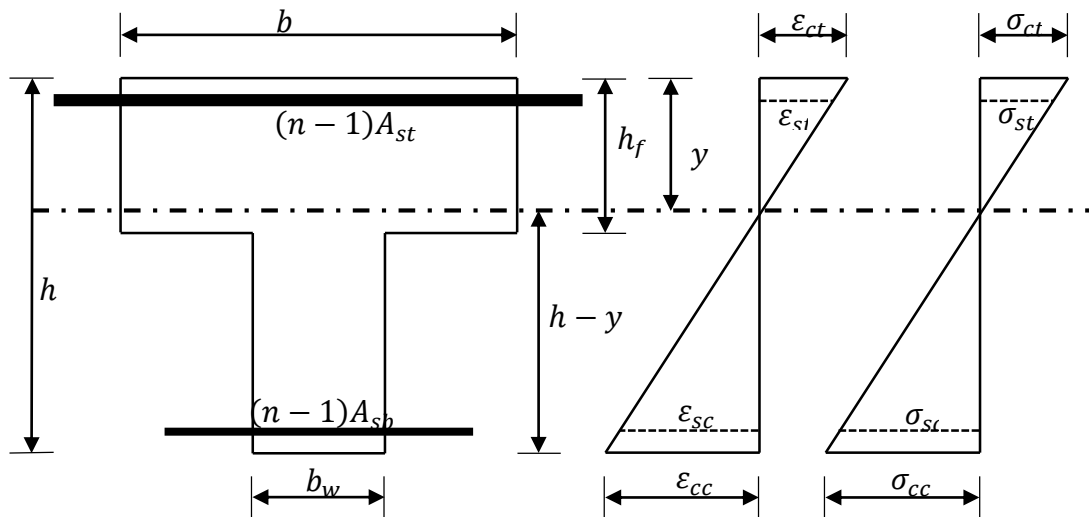
Figure A-18: Stress and strain distribution diagram for concrete section at cracking under the action of sagging moments, with the neutral axis in the flange

The strains are given by:

$$\frac{\varepsilon_{ct}}{h-y} = \frac{\varepsilon_{cc}}{y} = \frac{\varepsilon_{sb}}{h-y-d_b'} = \frac{\varepsilon_{st}}{y-d_t'} = \frac{\varepsilon_{cf}}{h_f-y}$$

The depth y of the neutral axis is found by dividing the first moments of the concrete and the steel areas taken about the outermost compressive fibre by the area of the section.

$$y = \frac{0.5b_w h^2 + 0.5(b-b_w)h_f^2 + (n-1)A_{sb}(h-d_b') + (n-1)A_{st}d_t'}{b_w h + (b-b_w)h_f + (n-1)A_{sb} + (n-1)A_{st}}$$

The compressive force in concrete is given by:

$$C_c = 0.5by\left(\frac{y}{h-y}\right)\varepsilon_{ct}E_c$$

The compressive force in the reinforcement is given by.

$$C_s = \left(\frac{n-1}{n}\right)A_{st}\left(\frac{y-d_t'}{h-y}\right)\varepsilon_{ct}E_s$$

The tension force in the steel reinforcement is given by.

$$T_s = \left[\frac{n-1}{n}\right]A_{sb}\left(\frac{h-y-d_b'}{h-y}\right)\varepsilon_{ct}E_c$$

The tension force in concrete is calculated in two parts; A and B. Part A consists of the tensile force that acts on the web of width b_w and depth $(h-y)$. Part B consists of the tension force that acts on the parts of the flange under tension. It acts on the flange parts of width $(b-b_w)$ and depth $(h_f - y)$.

Tensile force on part A of concrete in tension is given by

$$T_{CA} = 0.5b_w(h - y)\varepsilon_{ct}E_c$$

The tensile force on part B of concrete in tension is given by

$$T_{CB} = 0.5(b - b_w)(h_f - y)\left(\frac{h_f - y}{h - y}\right)\varepsilon_{ct}E_c$$

The cracking moment M_{cr} is found by calculating moments of the forces about the neutral axis.

$$M_{cr} = C_c\left(\frac{2}{3}y\right) + C_s(y - d_t') + T_s(h - y - d_b') + T_{CA}\left[\frac{2}{3}(h - y)\right]$$

$$+ T_{CB}\left[\frac{2}{3}(h_f - y)\right]$$

At the onset of cracking, the moment of inertia considered is the gross moment of inertia I_g. This is given by;

$$I_g = \frac{b_wh^3}{12} + b_wh(0.5h - y)^2 + \frac{(b - b_w)h_f^3}{12} + (b - b_w)h_f(h - y - 0.5h_f)^2$$

$$+ (n - 1)A_{sb}(y - d_b')^2 + (n - 1)A_{st}(y - d_t')^2$$

The cracking curvature $\emptyset_{cr}$ is given by:

$$\emptyset_{cr} = \frac{M_{cr}}{I_gE_c}$$

D.2   Neutral axis in the web

Consider Figure A-19 below, with the term as defined earlier.
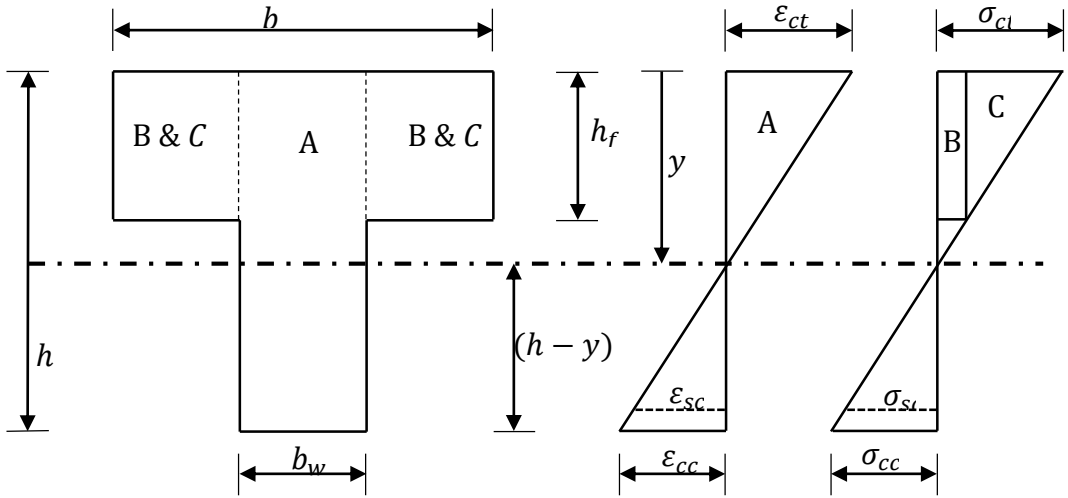
Figure A-19: Stress and strain distribution before cracking for a section under action of sagging moment, with the neutral axis in the web

The strains are given by:

$$\frac{\varepsilon_{ct}}{h-y} = \frac{\varepsilon_{cc}}{y} = \frac{\varepsilon_{sb}}{h-y-d'_b} = \frac{\varepsilon_{st}}{y-d'_t} = \frac{\varepsilon_{cf}}{h_f-y}$$

The tensile force in concrete is given by:

$$T_C = 0.5b_w(h-y)\varepsilon_{ct}E_c$$

The tensile force in steel is given by:

$$T_s = \left(\frac{n-1}{n}\right)A_{sb}\left(\frac{h-y-d'_b}{h-y}\right)\varepsilon_{ct}E_s$$

The compressive force in steel is given by:

$$C_s = \left(\frac{n-1}{n}\right)A_{st}\left(\frac{y-d'_t}{h-y}\right)\varepsilon_{ct}E_s$$

The compressive force in concrete is calculated in three parts A, B and C

148

Part A is the compressive force that acts on part labelled A, of width b_w, and depth y.

Part B is the compressive force on the flange, of width $(b - b_w)$, and height h_f, with a uniform stress (rectangular distribution) equal to the stress in concrete at the depth of the flange.

Part C is the compressive force on the flange of width $(b - b_w)$, and height h_f with a triangular stress distribution, equal to the total stress distribution less the stress distribution at the flange depth.

The compressive force in concrete due to part A is given by:

$$C_{CA} = 0.5 b_w y \left(\frac{y}{h - y} \right) \varepsilon_{ct} E_c$$

The compressive force in concrete due to concrete is given by:

$$C_{CA} = (b - b_w) h_f \left(\frac{y - h_f}{h - y} \right) \varepsilon_{ct} E_c$$

The compressive force in concrete due to part C is given by:

$$C_{CC} = 0.5 (b - b_w) h_f \left(\frac{h_f}{h - y} \right) \varepsilon_{ct} E_c$$

The depth of the neutral axis is given by:

$$y = \frac{0.5 b_w h^2 + 0.5 (b - b_w) h_f^2 + (n - 1) A_{sb} (h - d_b') + (n - 1) A_{st} d_t'}{b_w h + (b - b_w) h_f + (n - 1) A_{sb} + (n - 1) A_{st}}$$

The cracking moment is obtained by taking moments about the neutral axis

$$M_{cr} = T_c\left[\frac{2}{3}(h-y)\right] + T_s(h-y-d_b') + C_c(y-d_t') + C_{CA}\left(\frac{2}{3}y\right)$$

$$+ C_{CB}(y-0.5h_f) + C_{cc}\left(y-\frac{1}{3}h_f\right)$$

At the onset of cracking, the moment of inertia considered is the gross moment of inertia I_g. This is given by:

$$I_g = \frac{b_w h^3}{12} + b_w h(0.5h-y)^2 + \frac{(b-b_w)h_f^3}{12} + (b-b_w)h_f(h-y-0.5h_f)^2$$

$$+ (n-1)A_{sb}(y-d_b')^2 + (n-1)A_{st}(y-d_t')^2$$

The cracking curvature $\emptyset_{cr}$ is given by:

$$\emptyset_{cr} = \frac{M_{cr}}{I_g E_c}$$

D.3 STRESS – STRAIN RELATIONSHIP FOR BOTH STEEL AND CONFINED CONCRETE

D.3.1 Stress -strain curve for concrete
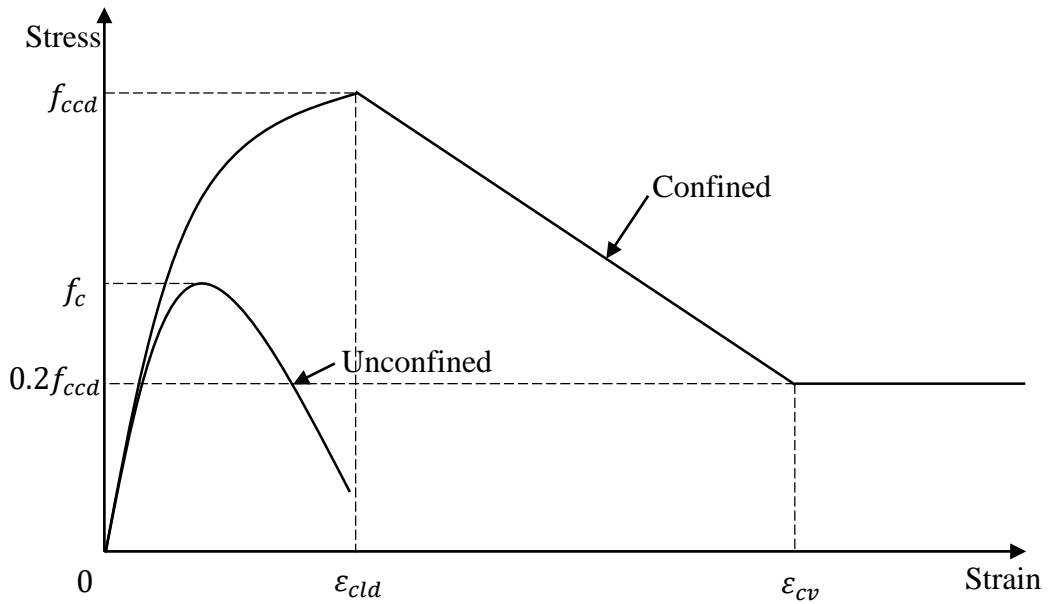
Figure A-20: Stress-strain diagram for confined concrete

The Park, Priestly and Gill (1982) model shall be used to represent the behaviour of confined concrete because it is based on adequate number of experimental data and it is simple (Kyakula, 2010). The model of the stress-strain relationship consists of an ascending parabolic branch, the descending linear branch and a constant stress linear portion as shown in figure A-20.

The ascending branch of stress-strain curve is Hognestad's parabola, given by

$$\sigma_{cc} = f_{ccd}\left[\frac{2\varepsilon_{cc}}{\varepsilon_{cld}} - \left(\frac{\varepsilon_{cc}}{\varepsilon_{cld}}\right)^2\right]$$

Where

f_{ccd} the maximum dynamic stress of confined concrete

ε_{cld} the strain corresponding to maximum stress

σ_{cc} is the compressive stress in concrete corresponding to a compressive strain ε_{cc}.

The descending branch of confined concrete under dynamic loading is given by:

$$\sigma_{cc} = f_{ccd}[1 - Z(\varepsilon_{cc} - \varepsilon_{cld})] \qquad (a)$$

Where;

$$Z = \frac{0.5}{\varepsilon_{cc50} - \varepsilon_{cld}}$$

ε_{cc50} is the strain corresponding to 50% f_{ccd} and is given by

$$\varepsilon_{cc50} = \frac{3 + 0.29f_c}{145f_c - 1000} + 0.75\rho_w \left(\frac{b_c}{s}\right)^{\frac{1}{2}}$$

ρ_w the volumetric ratio of hoops defined with respect to the outside perimeter of hoops

s the spacing of the hoops

b_c the size of the square confined core measured to the centroid of the peripheral hoop. For a beam section, where the hoops are normally rectangular, it is proposed to assume a square section with the same perimeter of hoops.

The ultimate strain of concrete ε_{cu}, is defined based on the $0.85f_c$, along the descending branch of the stress-strain curve. Where f_c is the strength of unconfined concrete.

$$\varepsilon_{cu} = \varepsilon_{cld} + \frac{k - 0.85}{Zk}$$

The constant stress branch of the stress-strain relationship is given by

$$\sigma_{cc} = 0.2f_{ccd} \tag{b}$$

The strain ε_{cv} at which the constant stress branch starts is found by setting $\varepsilon_{cv} = \varepsilon_{cc}$ in equation and equating equation (a) and (b) and solving for ε_{cv} is given by;

$$\varepsilon_{cv} = \frac{0.8}{Z} + \varepsilon_{cld}$$

D.3.2   The stress- strain relationship for steel

The stress strain relationship for steel is shown in Figure A-21.
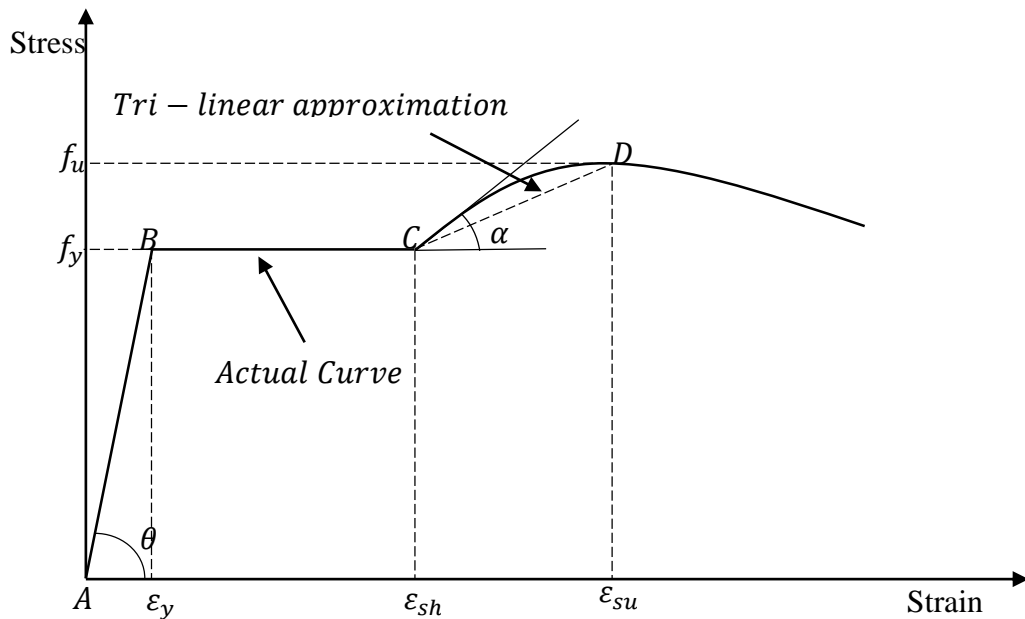
Figure A-21: Stress- Strain Curve for steel reinforcement

In the Figure A-21:

ε_y is the yield strain

ε_{sh} the strain at the end of the plastic region plateau or start of the strain hardening

153

ε_{su} is the ultimate strain

f_y is the yield stress

f_u is the ultimate stress

The curve consists of an elastic region AB, whose slope $Tan\theta = E_s$, the modulus of elasticity of steel. A plastic region BC, stretching from ε_y to ε_{sh} follows. Lastly, a strain hardening region CD. A tri-linear approximation is used in this research. Unloading and reloading before and after yielding follows a path parallel to the elastic curve.

ANNEX E: YIELD AND ULTIMATE MOMENTS WITH THE CORRESPONDING CURVATURES

E.1 INTRODUCTION

The rectangular stress block used for calculating the moment in most codes is a simplification of the assumption that the behaviour of concrete is represented by a parabolic stress-strain relationship up to a strain ε_{co}, then the strain increases with a constant stress up to an ultimate strain of 0.0035, (Kyakula, 2010).

According to Kyakula (2010), the rectangular stress block is not considered accurate for analysis of a confined concrete section under dynamic loading because:

e) Confinement and the dynamic loading increase the concrete strain

f) Confinement and dynamic loading also increase the concrete stress

g) The rectangular stress block assumes that at the time of yielding of the tension reinforcement, the concrete has reached its ultimate stress. This may not be the case, depending on the section dimensions, concrete strength, and area of tension reinforcement.

h) After the ultimate stress has been reached, the stress reduces uniformly as the strain increases, then becomes constant at 20% of the maximum stress.

Thus, the stress-strain relationship shown in Figure 3-10 is used to calculate the yield and ultimate moments and their corresponding curvatures.

The moment curvature relationships are calculated for both the sagging and hogging bending moments, considering whether the neutral axis is in the web or flange and

whether the strain at the outer most concrete fibre has exceeded ε_{cld}, ε_{cv}, given in Figure 3-10.

In the following section, formulae for various forces, moments, and curvatures acting on a section shall be simply stated, the derivation of which can be sourced from Kyakula (2010).

E.2 SAGGING MOMENTS AND CURVATURES

E.2.1 Compressive force in concrete when the neutral axis is in the flange

The strain and stress distribution diagrams across the section under sagging moments with neutral axis in the flange is shown in Figure A-22.
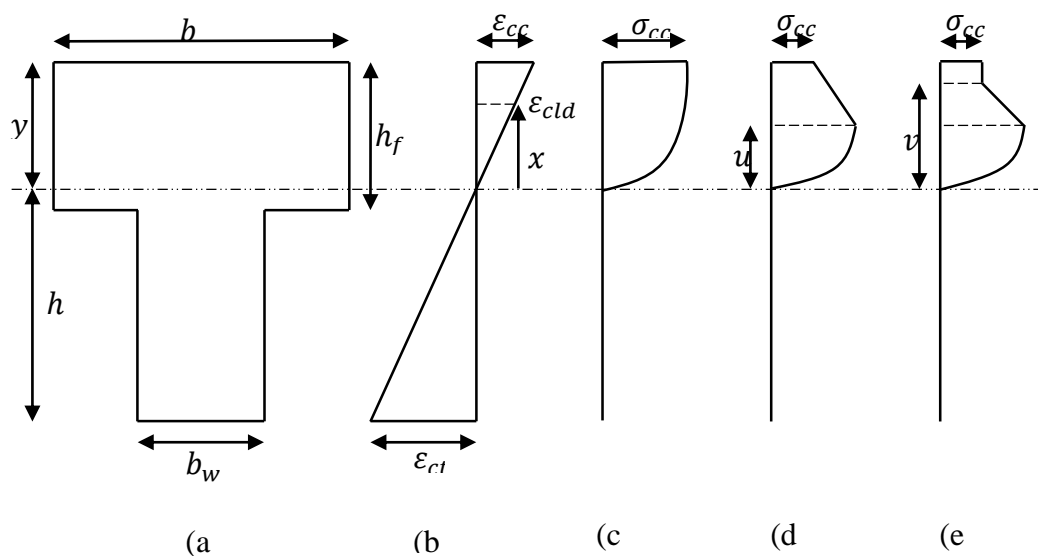
Figure A-22: Strain and stress distribution after cracking for a section under sagging moment with the neutral axis in the flange

b the flange width

b_w the web width

h the overall depth of the section

h_f the flange depth

ε_{ct} Refers to the tensile strain

ε_{cc} Refers to the maximum compressive strain

σ_{cld} Refers to the maximum stress

σ_{cc} Refers to the compressive stress in the outer most layer of concrete

ε_{cld} Refers to the strain corresponding to the maximum stress

y Refers to the depth of the neutral axis

The stress-strain relationship is as shown in Figure A-22. The stress diagram changes under increasing strain as shown in Figure A-22 (c), (d) and (e). The strain diagram is shown in Figure A-22 (b).

The stress diagram (c) corresponds to a case where the maximum compressive strain in concrete ε_{cc}, is less than the strain ε_{cld}, corresponding to the maximum stress.

Stress diagram (d) corresponds to a case where the maximum compressive strain in concrete ε_{cc}, is greater than the strain ε_{cld}, corresponding to the maximum stress, but less than the strain ε_{cv} at which the stress becomes constant.

Stress diagram (e) corresponds to the case where the maximum compressive strain in concrete ε_{cc}, is greater than the strain ε_{cv}, at which the stress becomes constant.

Consider the stress distribution shown in Figure A-22(e), where the strain at the outer most compressive concrete fibre is greater than the strain ε_{cv}.

The compressive force in concrete C_c is given by:

$$C_c = byf_{ccd}\left[\frac{2\varepsilon_{cld}}{3\varepsilon_{cc}} + \left(\frac{\varepsilon_{cv} - \varepsilon_{cld}}{\varepsilon_{cc}}\right)\left(1 - \frac{Z}{2}(\varepsilon_{cv} - \varepsilon_{cld})\right)\right.$$

$$\left. + 0.2\left(\frac{\varepsilon_{cc} - \varepsilon_{cv}}{\varepsilon_{cc}}\right)\right] \qquad (3.1)$$

If the topmost fibre strain ε_{cc} is equal to or less than ε_{cv}, as represented in Figure A-22 (d), the expression for the compressive force in concrete reduces to equation 3.2

$$C_c = byf_{ccd}\left[\left(1 - \frac{\varepsilon_{cld}}{3\varepsilon_{cc}}\right) + Z\left(\varepsilon_{cld} - 0.5\varepsilon_{cc} - \frac{0.5\varepsilon_{cld}^2}{\varepsilon_{cc}}\right)\right] \qquad (3.2)$$

Considering case (c), that is the stress-strain does not exceed that corresponding to the maximum stress, then the compressive force is given by:

$$C_c = byf_{ccd}\left[\frac{\varepsilon_{cc}}{\varepsilon_{cld}} - \frac{1}{3}\left(\frac{\varepsilon_{cc}}{\varepsilon_{cld}}\right)^2\right] \qquad (3.3)$$

The depth of the point of action $\bar{y}$, of the compressive force in concrete C_c, from the neutral axis is given by:

$$C_c\bar{y} = \frac{by^2 f_{ccd}}{12\varepsilon_{cc}^2}[5\varepsilon_{cld}^2 + 1.2(\varepsilon_{cc}^2 - \varepsilon_{cv}^2) + 6(1 + Z\varepsilon_{cld})(\varepsilon_{cv}^2 - \varepsilon_{cl}^2)$$

$$- 4Z(\varepsilon_{cv}^3 - \varepsilon_{cld}^3)] \qquad (3.4)$$

Considering case (d), where the strain does not exceed that corresponding to constant stress, then

$$C_c\bar{y} = \frac{by^2 f_{ccd}}{6}\left[\left(3 - 0.5\left(\frac{\varepsilon_{cld}}{\varepsilon_{cc}}\right)^2\right) + Z\left(3\varepsilon_{cld} - 2\varepsilon_{cc} - \frac{\varepsilon_{cld}^3}{\varepsilon_{cc}^2}\right)\right] \qquad (3.5)$$

Considering case (c), 9where the strain does not exceed that corresponding to the maximum stress, then

$$C_c\bar{y} = by^2 f_{ccd} \left[\frac{2}{3}\left(\frac{\varepsilon_{cc}}{\varepsilon_{cld}}\right) - \frac{1}{4}\left(\frac{\varepsilon_{cc}}{\varepsilon_{cld}}\right)^2 \right]$$ (3.6)

$$\bar{y} = \frac{C_c\bar{y}}{C_c}$$

E.2.2 Compressive force in concrete when the neutral axis is in the web

When concrete strain at the top is less than the strain corresponding to the maximum stress

The stress distribution diagram across the section when the compressive concrete strain at topmost fibre is less than the strain corresponding to maximum stress is shown in Figure A-23.
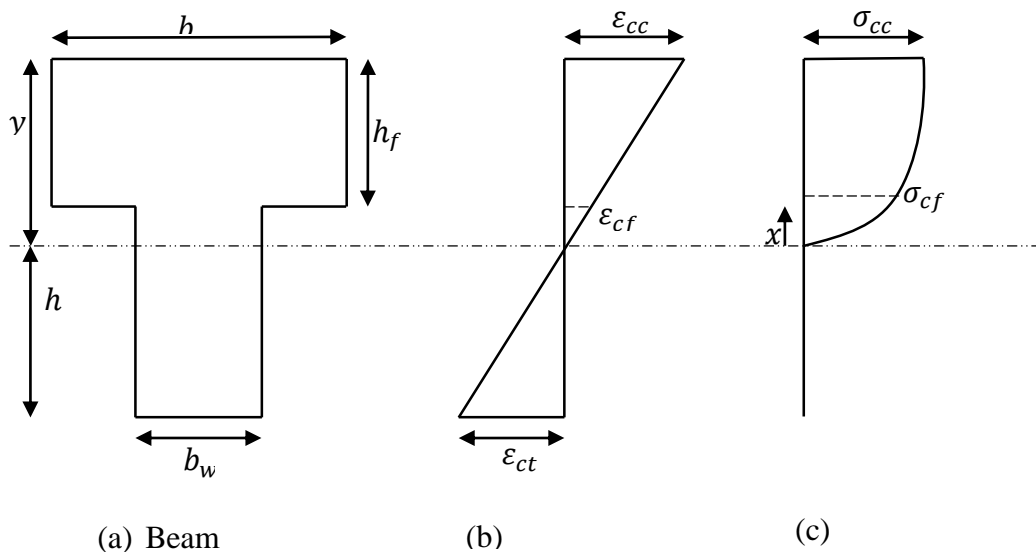

Figure A-23: Strain and stress distribution for a section under sagging moment with the neutral axis in the web and stress less than maximum stress

The compressive force in concrete C_c is obtained using equation 3.7:

$$C_c = byf_{ccd}\left[\frac{\varepsilon_{cc}}{\varepsilon_{cld}} - \frac{1}{3}\left(\frac{\varepsilon_{cc}}{\varepsilon_{cld}}\right)^2\right]$$

$$+ (b_w - b)f_{ccd}\left[\left(\frac{\varepsilon_{cc}}{\varepsilon_{cld}}\right)\frac{(y - h_f)^2}{y} - \left(\frac{\varepsilon_{cc}}{\varepsilon_{cld}}\right)^2\frac{(y - h_f)^3}{3y^2}\right] \qquad (3.7)$$

The depth of the point of action $\bar{y}$, of the compressive force in concrete C_c , from the neutral axis is determined using:

$$C_c\bar{y} = by^2 f_{ccd}\left[\frac{2}{3}\left(\frac{\varepsilon_{cc}}{\varepsilon_{cld}}\right) - \frac{1}{4}\left(\frac{\varepsilon_{cc}}{\varepsilon_{cld}}\right)^2\right]$$

$$+ f_{ccd}(b_w - b)\left[\frac{2\varepsilon_{cc}(y - h_f)^3}{3\varepsilon_{cld}y} - \left(\frac{\varepsilon_{cc}}{\varepsilon_{cld}}\right)^2\frac{(y - h_f)^4}{4y^2}\right]$$

$$\bar{y} = \frac{C_c\bar{y}}{C_c}$$

Concrete strain at the top is greater than the strain corresponding to maximum stress, which lies in the web

The stress and strain diagrams for a section under the action of sagging moments when the strain at the topmost fibre is greater than the strain ε_{cld} corresponding to the maximum stress, and the maximum stress lies within the web as shown in Figure A-24.

Considering case (d) where the strain is greater than ε_{cv} corresponding to the onset of the constant stress, then the compressive force in concrete shall be given by:

$$C_c = (b_w - b)f_{ccd}\left[(y - h_f) - \frac{Z\varepsilon_{cc}(y - h_f)^2}{2y} + Z\varepsilon_{cld}(y - h)\right]$$

$$- b_w f_{ccd}y\left[\frac{\varepsilon_{cld}}{3\varepsilon_{cc}} + \frac{Z\varepsilon_{cld}^2}{2\varepsilon_{cc}}\right] + byf_{ccd}\left[1 - \frac{Z\varepsilon_{cc}}{2} + Z\varepsilon_{cld}\right] \qquad (3.9)$$

(a) Beam   (b)   Strain   Stress diagrams
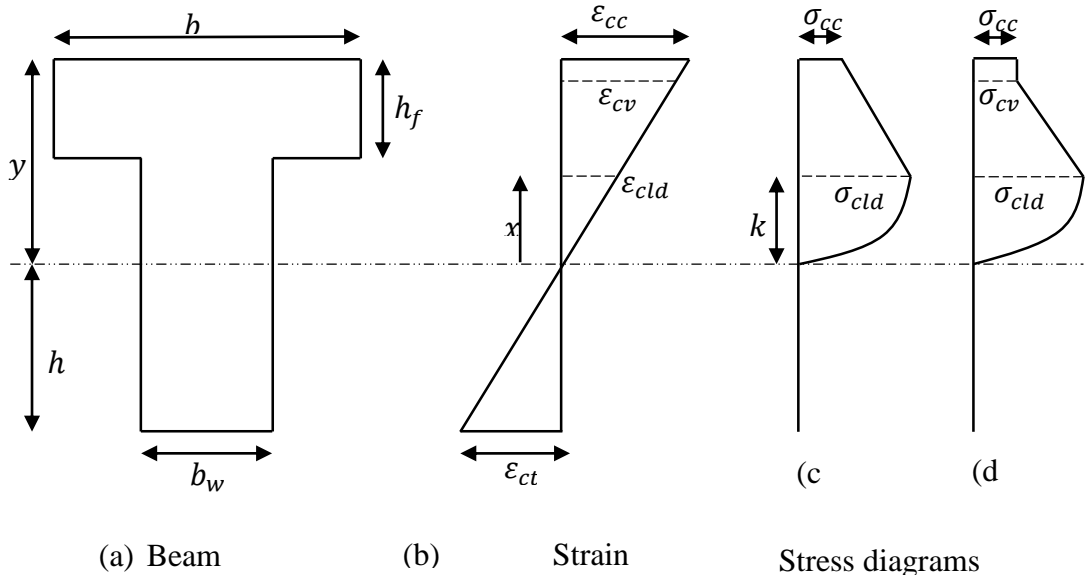
Figure A-24: Stress and Strain diagrams when the strain corresponding to maximum

stress has been exceeded and lies within the web

The point of action $\bar{y}$, of the compressive force in concrete C_c from the neutral axis is

given by:

$$C_c\bar{y} = \frac{y^2 f_{ccd}}{12\varepsilon_{cc}^2}[5b_w\varepsilon_{cld}^2 + 1.2b(\varepsilon_{cc}^2 - \varepsilon_{cv}^2)]$$

$$+ \frac{y^2 f_{ccd}}{12\varepsilon_{cc}^2}[6(1 + Z\varepsilon_{cld})(b\varepsilon_{cv}^2 - b_w\varepsilon_{cld}^2) - 4Z(b\varepsilon_{cv}^2 - b_w\varepsilon_{cld}^3)]$$

$$+ (b - b_w)f_{ccd}\left[\frac{(y - h_f)^2}{2} - \frac{Z\varepsilon_{cc}}{3y}(y - h_f)^3\right.$$

$$\left. + \frac{Z\varepsilon_{cld}}{2}(y - h_f)^2\right] \qquad (3.10)$$

Considering case (c), where the strain does not exceed that corresponding to constant

stress, then the $C_c\bar{y}$ reduces to:

$$C_c \bar{y} = \frac{(b_w - b)}{6} f_{ccd} \left[3(y - h_f)^2 - \frac{2Z\varepsilon_{cc}}{y}(y - h_f)^3 + 3\varepsilon_{cld}(y - h_f)^2 \right]$$

$$+ \frac{by^2 f_{ccd}}{6} [3 - 2Z\varepsilon_{cc} + 3\varepsilon_{cld}]$$

$$- \frac{b_w y^2 f_{ccd}}{6} \left[0.5 \left(\frac{\varepsilon_{cld}}{\varepsilon_{cc}} \right)^2 + \frac{Z\varepsilon_{cld}^3}{\varepsilon_{cc}^2} \right] \tag{3.11}$$

The depth from the neutral axis to centroid of compressive concrete is given by:

$$\bar{y} = \frac{C_c \bar{y}}{C_c}$$

E.2.3   When concrete strain at the top is greater than the strain corresponding to the maximum stress, which is in the flange.

The stress and strain diagrams for a section under action of sagging moments when the strain at the topmost fibre is greater than the strain ε_{cld} corresponding to the maximum stress lies within the flange as shown in Figure 3-15.

The compressive force in concrete C_c is obtained by:

$$C_c = byf_{ccd} \left[\left(\frac{\varepsilon_{cv}}{\varepsilon_{cc}} - \frac{\varepsilon_{cld}}{3\varepsilon_{cc}} \right) + Z \left(\frac{\varepsilon_{cld}\varepsilon_{cv}}{\varepsilon_{cc}} - \frac{\varepsilon_{cv}^2}{2\varepsilon_{cc}} - \frac{\varepsilon_{cld}^2}{2\varepsilon_{cc}} \right) + 0.2 \left(1 - \frac{\varepsilon_{cv}}{\varepsilon_{cc}} \right) \right]$$

$$- (b - b_w) f_{ccd} \left[\left(\frac{\varepsilon_{cc}}{\varepsilon_{cld}} \right) \frac{(y - h_f)^2}{y} - \left(\frac{\varepsilon_{cc}}{\varepsilon_{cld}} \right)^2 \frac{(y - h_f)^3}{3y^2} \right] \tag{3.12}$$

Considering case (c), where the strain does not exceed that corresponding to constant stress, then $\varepsilon_{cv} = \varepsilon_{cc}$, they compressive force in concrete reduces to:

$$C_c = by f_{ccd} \left[\left(1 - \frac{\varepsilon_{cld}}{3\varepsilon_{cc}} \right) + Z \left(\varepsilon_{cld} - \frac{\varepsilon_{cc}}{2} - \frac{\varepsilon_{cld}^2}{2\varepsilon_{cc}} \right) \right]$$

$$- (b - b_w) f_{ccd} \left[\left(\frac{\varepsilon_{cc}}{\varepsilon_{cld}} \right) \frac{(y - h_f)^2}{y} - \left(\frac{\varepsilon_{cc}}{\varepsilon_{cld}} \right)^2 \frac{(y - h_f)^3}{3y^2} \right] \qquad (3.13)$$

Considering case (d), the point of action $\bar{y}$ of the compressive force in concrete C_c from the neutral axis is determined by taking moment about the neutral axis to obtain $C_c \bar{y}$, and dividing the moments $C_c \bar{y}$ by the force C_c.

(b) Beam   (b)   Strain   Stress diagrams
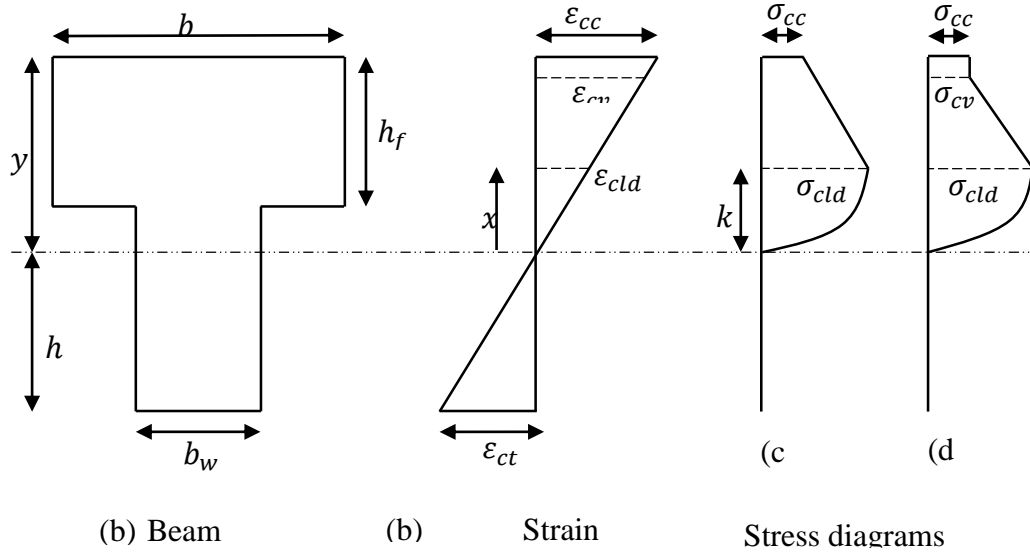
Figure A-25: Stress and Strain diagrams when the strain corresponding to maximum stress has been exceeded and lies within the flange

$$C_c \bar{y} = \frac{by^2 f_{ccd}}{12} \left[\left(\frac{6\varepsilon_{cv}^2}{\varepsilon_{cc}^2} - \frac{\varepsilon_{cld}^2}{\varepsilon_{cc}^2} \right) + Z \left(\frac{6\varepsilon_{cld}\varepsilon_{cv}^2}{\varepsilon_{cc}^2} - \frac{4\varepsilon_{cv}^3}{\varepsilon_{cc}^2} - \frac{2\varepsilon_{cld}^3}{\varepsilon_{cc}^2} \right) + 1.2 \left(1 - \frac{\varepsilon_{cv}^2}{\varepsilon_{cc}^2} \right) \right]$$

$$+ (b_w - b) f_{ccd} \left[\left(\frac{2\varepsilon_{cc}}{3y\varepsilon_{cld}} \right) (y - h_f)^3 - \left(\frac{\varepsilon_{cc}}{\varepsilon_{cld}} \right)^2 \frac{(y - h_f)^4}{4y^2} \right] \qquad (3.14)$$

Considering case (c), where the strain does not exceed that corresponding to constant stress, then $\varepsilon_{cv} = \varepsilon_{cc}$ and the $C_c \bar{y}$ reduces to:

$$C_c \bar{y} = \frac{by^2 f_{ccd}}{12}\left[\left(6 - \frac{\varepsilon_{cld}^2}{\varepsilon_{cc}^2}\right) + Z\left(6\varepsilon_{cld} - 4\varepsilon_{cc} - \frac{2\varepsilon_{cld}^3}{\varepsilon_{cc}^2}\right)\right]$$

$$+ (b_w - b)f_{ccd}\left[\left(\frac{2\varepsilon_{cc}}{3y\varepsilon_{cld}}\right)(y - h_f)^3 - \left(\frac{\varepsilon_{cc}}{\varepsilon_{cld}}\right)^2 \frac{(y - h_f)^4}{4y^2}\right] \quad (3.15)$$

The depth of the neutral axis to the centroid of the concrete block is given by:

$$\bar{y} = \frac{C_c \bar{y}}{C_c}$$

E.2.4   Tensile and compressive force in reinforcement

The yield moment and curvature is assumed to be the point at which the reinforcement under tension reaches yield strain.

When the reinforcement under tension (bottom reinforcement) reaches yield strain ε_y, the tensile force in concrete is zero, since concrete will have cracked, (Kyakula, 2010)

The tensile force in the reinforcement T_s is given by:

$$T_s = f_y A_{sb}$$

If the strain ε_{sb} in the tensile steel has exceeded the strain hardening strain ε_{sh}, but is less than the ultimate strain ε_{su} then the tensile force in steel is given by:

$$T_s = A_{sb}\left[f_y + \left(\frac{\varepsilon_{sb} - \varepsilon_{sh}}{\varepsilon_{su} - \varepsilon_{sh}}\right)(f_u - f_y)\right]$$

f_y Refers to the characteristic strength of reinforcement

f_u Refers to the ultimate strength of the reinforcement after strain hardening

If the strain in the tensile steel is equal to the ultimate strain ε_{su}, the tensile force is given by:

$$T_s = f_u A_{sb}$$

If at or after yielding of the tensile steel, the compression steel has not reached the yield strain, the compressive force in the reinforcement under compression at the top is obtained by considering the strain relationships from the strain diagram.

$$\frac{\varepsilon_{sy}}{h - y - d_b'} = \frac{\varepsilon_{st}}{y - d_t'}$$

d_b', d_t' the cover to the centreline of the bottom and top reinforcement respectively

ε_{st} the strain in the top reinforcement

The force in the compression reinforcement is given by:

$$C_s = \left(\frac{n-1}{n}\right) A_{st} \left(\frac{y - d_t'}{h - y - d_b'}\right) \varepsilon_y E_s$$

On the other hand, if the strain ε_{st} in the compressive reinforcement at the top is greater than the yield strain ε_y , but less than the strain hardening strain ε_{sh} , the force in compressive reinforcement is given by:

$$C_s = \left(\frac{n-1}{n}\right) A_{st} f_y$$

If the strain ε_{st} in the compressive reinforcement at the top is greater than the strain hardening strain ε_{sh} , but less than the ultimate strain ε_{su} then the compressive force in the reinforcement is given by:

$$C_s = \left(\frac{n-1}{n}\right) A_{st} \left[f_y + \left(\frac{\varepsilon_{st} - \varepsilon_{sh}}{\varepsilon_{su} - \varepsilon_{sh}}\right)(f_u - f_y)\right]$$

The compressive steel is not expected to reach the ultimate strain before crushing of the concrete around it, (Kyakula, 2010). But if it was to, the compressive force would be given by:

$$C_s = \left(\frac{n-1}{n}\right) A_{st} f_u$$

E.2.5 Determination of the neutral axis y:

Neutral axis at yield

The neutral axis is the point where the compressive and tensile forces are equal. For a given yield strain in steel, the neutral axis is obtained as follows:

The compressive force C is obtained by adding the compressive force C_c in concrete to the compressive force C_s in steel.

$$C = C_c + C_s$$

The tensile force in concrete at yield or ultimate stress shall be neglected because it is small compared to the other forces. Only the tensile force T_s in steel is to be considered.

Starting at a depth y_1 equal to the depth of the compression steel from the outer most compressive fibre, forces C_c , C_s and T_s shall be computed. The tensile force shall then be subtracted from the compressive force to get a difference $\Delta T C_1$.

$$\Delta T C_1 = C - T_s$$

The value of y_1 shall then be increased by a small amount Δy to give a new depth y_2 as shown in equation (3.26).

For the value of y_2, the forces C_c, C_s and T_s shall be computed. Typical values for Δy shall be $0.0001m$ as was considered by (Kyakula, 2010).

The tensile force shall again be subtracted from the compressive forces to get a tolerance ΔTC_2 and the previous value of y_2 and ΔTC_2 renamed y_1 and ΔTC_1 respectively.

$$y_2 = y_1 + \Delta y \qquad (3.26)$$

$$\Delta TC_2 = C - T_s \qquad (3.27)$$

$$y_1 = y_{2(previous)}$$

$$\Delta TC_1 = \Delta TC_{2(previous)}$$

The process is to be continued up to a depth equal to half the overall depth. $y_2 = 0.5h$

Except of a single increment of Δy, if the tensile force is not equal to the compressive force, the product $(\Delta TC_1 . \Delta TC_2)$ is always positive because both ΔTC_1 and ΔTC_2 are either positive or negative. When the tensile force is equal to the compressive force the product $(\Delta TC_1 . \Delta TC_2)$ is zero. The exception occurs when depth y_1 is less and y_2 is greater than the neutral axis depth y. Then ΔTC_2 and ΔTC_1 have opposite signs and the product $(\Delta TC_1 . \Delta TC_2)$ is negative. Therefore, the neutral axis depth is found by tracing the point at which the difference between the tensile and compressive forces changes signs. This is done by interpolation as shown in equation (3.28) and illustrated in Figure A-26.

$$y = y_2 - \Delta y \left(\frac{\Delta TC_2}{\Delta TC_2 - \Delta TC_1} \right) \qquad (3.28)$$
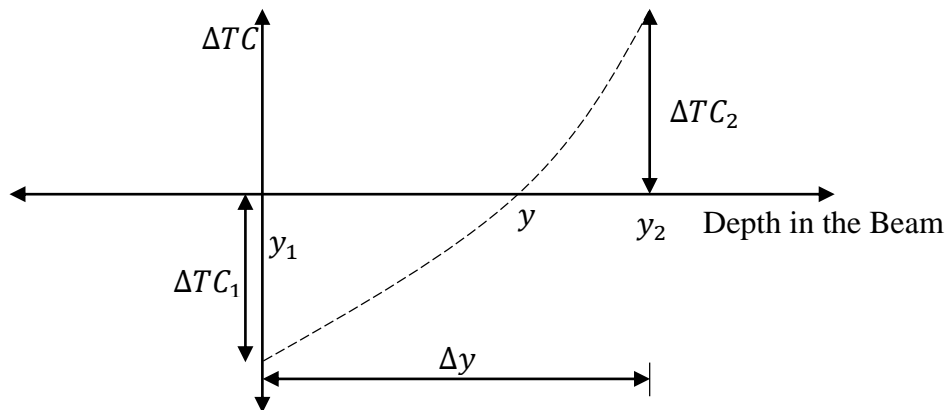
Figure A-26: Difference ΔTC between compressive and tensile force for incremental depth Δy at the neutral axis

Neutral axis at ultimate moment

The neutral axis at ultimate shall be found the same way as outlined for the neutral axis at yield moment except that steel strains ranging from 0.0024 to 0.15 shall be considered. The yield strain for $f_y = 460 \, N/mm^2$ is 0.0023. The neutral axis depth shall be determined based on the following:

  e) The neutral axis depth shall be greater than the depth to the compression reinforcement

  f) The neutral axis depth shall be smaller than that of the yield moment

  g) The ultimate moment shall be greater than the yield moment

  h) The ultimate curvature shall be greater than the yield curvature.

The highest moment to satisfy conditions (a) to (d) shall be the ultimate moment and its corresponding curvature and neutral axis depth as the ultimate curvature and neutral axis depth at ultimate moment.

Determination of the section moment capacity

The moment was found by taking moments about the centreline of the tensile steel reinforcement. The lever arm Z_c, to the compressive force in concrete and that to the compressive steel Z_s are given by:

$$Z_c = d_{sb} - y + \bar{y}$$

$$Z_s = d_{sb} - d_t'$$

Equating the compressive and the tensile forces gives the neutral axis depth y.

The moment is given by:

$$M = C_c Z_c + C_s Z_s$$

The yield moment of the section is the moment corresponding to the yield strain in the tensile reinforcement. On the other hand, the determination of the ultimate moment involves comparing the moment for the current strain value satisfying the four conditions for the ultimate moment with the current ultimate moment.

Determination of curvature

The curvature at yield $\emptyset_y$, and ultimate strain $\emptyset_u$, are respectively given by:

$$\emptyset_y = \frac{\varepsilon_{ccy}}{y}$$

$$\emptyset_u = \frac{\varepsilon_{ccu}}{y}$$

Where

ε_{ccy} and ε_{ccu} are the concrete strains at the outer most compressive fibre at yield and ultimate moments, respectively. Given the value of the tensile steel strain ε_{st} the concrete strain at the outer most compressive fibre is given by:

$$\varepsilon_{cc} = \left(\frac{y}{d-y}\right)\varepsilon_{st}$$

E.3 HOGGING MOMENTS AND CURVATURES

The strain and stress diagrams across the section under the action of hogging moments with the neutral axis in the web are shown in Figure 6-26.
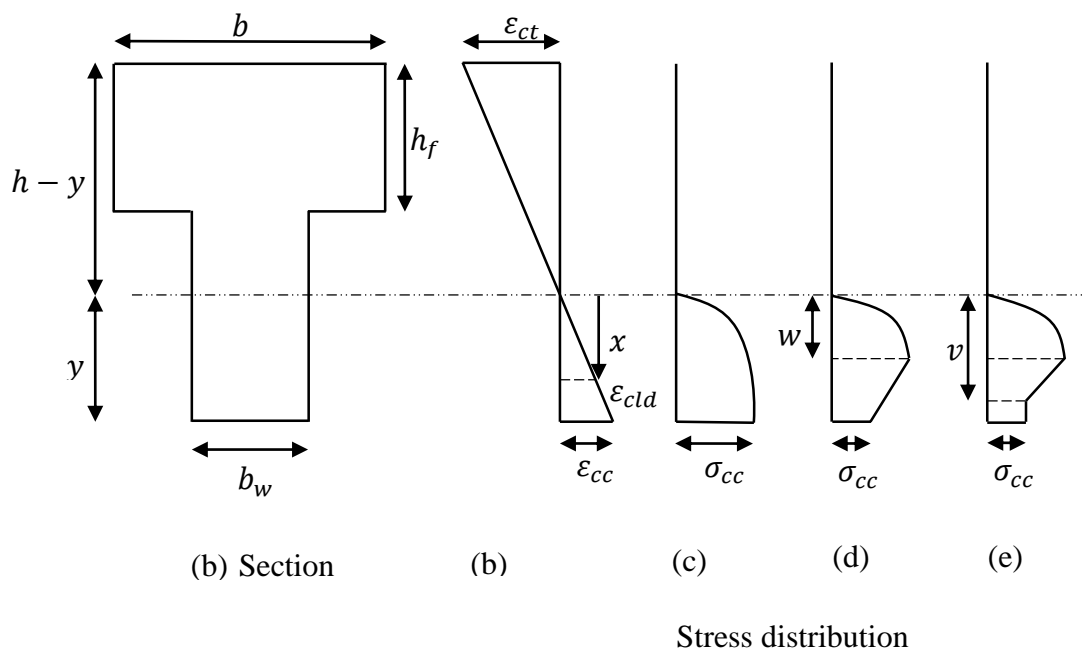

(b) Section   (b)   (c)   (d)   (e)

Stress distribution

Figure A-27: Strain and stress distribution for a section under hogging moment with the neutral axis in the web

In the Figure A-27:

b refers to the flange width

b_w refers to the web width

h refers to the overall depth of the section

h_f refers to the flange depth

$\varepsilon_{ct}, \varepsilon_{cc}, \sigma_{cld}, \sigma_{cc}$ Refer to the tensile strain, maximum compressive strain, maximum stress, and compressive stress in the outer most layer of concrete respectively.

ε_{cld} the strain corresponding to the maximum stress

y the depth of the neutral axis

Stress diagram (c) corresponds to a case where the maximum compressive strain in concrete ε_{cc}, is less than the strain ε_{cld}, corresponding to the maximum stress.

Stress diagram (d) corresponds to a case where the maximum compressive strain in concrete ε_{cc}, is greater than the strain ε_{cld}, corresponding to the maximum stress, but less than the strain ε_{cv} at which the stress becomes constant.

From the proportionality of the strain diagram, the concrete strain ε_{cx} at the height x above the neutral axis is given by:

$$\varepsilon_{cx} = \varepsilon_{cc}\left(\frac{x}{y}\right)$$

w - the depth from the neutral axis to the point of maximum stress. From the proportionality of the strain diagram, this is given by:

$$w = \frac{\varepsilon_{cld}}{\varepsilon_{cc}}y$$

v - the depth from the neutral axis to the point of constant stress. From the proportionality of the strain diagram, this is given by:

$$v = \frac{\varepsilon_{cv}}{\varepsilon_{cc}}y$$

Considering the stress distribution (e),

The compressive force in concrete C_c is given by

$$C_c = \frac{b_w y f_{ccd}}{\varepsilon_{cc}}\left[\frac{2\varepsilon_{cld}}{3} + (\varepsilon_{cv} - \varepsilon_{cld})\left\{(1 + Z\varepsilon_{cld}) - \frac{Z}{2}(\varepsilon_{cv} + \varepsilon_{cld})\right\}\right.$$
$$\left. + 0.2(\varepsilon_{cc} - \varepsilon_{cv})\right] \tag{3.29}$$

Considering case (d), where the stress doesn't exceed that corresponding to constant stress then $\varepsilon_{cv} = \varepsilon_{cc}$, the compressive force in concrete reduces to

$$C_c = b_w y f_{ccd}\left[\left(1 - \frac{\varepsilon_{cld}}{3\varepsilon_{cc}}\right) + Z\left(\varepsilon_{cld} - 0.5\varepsilon_{cc} - \frac{0.5\varepsilon_{cld}^2}{\varepsilon_{cc}}\right)\right] \tag{3.30}$$

Considering case (c), when the stress doesn't exceed that corresponding to maximum stress, the compressive force in concrete is given by

$$C_c = b_w y f_{ccd}\left[\frac{\varepsilon_{cc}}{\varepsilon_{cld}} - \frac{1}{3}\left(\frac{\varepsilon_{cc}}{\varepsilon_{cld}}\right)^2\right] \tag{3.31}$$

The depth of the point of action $\bar{y}$, of the compressive force in concrete C_c, from the neutral axis is determined as follows:

Considering the stress distribution in Figure A-27(e),

$$C_c\bar{y} = \frac{b_w y^2 f_{ccd}}{12\varepsilon_{cc}^2}[5\varepsilon_{cld}^2 + 6(1 + Z\varepsilon_{cld})(\varepsilon_{cv}^2 - \varepsilon_{cld}^2) - 4Z(\varepsilon_{cv}^3 - \varepsilon_{cld}^3)$$

$$+ 1.2(\varepsilon_{cc}^2 - \varepsilon_{cv}^2)]$$

Considering case (d), where the stress doesn't exceed that corresponding to constant stress, then $\varepsilon_{cv} = \varepsilon_{cc}$,

$$C_c\bar{y} = \frac{b_w y^2 f_{ccd}}{12}\left[\left(6 - \left(\frac{\varepsilon_{cld}}{\varepsilon_{cc}}\right)^2\right) + Z\left(6\varepsilon_{cld} - 4\varepsilon_{cc} - \frac{2\varepsilon_{cld}^2}{\varepsilon_{cc}^2}\right)\right] \tag{3.33}$$

Considering case (c), where the stress does not exceed that corresponding to the maximum stress,

$$C_c\bar{y} = b_w y^2 f_{ccd}\left[\frac{2}{3}\left(\frac{\varepsilon_{cc}}{\varepsilon_{cld}}\right) - \frac{1}{4}\left(\frac{\varepsilon_{cc}}{\varepsilon_{cld}}\right)^2\right] \tag{3.34}$$

$$\bar{y} = \frac{C_c\bar{y}}{C_c}$$

E.3.1   Compressive force in concrete when the neutral axis is in the flange

When concrete strain at the bottom is less than the strain corresponding to maximum stress
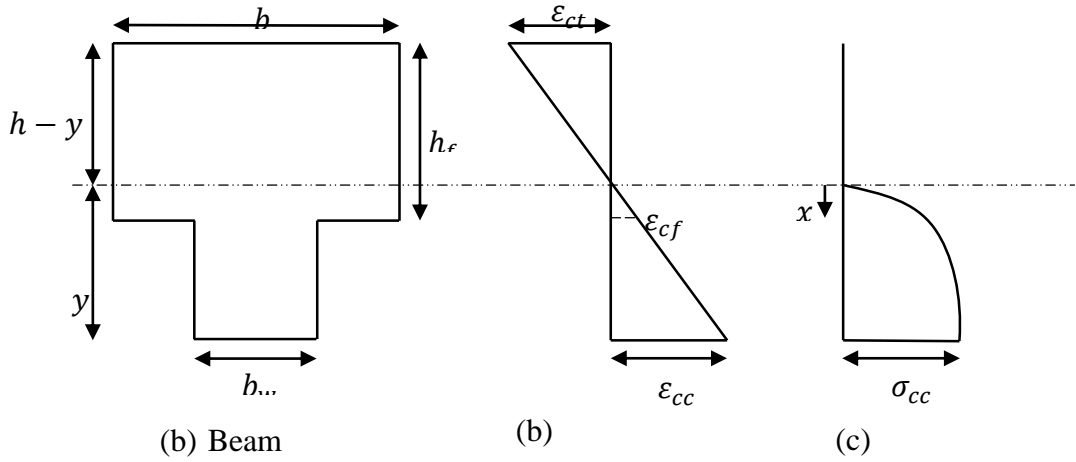
Figure A-28: Strain and stress distribution for a section under hogging moment with the neutral axis in the flange and stress less than the maximum stress

The symbols in Figure A-28 carry the same meaning as defined in A-27.

The compressive force in concrete C_c shall be given by

$$C_c = b_w y f_{ccd} \left[\frac{\varepsilon_{cc}}{\varepsilon_{cld}} - \frac{1}{3}\left(\frac{\varepsilon_{cc}}{\varepsilon_{cld}}\right)^2 \right] + (b - b_w) f_{ccd} \left[\frac{\varepsilon_{cc} q^2}{\varepsilon_{cld} y} - \left(\frac{\varepsilon_{cc}}{\varepsilon_{cld}}\right)^2 \frac{q^3}{3y^2} \right] \qquad (3.35)$$

Where,

$$q = h_f + y - h$$

The depth of the point of action $\bar{y}$, of the compressive force in concrete C_c, from the neutral axis is determined using

$$C_c \bar{y} = b_w y^2 f_{ccd} \left[\frac{2}{3}\left(\frac{\varepsilon_{cc}}{\varepsilon_{cld}}\right) - \frac{1}{4}\left(\frac{\varepsilon_{cc}}{\varepsilon_{cld}}\right)^2 \right] + (b - b_w) f_{ccd} \left[\frac{2q^3}{3y}\left(\frac{\varepsilon_{cc}}{\varepsilon_{cld}}\right) - \frac{q^4}{4y^2}\left(\frac{\varepsilon_{cc}}{\varepsilon_{cld}}\right)^2 \right]$$

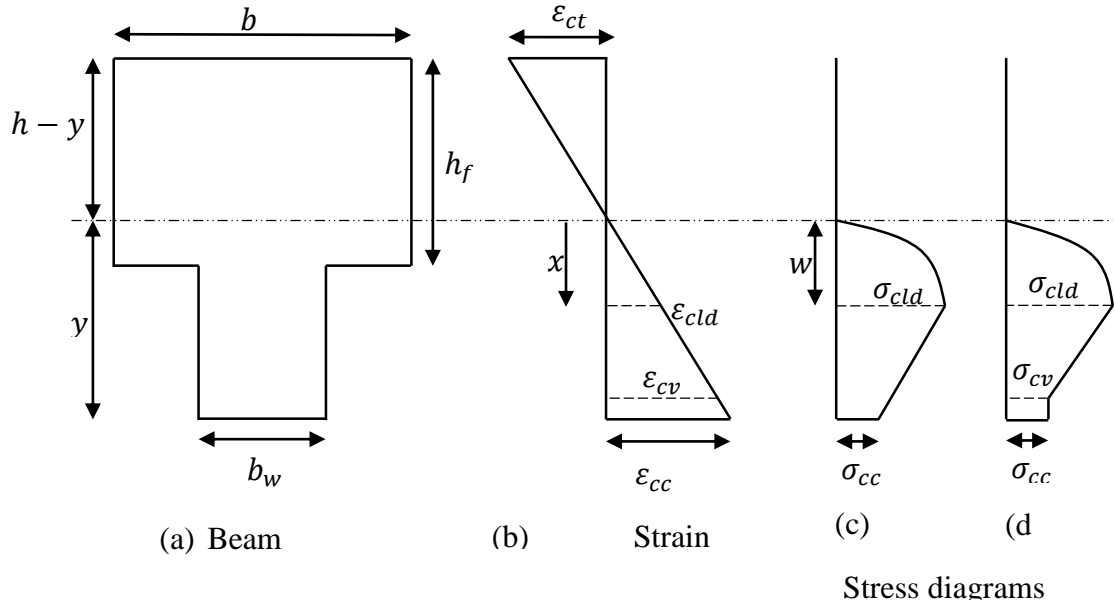$$\bar{y} = \frac{C_c \bar{y}}{C_c}$$

174

Figure A-29: Strain and Stress distribution for a section under hogging moment with the neutral axis in the flange and maximum stress greater than that corresponding to maximum stress

Considering the stress distribution (d), the compressive force in concrete C_c shall be given by

$$C_c = \frac{b_w y f_{ccd}}{\varepsilon_{cc}} \left[\frac{2}{3} \varepsilon_{cld} + 0.2(\varepsilon_{cc} - \varepsilon_{cv}) + (1 + Z\varepsilon_{cld})(\varepsilon_{cv} - \varepsilon_{cld}) - \frac{Z}{2}(\varepsilon_{cv}^2 - \varepsilon_{cld}^2) \right]$$

$$+ (b - b_w) y f_{ccd} \frac{\varepsilon_{cf}^2}{\varepsilon_{cld}\varepsilon_{cc}} \left(1 - \frac{\varepsilon_{cf}}{3\varepsilon_{cld}} \right)$$

Considering case (c) where the stress does not exceed that corresponding to constant stress, then the compressive force in concrete shall be given by

$$C_c = \frac{b_w y f_{ccd}}{\varepsilon_{cc}} \left[\frac{2}{3} \varepsilon_{cld} + (1 + Z\varepsilon_{cld})(\varepsilon_{cc} - \varepsilon_{cld}) - \frac{Z}{2}(\varepsilon_{cc}^2 - \varepsilon_{cld}^2) \right]$$

$$+ (b - b_w) y f_{ccd} \frac{\varepsilon_{cf}^2}{\varepsilon_{cld}\varepsilon_{cc}} \left(1 - \frac{\varepsilon_{cf}}{3\varepsilon_{cld}} \right)$$

The depth of the point of action $\bar{y}$, of the compressive force in concrete C_c, from the

neutral axis is given by

$$C_c \bar{y} = \frac{b_w y^2 f_{ccd}}{12\varepsilon_{cc}^2} [5\varepsilon_{cld}^2 + 1.2(\varepsilon_{cc}^2 - \varepsilon_{cv}^2) + 6(1 + Z\varepsilon_{cld})(\varepsilon_{cv}^2 - \varepsilon_{cld}^2)$$

$$- 4Z(\varepsilon_{cv}^2 - \varepsilon_{cld}^3)] + (b - b_w) y^2 f_{ccd} \frac{\varepsilon_{cf}^2}{\varepsilon_{cc}^2} \left[\frac{2}{3}\left(\frac{\varepsilon_{cf}}{\varepsilon_{cld}}\right) - \frac{1}{4}\left(\frac{\varepsilon_{cf}}{\varepsilon_{cld}}\right)^2 \right]$$

Considering case (c), that is when the stress does not exceed that corresponding to

constant stress, then

$$C_c \bar{y} = \frac{b_w y^2 f_{ccd}}{12\varepsilon_{cc}^2} [5\varepsilon_{cld}^2 + 6(1 + Z\varepsilon_{cld})(\varepsilon_{cc}^2 - \varepsilon_{cld}^2) - 4Z(\varepsilon_{cc}^3 - \varepsilon_{cld}^3)]$$

$$+ (b - b_w) y^2 f_{ccd} \frac{\varepsilon_{cf}^2}{\varepsilon_{cc}^2} \left[\frac{2}{3}\left(\frac{\varepsilon_{cf}}{\varepsilon_{cld}}\right) - \frac{1}{4}\left(\frac{\varepsilon_{cf}}{\varepsilon_{cld}}\right)^2 \right]$$

$$\bar{y} = \frac{C_c \bar{y}}{C_c}$$

E.3.3 Compressive force in concrete when concrete strain at the bottom is greater than the strain corresponding to the maximum stress, which lies in the flange
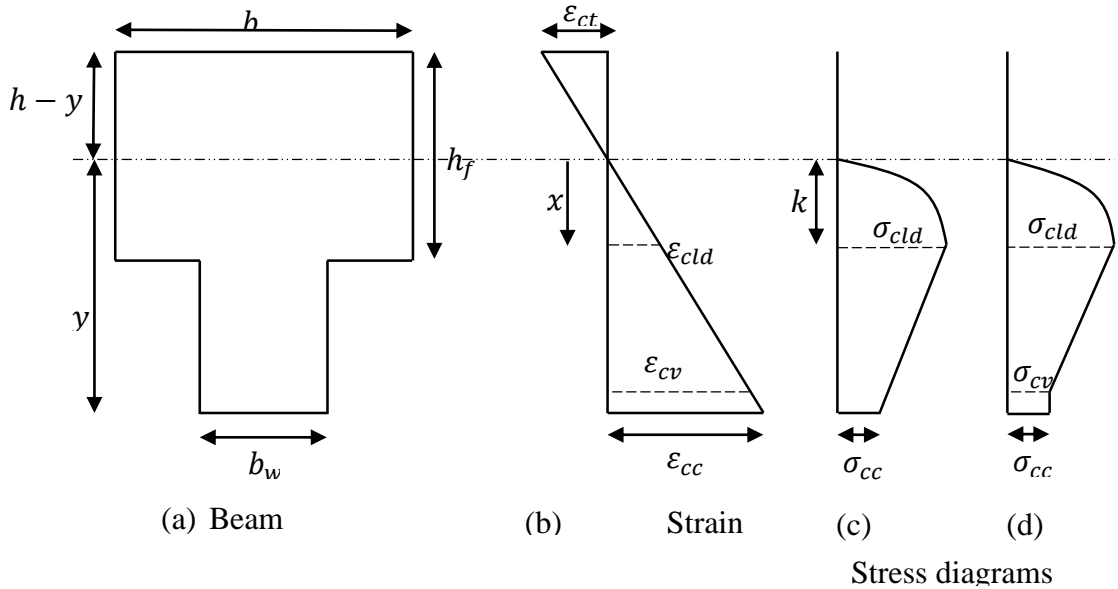

Figure A-30: Strain and Stress distribution for a section under hogging moment with neutral axis in the flange and strain greater than that corresponding to maximum stress

Considering the stress distribution (d)

The compressive force in concrete C_c is given by

$$C_c = \frac{y f_{ccd}}{\varepsilon_{cc}} \left[(b - b_w)\varepsilon_{cf} \left(1 - \frac{Z\varepsilon_{cf}}{2} + Z\varepsilon_{cld} \right) + b_w \varepsilon_{cv} \left(1 - \frac{Z\varepsilon_{cv}}{2} + Z\varepsilon_{cld} \right) \right.$$

$$\left. - b\varepsilon_{cld} \left(\frac{1}{3} + \frac{Z\varepsilon_{cld}}{2} \right) + 0.2 b_w (\varepsilon_{cc} - \varepsilon_{cv}) \right]$$

Considering case (c), when the stress does not exceed that corresponding to constant stress, then the compressive force in concrete is given by

$$C_c = \frac{y f_{ccd}}{\varepsilon_{cc}} \left[(b - b_w)\varepsilon_{cf} \left(1 - \frac{Z\varepsilon_{cf}}{2} + Z\varepsilon_{cld} \right) + b_w \varepsilon_{cc} \left(1 - \frac{Z\varepsilon_{cc}}{2} + Z\varepsilon_{cld} \right) \right.$$

$$\left. + b\varepsilon_{cld} \left(\frac{1}{3} + \frac{Z\varepsilon_{cld}}{2} \right) \right]$$

The depth of the point of action $\bar{y}$, of the compressive force in concrete C_c, from the neutral axis is given by

$$C_c\bar{y} = \frac{y^2 f_{ccd}}{12\varepsilon_{cc}^2} \left[(b - b_w)\varepsilon_{cf}^2 \left(6 - 4Z\varepsilon_{cf} + 6Z\varepsilon_{cld} \right) + b_w\varepsilon_{cv}^2 (6 - 4Z\varepsilon_{cv} + 6Z\varepsilon_{cld}) \right.$$

$$\left. - b\varepsilon_{cld}^2 (1 + 2Z\varepsilon_{cld}) \right] + \frac{b_w y^2 f_{ccd}}{10\varepsilon_{cc}^2} (\varepsilon_{cc}^2 - \varepsilon_{cv}^2)$$

Considering case (c), where the stress does not exceed that corresponding to constant stress then $C_c\bar{y}$ is given by

$$C_c\bar{y} = \frac{y^2 f_{ccd}}{12\varepsilon_{cc}^2} \left[(b - b_w)\varepsilon_{cf}^2 \left(6 - 4Z\varepsilon_{cf} + 6Z\varepsilon_{cld} \right) + b_w\varepsilon_{cc}^2 (6 - 4\varepsilon_{cc} + 6Z\varepsilon_{cld}) \right.$$

$$\left. - b\varepsilon_{cld}^2 (1 + 2Z\varepsilon_{cld}) \right]$$

E.4 TENSILE AND COMPRESSIVE FORCE IN THE REINFORCEMENT

The yield moment and curvature are assumed to be the point at which the reinforcement under tension reaches a yield strain. When the reinforcement under tension (top reinforcement) reaches a yield strain ε_{sy}, the tensile force in the reinforcement T_s is given by:

$$T_s = f_y A_{st} \tag{3.46}$$

If the strain ε_{st} in the tensile steel at the top has exceeded the strain hardening value ε_{sh}, but less than the ultimate strain ε_{su} , then the tensile force in steel is given by:

$$T_s = A_{st} \left[f_y + \left(\frac{\varepsilon_{st} - \varepsilon_{sh}}{\varepsilon_{su} - \varepsilon_{sh}} \right) (f_u - f_y) \right]$$
(3.47)

At the ultimate strain of the tensile steel, the tensile force is given by

$$T_s = f_u A_{st}$$
(3.48)

If the steel under compression has not reached the yield strain, the compressive force in the reinforcement at the bottom is given by

$$C_s = \left(\frac{n-1}{n} \right) A_{sb} \left(\frac{y - d_b'}{h - y - d_t'} \right) \varepsilon_y E_s$$
(3.49)

If the strain in the compressive reinforcement (at the bottom) is greater than the yield strain ε_y, but less than the strain hardening strain, the force in compressive reinforcement is given by:

$$C_s = \left(\frac{n-1}{n} \right) A_{sb} \left[f_y + \left(\frac{\varepsilon_{sb} - \varepsilon_{sh}}{\varepsilon_{su} - \varepsilon_{sh}} \right) (f_u - f_y) \right]$$
(3.50)

The determination of the neutral axis, yield and ultimate moments and curvatures are carried out as detailed in section 3.6.1.

Annex F: Analysis and Design of the beam sections

REF:	CALCULATIONS	RES.
Clause: *5.3.2.1* *Eqn:5.7* *Eqn:5.7a*	The figure below shows a section through an interior beam which forms part of a concrete beam and slab floor with the slab spanning between beams and the areas of the slab acting as the flanges of the beam. When interior beams are resisting sagging moments, the slab acts as a compression flange and the members are designed as T beams. With hogging moments, the slab will be in tension and assumed to be cracked; therefore the beam must be designed as a rectangular section with width b_w and an overall depth h. b_{eff} Transverse steel in flange b_{eff1} b_w b_{eff2} *Figure A-31: Beam cross section* The effective flange width $b_{eff} = b_w + \sum b_{eff,i}$ Where;	

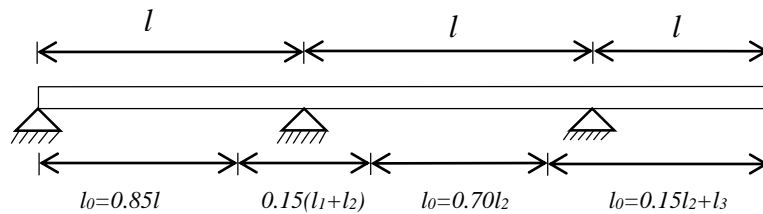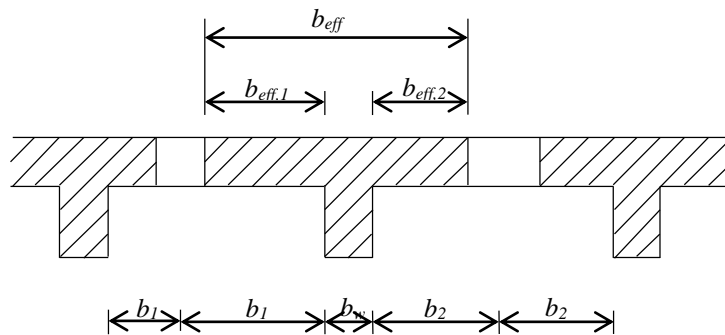|	
	$$b_{eff,i} = 0.2b_i + 0.1l_0 \leq 0.2l_0 \text{ and also } b_{eff,i} \leq b_i$$ $2b_i$ - the clear distance between the webs of adjacent beams l_0 - the distance between the points of contra flexure along the beam as shown in Figure A-32
Clause: *5.3.2.1.(2)* *Figure 5.2*	$l_0=0.85l \qquad 0.15(l_1+l_2) \qquad l_0=0.70l_2 \qquad l_0=0.15l_2+l_3$ *Figure A-32: Showing distance between points of contra flexure along the beam*
Figure 5.3	$b_1 \qquad b_1 \qquad b_w \qquad b_2 \qquad b_2$ *Figure A-33: Effective Flange width* $$b_{eff} = \sum b_{eff,i} + b_w \leq b$$ Where; $$b_{eff,i} = 0.2b_i + 0.1l_0 \leq 0.2l_0$$ $$l_0 = 0.7l = 0.7x7000 = 4900mm, b_w = 300mm,$$

$$b_i = {^{6000}}/_2 = 3000mm$$

$$b_{eff,1} = b_{eff,2} = 0.2x3000 + 0.1x4900 = 1090mm$$

$$b_{eff} = 1090x2 + 300 = 2480mm$$

For sagging moments, the flanges act as a large compressive area. Therefore, the stress block for the flanged beam section usually falls within the flange thickness. For this position of the stress block, the section may be designed as an equivalent rectangular section of breadth b_f.

Transverse reinforcement should be placed across the full width of the flange to resist the shear developed between the web and the flange. Quite often this reinforcement is adequately provided for by the top steel of the bending reinforcement in the slab supported by the beam.
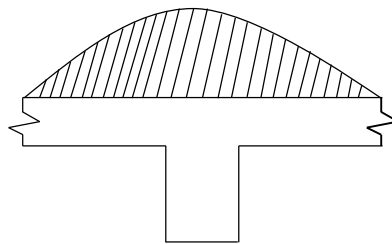
Figure A-34: Stress distribution over a flanged beam

Design procedure for a flanged beam subject to a sagging moment.

Estimation of design beam loading, W_{Ed}

Permanent load, g_k

Assuming unit weight of concrete to be $25 \, kN/m^2$

$g_k = Weight \; of \; solid \; concrete \; slab + Weight \; of \; Beam$

$g_k = (0.2x3.5 + 0.3x0.3)x25 = 19.75kN/m$

Variable load, q_k

Assuming office floor space having an average loading of $1.5 \, kN/m^2$

$q_k = 1.5x \, {^{3.5}/_2} = 2.625kN/m$

Ultimate Design load, W_{Ed}

$W_{Ed} = 1.35g_k + 1.5q_k$

$W_{Ed} = 1.35x19.75 + 1.5x2.625$

$W_{Ed} = 30.6 \, kN/m$

Maximum sagging moment, M_{sag}

$$M_{sag} = \frac{wl^2}{24} = \frac{30.6x7^2}{24} = 62.48kNm$$

1. Calculate $K = \dfrac{M}{b_f d^2 f_{ck}}$

$$d = h - cover - \emptyset link - {^1/_2} \emptyset bar$$

$$d = 500 - 25 - 8 - {^{16}/_2} = 459mm$$

$$K = \frac{62.48x10^6}{2480x459^2x25} = 0.0048 < 0.167.$$

To be designed as a singly reinforced beam

2. Determine the lever-arm distance, z , from the equation

$$z = d\left[0.5 + \sqrt{\left(0.25 - K/1.134\right)}\right]$$

$$z = d\left[0.5 + \sqrt{\left(0.25 - 0.0048/1.134\right)}\right]$$

$$z = 0.996d > 0.82d,$$

$$Take\ z = 0.82d = 0.82x459 = 376.38mm$$

3. Compute the depth of the stress block

$$s = 2(d - z)$$

$$s = 2(459 - 376.38) = 165.24 < h = 200m$$

If $s \leq h$ the stress block falls within the flange depth, and the design may proceed as for rectangular section, breadth b_f.

4. Calculate the area of tension steel required from;

$$A_s = \frac{M}{0.87f_{yk}z}$$

$$A_s = \frac{62.48x10^6}{0.87x460x376.38}$$

$$A_s = 414.8mm^2$$

Provide $3T16$ bars at the bottom of the beam.

$$A_{s,prov} = 201x3 = 603mm^2$$

Design procedure for a rectangular beam subject to a

hogging moment.

Maximum hogging moment, M_{hog}

$$M_{hog} = \frac{wl^2}{12} = \frac{30.6 x 7^2}{12} = 124.95 kNm$$

1. Calculate

$$K = \frac{M}{b_w d^2 f_{ck}}$$

$$d = h - cover - \emptyset link - {}^1/_2 \emptyset bar$$

$$d = 500 - 25 - 8 - {}^{16}/_2 = 459mm$$

$$K = \frac{124.95 x 10^6}{300 x 459^2 x 25} = 0.079 < 0.167.$$

To be designed as a singly reinforced section

2. Determine the lever-arm distance, Z , from the

equation

$$z = d \left[0.5 + \sqrt{\left(0.25 - {K}/{1.134} \right)} \right]$$

$$z = d \left[0.5 + \sqrt{\left(0.25 - {0.079}/{1.134} \right)} \right]$$

$$z = 0.92d > 0.82d,$$

$$Take\ z = 0.82d = 0.82 x 459 = 376.38mm$$

5. Calculate the area of tension steel required from;

$$A_s = \frac{M}{0.87 f_{yk} z}$$

	$$A_s = \frac{124.95x10^6}{0.87x460x376.38}$$ $$A_s = 829.53mm^2$$ Provide $3T20$ bars at the bottom of the beam. $$A_{s,prov} = 314.159x3 = 942.48mm^2$$	
Clause: **6.2.3**	**Members requiring design shear reinforcement** **Design for shear at the support** For members with vertical shear reinforcement, the shear resistance, V_{Rd} is the smaller value of:	
Eqn:6.8	$$V_{Rd,s} = \frac{A_{sw}}{s}.z.f_{ywd}.\cot\theta$$ and	
Eqn:6.9	$$V_{Rd,max} = \alpha_{cw}b_w z v_1 f_{cd} \Big/ (\cot\theta + \tan\theta)$$ ere: A_{sw} the cross-sectional area reinforcement s the spacing of the stirrups f_{ywd} the design yield strength of the shear reinforcement v_1 strength reduction factor for concrete cracked in shear α_{cw} coefficient taking account of the state of the stress in the compression chord. **Note 1**: the value of v_1 and α_{cw} for use in a country may be found in its national annex. The recommended value of v_1 is v.	
Eqn:6.6N	$v = 0.6\left[1 - \frac{f_{ck}}{250}\right]$ (f_{ck} in Mpa)	

Note 2: the recommended value of α_{cw} is as follows:

1 for non- prestressed structures.

Computation

Shear force at center of supports, V_{ef}

$$V_{ef} = \frac{wl}{2} = \frac{30.6x7}{2} = 107.1kN$$

Shear force at the face of the support, V_{sf}

$$V_{sf} = shear force\ at\ the\ center$$

$$- \frac{w\ x\ \sup p\ ort\ width}{2}$$

$$V_{sf} = 107.1 - \frac{30.6x0.5}{2}$$

$$V_{sf} = 99.45kN$$

Shear force at the critical section, V_{sd}

$$V_{sd} = V_{sf} - wd$$

$$V_{sd} = 99.45 - 30.6x0.459$$

$$V_{sd} = 85.41kN$$

Check for maximum shear force which can be sustained by the member,

$$V_{Rd,max} = 0.6[1 - f_{ck}/250]$$

$$v = 0.6x[1 - 25/250] = 0.54$$

$$z = 376.38mm, b_w = 300mm, v_1 = 0.54, f_{cd} = \frac{25}{1.5}$$

$$= 16.67, \cot\theta = 1, \tan\theta = 0$$

$$V_{Rd,max} = {\alpha_{cw}b_w z v_1 f_{cd}}\Big/{(\cot\theta + \tan\theta)}$$

$$V_{Rd,max} = \frac{1 x 300 x 376.38 x 0.54 x 16.67}{1} = 1016.4 kN$$

$$> 85.41 kN$$

Design for shear reinforcement

$$\left(\frac{A_{sw}}{s}\right) = 1.28\frac{(V_{sd} - V_{Rd,c})}{d f_{yk}}$$

where:

The design value for the shear resistance $V_{Rd,c}$ is given by:

$$V_{Rd,c} = \left[C_{Rd,c}k(100\rho_1 f_{ck})^{1/3} + k_1\sigma_{cp}\right]b_w d$$

With a minimum of

$$V_{Rd,c} = (v_{min} + k_1\sigma_{cp})b_w d\text{ere:}$$

f_{ck} is in MPa

$k = 1 + \sqrt{\frac{200}{d}} \leq 2.0$with, d in mm

$\rho_1 = \frac{A_{sl}}{b_w d} \leq 0.02$

A_{sl} Is the area of the tensile reinforcement, which extends $\geq$

$(l_{bd} + d)$beyond the section, considered

b_w the smallest width of the cross-section in the tensile area

(mm)

$\sigma_{cp} = N_{Ed}/A_c < 0.2 f_{cd}[MPa]$

N_{Ed} the axial force in the cross-section due to loading or prestressing [in N]

A_c the area of the concrete section [mm²]

$V_{Rd,c}$ is [N]

$$k = 1 + \sqrt{\frac{200}{d}} = 1 + \sqrt{\frac{200}{459}} = 1.66 \leq 2.0$$

$$\rho_1 = \frac{A_{sl}}{b_w d} = \frac{603}{300x459} = 0.0044 \leq 0.02$$

$$C_{Rd,c} = 0.18/\gamma_c = 0.18/1.5 = 0.12, k_1 = 0.15$$

$$V_{Rd,c} = \left[0.12x1.66x(100x0.0044x25)^{1/3}\right]x300x459x10^{-3}$$

$$V_{Rd,c} = 61.0kN$$

Therefore:

$$\left(\frac{A_{sw}}{s}\right) = 1.28\frac{(V_{sd} - V_{Rd,c})}{df_{yk}}$$

$$\left(\frac{A_{sw}}{s}\right) = 1.28x\frac{(85.41 - 61.0)x10^3}{459x450}$$

$$\left(\frac{A_{sw}}{s}\right) = 0.151$$

For 2 R08 bars, $A_{sw} = 100.6mm^2$

$$s = \frac{A_{sw}}{0.151} = \frac{100.6}{0.151} = 666.23mm$$

Provide R08 bars at 200mm c/c.

REFERENCES

Aktan, A. E. & Nelson, G. E., 1989. Problems in predicting seismic responses of RC buildings. *Journal of Structural Engineering,* pp. 2036-2056.

Antoniou, S. & Pinho, R., 2004. Advantages and limitations of adaptive and non-adaptive force-based pushover proceedures. *Journal of Earthquake Engineering,* 8(4), pp. 497-522.

Aristizabal-Ochoa & Dario, J., 1983. Cracking and Shear effects on structural walls. *Journal of structural Engineering,* pp. 1267-1277.

Bhabha Atomic Research Centre, 2012. *Nonlinear Seismic Analysis of Reinforced Concrete Framed Structure considering Joint Distortion,* Mumbai: Head, Scientific Information Resource Division,.

BSI, 2000. *Eurocode 8: Design of structures for earthquake resistance - Part 1: General rules, seismic actions and rules for buildings.* s.l.:European Committee for Standardization (CEN).

BSI, 2004. *Eurocode 2: Design of concrete structures - Part 1: General rules and rules for buildings.* B-1050 Brussels: European Committee for Standardization (CEN).

Filippou, F. C. & Issa, A., 1988. *Nonlinear Analysis of Reinforced Concrete Frames under Cyclic Load Reversals.* Berkeley: Earthquake Engineering Research Center.

Galeb & Alaa, 2018. Optimum design of doubly reinforced concrete beams using simulated annealing. *International Journal of Civil Engineering and Technology,* 9(10), pp. 61-70.

Jack, M., Terry & Cavanagh, 1985. Confinement effectiveness of crossties in RC. *Journal of Structural Engineering.*

Krawinkler, H. & Seneviratna, G. D. P. K., 1997. Pros and ons of a pushover analysis of seismic performance evaluation. *Elsevier Science Ltd,* Volume 20, pp. 452-464.

Kyakula Michael, S. W., 2004. *The effect of the length and location of yield zones on the accuracy of the spread plasticity models.* Vancouver, B.C, Canada, s.n.

Kyakula, M., 2010. *A versatile Spread Plasticity Model for Seismic Analysis of RC Frames.* Saarbrucken: LAP LAMBERT Academic Publishing GmbH & Co. KG.

Kyakula, M. & Wilkinson, S., 2004. *An improved spread plasticity model for inelastic analysis of R/C. frames subjected to seismic loading.* Vancouver, B.C, s.n.

Montaignac, R. d., Massicotte, B., Charron, J.-P. & Nour, A., 2012. Design of SFRC structural elements: post-cracking tensile strength measurements. *ResearchGate,* p. 15.

Pantazopoulou, S. J., Moehle, J. P. & Shahrooz, B. M., 1988. Simple Analytical model for T-Beams in flexure. *Journal of structural Engineering.*

Penelis, G. G. & Kappos, A. J., 1997. *Earthquake Resistant Concrete Structures.* 2 Park Square, Milton Park, Abingdon, Oxon,: Taylor & Francis.

Regina Gaiotti, B. S. S., 1989. P-Delta Analysis of building structures. *Journal of Strucutral Engineering.*

Riva, P. & Cohn, M. Z., 1990. Engineering approach to nonlinear analysis of concrete structures. *Journal of Structural Engineering.*

Sheikh, S. & Uzumeri, S., 1980. Strength and Ductility of Tied Concrete Columns. *Journal of the Structural Division.*

Watson, S., Zahn, F. A. & Park, R., 1994. Confining Reinforcement for Concrete Columns. *Journal of Structural Engineering,* 120(6), pp. 1798-1824.